

# Modeling the Spatial and Temporal Variability of Marine Radiocarbon Reservoir Ages in the Late Quaternary

Dissertation zur Erlangung des Doktorgrades der Naturwissenschaften  
am Fachbereich Geowissenschaften der Universität Bremen

vorgelegt von **Jörg Franke**

Betreuer und 1. Gutachter :	<b>Prof. Dr. M. Schulz</b>
2. Gutachterin:	<b>Prof. Dr. G. Mollenhauer</b>

Eingereicht am 04.02.2008



Life is like riding a bicycle. To keep your balance you must keep moving.

- Albert Einstein -



# Abstract

In paleoceanography and paleoclimatology radiocarbon ( $^{14}\text{C}$ ) is frequently used to date carbonaceous samples of the past 50,000 years and as a proxy to reconstruct circulation states of the ocean. Temporal variations of the atmospheric  $^{14}\text{C}$  concentration ( $\Delta^{14}\text{C}_{atm}$ ), caused by a varying  $^{14}\text{C}$  production rate or changes in the global carbon cycle, lead to dating uncertainties and also limit the usability of  $^{14}\text{C}$  as an oceanographic proxy. In order to analyze and correct the influence of varying atmospheric  $^{14}\text{C}$  on the ocean, radiocarbon has been included as a tracer to a global climate model (University of Victoria Earth System Climate Model). This model was forced by the reconstructed atmospheric  $^{14}\text{C}$  production rate, to predict differences between atmospheric and marine  $^{14}\text{C}$  age, the so-called reservoir age, spatially and temporally. The model simulations confirmed the earlier results of box models that the reconstructed  $\Delta^{14}\text{C}$  in the atmosphere cannot be explained by  $^{14}\text{C}$  production-rate changes alone. Major changes in the carbon cycle are required. In order to take the entire range of atmospheric variations such as the decreasing  $\Delta^{14}\text{C}$  trend of the past 27,000 years and the influence of oceanic circulation changes into account, the model was forced by the reconstructed  $\Delta^{14}\text{C}$  in a second simulation. The range of reservoir-age variations is similar in both experiments, because the temporal variations of atmospheric  $\Delta^{14}\text{C}$  mainly influence the reservoir age and not the absolute  $\Delta^{14}\text{C}$  value. In the time period between 45,000 and 27,000 years before present (BP) where  $\Delta^{14}\text{C}$  reconstructions show a lot of scatter and major  $\Delta^{14}\text{C}$  variations can be explained by  $^{14}\text{C}$  production-rate changes, the production-rate model forcing is supposed to result in more reliable reservoir-age variations. From 27,000 years BP until present day  $\Delta^{14}\text{C}$  reconstructions have less uncertainties and carbon-cycle changes are held responsible for major  $\Delta^{14}\text{C}$  variations in the atmosphere. Thus,  $\Delta^{14}\text{C}$  forced reservoir-age variations are supposed to be more reliable. Modeled temporal reservoir-age variations range from  $\sim 300$  years in low latitudes and  $\sim 1000$  years in high latitudes highlight the need to consider these variations at any location when marine samples are dated by the  $^{14}\text{C}$  method. Neglecting them can lead to a the wrong interpretation of cause and effect in time-series analysis. Modeled reservoir ages are now an alternative to the constant present day reservoir ages and are available as maps, diagrams or raw data via an internet database ([www.reservoirage.uni-bremen.de](http://www.reservoirage.uni-bremen.de)).

Reconstructions of past ocean circulation changes are often based on the difference between surface ocean and deep ocean  $^{14}\text{C}$  age (“top-to-bottom ages” or “benthic minus planktonic ages”) or on the calculation of projection ages ( $^{14}\text{C}$  decay is calculated backwards through time to the intersection with the  $\Delta^{14}\text{C}$  evolution of the atmosphere). To analyze which method is less influenced by atmospheric  $\Delta^{14}\text{C}$  variations, the model was forced by a idealized atmospheric  $\Delta^{14}\text{C}$  variation. This experiment shows that apparent age variations using both methods are not necessarily caused by ocean-circulation changes as long as they do not exceed a several hundreds of years. Top-to-bottom and projection ages in the Atlantic are less sensitive to atmospheric  $\Delta^{14}\text{C}$  variations than in the Pacific because of the shorter distance to the deep-water formation areas and the smaller influence of mixing processes. Both methods indicate circulation changes of similar magnitude, when they are forced by the idealized  $\Delta^{14}\text{C}$  variations in the atmosphere. The projection-age method has the advantage not to predict a long-lasting trend if such a trend exists in the atmospheric  $\Delta^{14}\text{C}$  evolution. In contrast, the top to bottom age method takes the surface ocean into account and is therefore less influenced by reservoir-age variations and changes in the atmosphere-ocean gas exchange. Improvements of the projections-age method, especially the substitution of the atmospheric  $^{14}\text{C}$  history by a marine reconstruction, has the potential, to make this method highly independent from atmospheric  $^{14}\text{C}$  variations. On-going research will further improve the quality of  $^{14}\text{C}$  as a proxy in paleoclimatic and paleoceanographic research.

# Kurzfassung

In der Paläoozeanographie und Paläoklimatologie wird Radiokohlenstoff ( $^{14}\text{C}$ ) vor allem zur Datierung von Proben der vergangenen 50.000 Jahre eingesetzt, aber auch zur Rekonstruktion von Zirkulationsänderungen des Ozeans. Zeitliche Schwankungen atmosphärischer  $^{14}\text{C}$ -Konzentrationen ( $\Delta^{14}\text{C}_{\text{atm}}$ ), verursacht durch Änderungen der atmosphärischen  $^{14}\text{C}$ -Produktionsrate oder Veränderungen im globalen Kohlenstoffkreislauf, schränken die Nutzungsmöglichkeiten ein oder führen zu Unsicherheiten in den Ergebnissen. Um den Einfluss von variierendem atmosphärischem  $\Delta^{14}\text{C}$  auf den Ozean zu analysieren und korrigieren, wurde Radiokohlenstoff in ein globales Klimamodell, das University of Victoria Earth System Climate Model, integriert. Dieses Modell wurde zunächst mit rekonstruierten Änderungen der atmosphärischen  $^{14}\text{C}$ -Produktionsrate angetrieben, um die Differenzen zwischen atmosphärischen und marinem  $^{14}\text{C}$ -Alter, die sogenannten Reservoiralter, räumlich und zeitlich zu prognostizieren. Dabei bestätigte es die Ergebnisse vorangegangener Experimente mit Box-Modellen, dass sich die rekonstruierten  $^{14}\text{C}$ -Gehalte der Atmosphäre im letzten Glazial nicht allein mit  $^{14}\text{C}$ -Produktionsratenschwankungen erklären lassen, sondern gravierende Änderungen im Kohlenstoffkreislauf notwendig sind. Um alle atmosphärischen  $\Delta^{14}\text{C}$ -Variationen wie den negativen Trend der vergangenen 27.000 Jahre und den Einfluss von Änderungen in der ozeanischen Zirkulation zu berücksichtigen, wurde das Modell ebenfalls mit rekonstruierten  $\Delta^{14}\text{C}_{\text{atm}}$  angetrieben. Da aber die zeitlichen Veränderungen atmosphärischen  $\Delta^{14}\text{C}$  maßgeblich über die Reservoiraltervariation bestimmen und nicht der absolute  $\Delta^{14}\text{C}$ -Wert, ist die Spannweite der Variationen unter beiden Modellantrieben ähnlich. In der Zeit zwischen 45.000 und 27.000 Jahren vor heute, in der die  $\Delta^{14}\text{C}$ -Rekonstruktionen eine große Streuung aufweisen und sich die wesentlichen  $\Delta^{14}\text{C}$ -Variationen durch  $^{14}\text{C}$ -Produktionsratenschwankungen erklären lassen, sind die mit der  $^{14}\text{C}$ -Produktionsrate modellierten Reservoiralter vermutlich verlässlicher. Von 27.000 Jahren vor heute bis heute zeigen die  $\Delta^{14}\text{C}$ -Rekonstruktionen eine geringere Streuung. Für viele der atmosphärischen  $\Delta^{14}\text{C}$ -Variationen werden Änderungen im globalen Kohlenstoffkreislauf verantwortlich gemacht. Deshalb sind in diesem Zeitraum vermutlich die mit  $\Delta^{14}\text{C}$ -Rekonstruktionen modellierten Reservoiralter vertrauenswürdiger. Modellerte zeitliche Variationen der Reservoiralter von  $\sim 300$  Jahren in niedrigen Breiten bis zu  $\sim 1000$  Jahren in hohen Breiten machen deutlich, dass überall im Ozean eine Korrektur um zeitlich veränderliche Reservoiralter bei der Datierung mariner Proben er-

forderlich ist. Ohne diese ist eine korrekte Interpretation von Zeitreihen wie die Trennung von Ursachen und Wirkungen unmöglich. Bislang konnten aus Mangel an rekonstruierten Reservoiraltern fast ausschließlich konstante moderne Reservoiralter zur Korrektur herangezogen werden. Mit diesen Modellergebnissen steht jetzt eine Alternative zur Berücksichtigung dieser Variationen zu Verfügung. Die modellierten Reservoiralter sind in einer Internet-Datenbank ([www.reservoirage.uni-bremen.de](http://www.reservoirage.uni-bremen.de)) zugänglich und können für jegliche Dimension in Form von Karten, Diagrammen oder Rohdaten abgerufen werden.

Rückschlüsse auf Veränderungen in der Ozeanzirkulation der Vergangenheit auf Basis von  $^{14}\text{C}$  werden in der Regel mittels der Alterdifferenz zwischen Tiefen- und Oberflächenwasser (benthisches minus planktonisches Alter) angegeben oder durch die Berechnung von Projektionsaltern (der  $^{14}\text{C}$ -Zerfall wird in der Zeit zurückgerechnet bis der Schnittpunkt und der atmosphärischen  $\Delta^{14}\text{C}$ -Entwicklung erreicht ist) bestimmt. Zur Analyse welche Methode weniger von atmosphärischen  $^{14}\text{C}$ -Variationen beeinflusst wird, wurde das Model mit einer theoretischen Schwankung angetrieben. Dabei zeigte sich, dass Altersvariationen bei beiden Methoden nicht durch Zirkulationsänderungen begründet sein müssen, solange sie nicht einige hundert Jahre überschreiten. Sowohl die Altersdifferenzen zwischen Tiefen- und Oberflächenwasser als auch die Projektionsalter sind im Atlantik weniger empfindlich gegenüber den atmosphärischen Schwankungen als im Pazifik, vor allem weil das Tiefenwasser näher an seiner Bildungsregion ist und damit weniger Zeit seit dem Gasaustausch mit der Atmosphäre vergangen ist und ebenfalls weil Vermischungsprozesse im Ozean weniger Einfluss haben. Trotz der methodischen Differenzen, deuten beide Methoden nicht vorhandene Zirkulationsänderungen in vergleichbarer Größenordnung an. Die Projektionsaltermethode hat den Vorteil, keinen langfristigen Trend in den Projektionsaltern zu prognostizieren, wenn ein solcher in der Atmosphäre vorliegt. Die Altersdifferenzen zwischen Tiefen- und Oberflächenwasser berücksichtigen hingegen den Oberflächenozean und sind damit weniger von Reservoiraltervariationen oder Änderungen im Gasaustausch zwischen Ozean und Atmosphäre betroffen. Weiterentwicklungen an der Projektionsaltermethode, insbesondere der Austausch der atmosphärischen  $\Delta^{14}\text{C}$ -Geschichte durch marine Rekonstruktionen, haben das Potential, diese Methode weitgehend von atmosphärischen  $\Delta^{14}\text{C}$ -Variationen zu entkoppeln. Die Qualität von  $^{14}\text{C}$  als Proxy für Zirkulationsvariationen wird damit in Zukunft weiter steigen.



# Acknowledgements

The work in this thesis was supported by the Deutsche Forschungsgemeinschaft (DFG) and was carried out at the Department of Geosciences of the University of Bremen.

Many thanks to Michael Schulz and André Paul for being ideal supervisors and for offering me the opportunity to work in such an inspiring and motivating environment. I greatly appreciate their guidance, all the helpful feedbacks and their support in general that allowed me to improve my scientific skills and to realize this dissertation. Thanks to Michael especially for sharing creative ideas and for many constructive improvements on my manuscripts. Thanks to André, in particular for patiently introducing me into the world of climate modeling and always taking time for any of my questions. I also want to thank Andreas Manschke for solving quickly all computer trouble as well as Leslie Sütterlin for her great help with all administration-related topics.

I am much obliged for the opportunity to work with Jess F. Adkins, who effectively assisted me in understanding the background behind his projection-age method, also for the reviews of and suggestions to improve my manuscript, co-operations on other projects and motivating discussions.

I also thank Carlo Laj who offered his paleointensity reconstructions (GLOPIS-75) and the derived atmospheric radiocarbon production rates. Discussions with Mea Cook and Luke Skinner, which gave me new ideas and opened my eyes for some details, were very much appreciated as well. Jürg Beer created a figure of the  $^{14}\text{C}$  production-rate dependency on the intensity of the geomagnetic field. Michael Eby explained me in his extensive e-mails how to modify the UVic ESCM for my purpose. Ansley Manke gave me many hints how changes to the Live Access Server can be made. I was very glad to receive their help.

I am also grateful for the support of Marina Escala, Heather Johnstone and Stijn de Schepper who proofread this thesis. All other PhD, Postdocs and Scientists I met in Bremen as well as in the courses and conferences all around the world made this time unforgettable, especially my office-mate Iga and the entire “palmod” group. Thanks for all the little every-day help in the office and for the shortwhiling lunch and coffee breaks which made my stay in Bremen such a nice time.

Finally, I would like to express my entire gratitude to my parents, Brigitte and Dieter<sup>†</sup> Franke who supported me throughout my whole life.



# Contents

<b>1</b>	<b>Introduction</b>	<b>1</b>
1.1	Radiocarbon dating . . . . .	1
1.2	Reservoir ages . . . . .	4
1.3	Objectives and strategy . . . . .	8
<b>2</b>	<b>Radiocarbon and the UVic ESCM</b>	<b>11</b>
2.1	The UVic ESCM . . . . .	11
2.2	Radiocarbon in the model . . . . .	12
2.3	Model tuning . . . . .	13
2.3.1	Present-day ocean circulation . . . . .	14
2.3.2	Radiocarbon distribution . . . . .	15
2.3.3	Last glacial maximum ocean circulation . . . . .	16
2.4	Model validation . . . . .	18
<b>3</b>	<b>Modeling marine reservoir-age variations</b>	<b>23</b>
3.1	$^{14}\text{C}$ production-rate forcing . . . . .	23
3.1.1	Model experiment . . . . .	26
3.1.2	Results . . . . .	27
3.1.3	Discussion . . . . .	28
3.1.4	Conclusions . . . . .	29

3.2	Modeling reservoir-age variations forced by $\Delta^{14}\text{C}_{atm}$ . . . . .	31
3.2.1	Abstract . . . . .	31
3.2.2	Introduction . . . . .	31
3.2.3	Model setup . . . . .	32
3.2.4	Experiments and model forcing . . . . .	35
3.2.5	Results . . . . .	37
3.2.6	Discussion . . . . .	43
3.2.7	Conclusions . . . . .	47
3.3	Comparison of $\Delta^{14}\text{C}$ and $^{14}\text{C}$ production-rate forcings . . . . .	49
3.3.1	Results . . . . .	49
3.3.2	Discussion . . . . .	51
3.3.3	Conclusions . . . . .	55
<b>4</b>	<b>The reservoir-age database</b>	<b>57</b>
4.1	The Live Access Server . . . . .	57
4.2	Time axis . . . . .	58
4.3	Reservoir-age request . . . . .	60
<b>5</b>	<b><math>^{14}\text{C}</math> Projection-age method</b>	<b>63</b>
5.1	Abstract . . . . .	63
5.2	Introduction . . . . .	64
5.3	Model description and simulation setup . . . . .	65
5.4	Results . . . . .	68
5.4.1	Control run . . . . .	68
5.4.2	Experiment with decreasing atmospheric $\Delta^{14}\text{C}$ . . . . .	68
5.4.3	Experiment with 1000-year long atmospheric $\Delta^{14}\text{C}$ increase . . . . .	72

5.5	Discussion . . . . .	74
5.5.1	Control run . . . . .	74
5.5.2	Transient atmospheric $\Delta^{14}\text{C}$ variations . . . . .	75
5.5.3	Assessing potential sources of error . . . . .	80
5.5.4	Improved projection-age method . . . . .	81
5.6	Conclusions . . . . .	83
<b>6</b>	<b>Discussion</b>	<b>85</b>
<b>7</b>	<b>Conclusions and outlook</b>	<b>89</b>
	<b>Bibliography</b>	<b>93</b>
<b>A</b>	<b>The Live Access Server</b>	<b>109</b>
A.1	Installation and operation of the server . . . . .	109
A.2	LAS modifications . . . . .	116
A.3	Preparing model data for LAS . . . . .	117
A.4	Time-axis conversion . . . . .	118
A.5	NetCDF descriptor file . . . . .	120
A.6	Adding files to LAS . . . . .	122



# Chapter 1

## Introduction

### 1.1 Radiocarbon dating

Scientists researching phenomena of the past need techniques to accurately date events. Many dating methods take advantage of the decay of radioactive isotopes which change the ratio between stable and unstable isotopes. Depending on the geological time targeted for study, different isotopes are chosen due to their half-lives. Another important factor is the occurrence of the isotope in the sample as many radioactive isotopes are rare e.g. U/Th ratios can only be used in corals and speleothems.

Carbon is one of the most prevalent elements on Earth. All organisms fix carbon from the surrounding air or water during their life. It can be found in organic structures, e.g. plant or animal tissue but carbon also occurs in an inorganic form as in stalagmites, CO<sub>2</sub> bubbles in ice cores or calcareous plankton. In the 1940s Willard Libby and his colleagues were the first who suggested and finally proved that a radioactive carbon isotope, radiocarbon (<sup>14</sup>C), is embedded in all carbon containing matter (Bowman, 1995). Radiocarbon originates in Earth's atmosphere, where cosmic rays collide with atmospheric atoms and produce free neutrons. Such neutrons can react with the core of a nitrogen atom (<sup>14</sup>N). If one proton is exchanged with a neutron, a new <sup>14</sup>C isotope is generated. This <sup>14</sup>C isotope is radioactive and decays back to <sup>14</sup>N ( $\beta$  decay) with a half-life of  $5730 \pm 40$  years. Naturally <sup>14</sup>C only represents 1 part per trillion ( $10^{-12}$ ) of all the carbon on Earth, 98.89 % are <sup>12</sup>C and 1.11 % <sup>13</sup>C, both stable isotopes. Due to its half-life and the small amount, <sup>14</sup>C can be used to determine ages back to  $\sim 50,000$  years (50 kyr) before present (BP, defined as the

year 1950 Common Era, C.E.) with modern accelerator based mass-spectrometric (AMS) techniques. In older samples there is not enough  $^{14}\text{C}$  left to date them accurately.

After measuring the absolute concentration of  $^{14}\text{C}$  it is necessary to specify the  $^{14}\text{C}/^{12}\text{C}$  ratio to calculate how much  $^{14}\text{C}$  has decayed. Because the ratios are usually very small, it became common practice to use a delta notation, which shows the analyzed ratio compared to a standard.

$$\delta^{14}\text{C}[\text{‰}] = \left[ \frac{(^{14}\text{C}/^{12}\text{C})_{\text{Sample}}}{(^{14}\text{C}/^{12}\text{C})_{\text{Standard}}} - 1 \right] \times 1000.$$

In case of radiocarbon the international standard is:

$$(^{14}\text{C}/^{12}\text{C})_{\text{Standard}} = 1.176 \times 10^{-12}, \text{ (e.g. Keeling, 1981)}$$

During any transition of an element into another state of matter (e.g. from condensed to vapour phase) or by the assimilation of an organism, the ratio between the carbon isotopes changes, due to fractionation. Measurements have to be corrected for this effect if the ratio of different reservoirs should be comparable with each other. The fractionation corrected delta notation is indicated by a “ $\Delta$ ” instead of a “ $\delta$ ”. The ratio of the stable carbon isotopes  $^{12}\text{C}$  and  $^{13}\text{C}$  can be used to assess the extent of the fractionation and thus to calculate the corrected  $^{14}\text{C}/^{12}\text{C}$  ratio. For  $^{14}\text{C}$  this is done by normalizing the  $^{13}\text{C}$  fractionation to  $-25\text{‰}$ , the mean value of terrestrial wood (Stuiver and Polach, 1977).

$$\Delta^{14}\text{C}[\text{‰}] = \delta^{14}\text{C} - 2(\delta^{13}\text{C} + 25) \left( 1 + \frac{\delta^{14}\text{C}}{1000} \right)$$

Applying the equation for radiocarbon decay

$$\frac{d^{14}\text{C}}{dt} = -\lambda^{14}\text{C},$$

and the decay constant of

$$\lambda = \frac{1}{8267\text{yr}},$$



the  $^{14}\text{C}/^{12}\text{C}$  ratio can be used to calculate the “true”  $^{14}\text{C}$  age:

$$^{14}C_{age}[\text{yr}] = -8267 \cdot \ln \left( \frac{\Delta^{14}C}{1000} + 1 \right).$$

It is common practice to calculate the so-called conventional radiocarbon ages (CRA), applying the previously calculated half-life of Libby (1963) of 5568 years ( $\lambda = \frac{1}{8033\text{yr}}$ ), in order to avoid inconsistencies in raw  $^{14}\text{C}$  dates.

Variations in the carbon cycle, caused for example by changes in the  $^{14}\text{C}$  production rate or the release of  $^{14}\text{C}$ -free  $\text{CO}_2$  from volcanoes or changes in carbon reservoir sizes cause an offset between  $^{14}\text{C}$  ages and calendar ages. Calibration curves, based on the evolution of atmospheric  $^{14}\text{C}$ , have been developed to correct this error (Jöris and Weninger, 1998; Reimer et al., 2004; Fairbanks et al., 2005). Accurate  $^{14}\text{C}$ -age calibrations can be done for the past  $\sim 12$  kyr, because tree rings could be counted with annual resolution for this time span, parallel to  $^{14}\text{C}$  measurements. For the time period prior to the Younger Dryas ma-

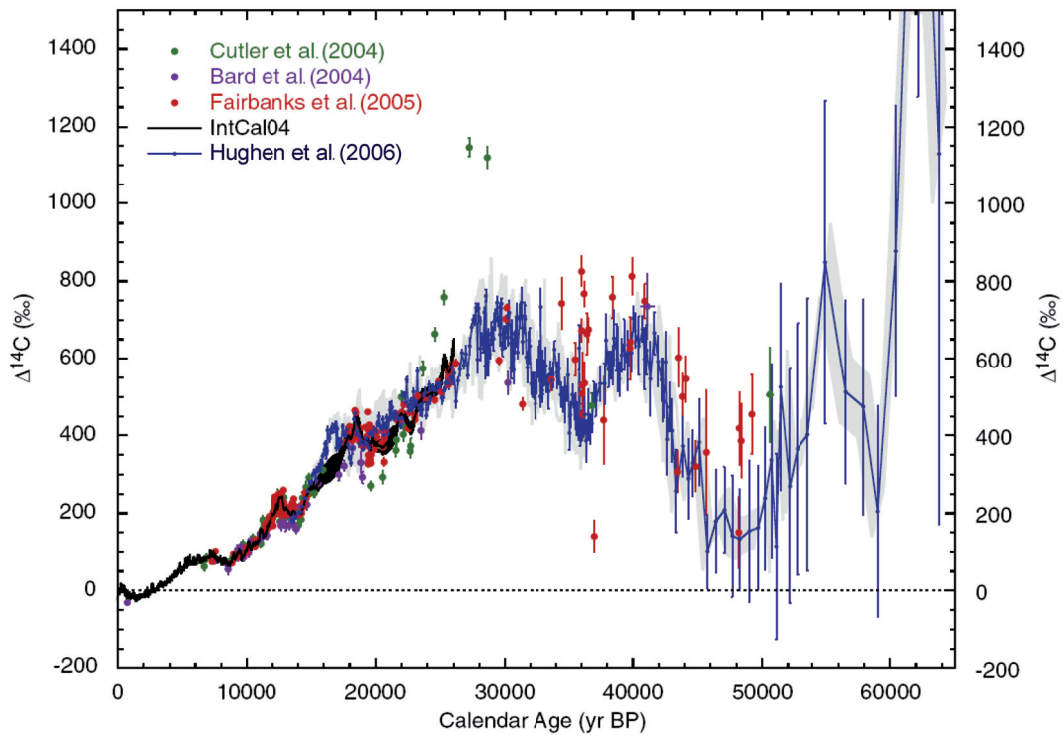


**Figure 1.1:** *Compilation of recent  $\Delta^{14}C_{atm}$  reconstructions and the  $1\sigma$  error (from Hughen et al., 2006).*

rine reconstructions of  $^{14}\text{C}$  in varved lake and ocean sediments (e.g. Kitagawa and Plicht, 2000; Hughen et al., 2006), corals (e.g. Burr et al., 1998; Bard et al., 2004; Cutler et al., 2004; Fairbanks et al., 2005) or speleothems (e.g. Beck et al., 2001) have been converted to atmospheric values. Although improvements in sample measurements over the last decade reduced the scatter of this calibration, the datasets still show differences, especially beyond 26 kyr BP (Fig. 1.1). The conversion of marine data can barely reach the accuracy of the tree ring calibration because the atmosphere-ocean gas exchange smoothes atmospheric variations and because of unknown reservoir-age variations. On-going research, for instance on pre-Holocene Kauri trees from New Zealand, might offer a more accurate atmospheric  $\Delta^{14}\text{C}$  ( $\Delta^{14}\text{C}_{\text{atm}}$ ) history up to 50 kyr BP in the future (Palmer et al., 2006; Turney et al., 2007).

Calibration curves, in which the calendar age is plotted vs.  $^{14}\text{C}$  age, do not always compare on a 1:1 basis, they even have plateaus, where the same  $^{14}\text{C}$  age potentially suggests many calendar ages. In such periods the dating accuracy is very low, which might result in misleading temporal relationships between past events. The aforementioned calibration curves of atmospheric  $^{14}\text{C}$  were developed to date terrestrial samples which took up  $\text{CO}_2$  from the atmosphere. In marine environments the correction of  $^{14}\text{C}$  ages to calendar ages becomes even more difficult due to the so-called reservoir ages.

## 1.2 Reservoir ages

In contrast to the atmosphere, which has spatially nearly homogeneous  $^{14}\text{C}$  concentrations, the oceanic  $^{14}\text{C}$  concentrations are very heterogeneously distributed, which makes the correction of  $^{14}\text{C}$  ages to calendar ages more difficult in marine samples. Radiocarbon enters into the ocean via a limited gas exchange from the atmosphere (e.g. Zhang and Cai, 2007), and there it is redistributed due to the ocean circulation while it continues decaying.

When deep, old ( $^{14}\text{C}$  depleted) waters mixes with young ( $^{14}\text{C}$  rich) surface water the  $^{14}\text{C}$  age of the surface water increases. Atmosphere-ocean gas exchange is kinetically limited and in many regions the residence time of surface waters is shorter than  $\sim 10$  years which would be needed to equilibrate the  $^{14}\text{C}$  concentrations (Broecker and Peng, 1982). For this reason the surface ocean has always a larger  $^{14}\text{C}$  age than the atmosphere. This difference

between surface oceanic and atmospheric  $^{14}\text{C}$  age, is defined as **reservoir age**. The global mean reservoir age at the pre-industrial state equals  $\sim 400$  years (Bard, 1988; Stuiver and Braziunas, 1993; Stuiver et al., 1998; Hughen et al., 2004a).

$$\text{Reservoir age [yr]} = {}^{14}\text{C age}_{\text{marine}} [\text{yr}] - {}^{14}\text{C age}_{\text{atmosphere}} [\text{yr}]$$

There are large regional deviations from the global mean especially where the gas exchange with the atmosphere is strongly reduced, for example below sea ice in the Southern Ocean. Here reservoir ages can reach up to 1300 years. On the other hand in well stratified, ice-free regions, such as the Mediterranean Sea, more gas exchange between atmosphere and surface ocean is possible and reservoir ages can be as small as 270 years (Stuiver and Braziunas, 1993).

Reservoir ages can also be influenced by seasonal and regional phenomena. A dependency on El Nino Southern Oscillation (ENSO) has been reported close to the Great Barrier Reef, the Christmas Islands, Rarotonga and the Galapagos Islands (Druffel and Griffin, 1999; Gagan et al., 2000; Guilderson et al., 2000; Schmidt et al., 2004). At these locations annual ENSO variations change the source regions of water, which are associated with different reservoir ages. A similar variation has been discussed for the Iceland Sea, which sometimes seems to be influenced by the Atlantic water mass and sometimes by the polar water mass (Eiriksson et al., 2004).

For dating of marine samples it is common practice to use an atmospheric correction curve and an estimate of the local present day (PD) reservoir age, to correct the age. This implies the assumption that reservoir ages have been temporally constant. All reconstructed reservoir ages from marine samples of 0 to 75 m water depth that were not influenced by anthropogenic  $^{14}\text{C}$  from nuclear weapon tests have been compiled in a database (Reimer and Reimer, 2001).

Another possibility is to use the calibration curve called MARINE04 that has been constructed especially for marine samples (Hughen et al., 2004a). Using a box diffusion model,  $^{14}\text{C}$  measurements of dendrochronologically dated tree-ring samples were converted to a global mean oceanic  $^{14}\text{C}$  concentration history back to 10.5 kyr BP. Before this age marine data from foraminifera in varved sediments and U/Th-dated corals, which were corrected for a site-specific but constant  $^{14}\text{C}$  reservoir age, have been used to construct the calibration curve (Hughen et al., 2004a). In both cases, this single global marine mixed-layer

calibration does not consider effects of ocean circulation, except for the advice that the user additionally has to correct for the PD local reservoir-age difference from the global mean.

Many reconstructions have proven that the assumption of constant reservoir ages is not justified for many time periods in the past. For the last deglaciation Sarnthein et al. (2007) and Sikes et al. (2000) reconstructed reservoir ages of  $\sim 2000$  years in the North Atlantic and close to New Zealand, respectively. Siani et al. (2001) found twice the PD reservoir age in the Mediterranean Sea during the same time period. Bondevik et al. (2006) reconstructed ages 400 to 600 years larger than at present around the coast of Norway for the Younger Dryas. Eiriksson et al. (2004) even found reservoir-age variations between 200 and 800 years in the Holocene period close to Iceland (Fig. 1.2). Variations at high latitudes are assumed to be larger than at low latitudes (Bard et al., 2004). These reservoir-age variations of several hundreds of years can cause uncertainties and misinterpretations, since the resolution of late Quaternary paleoclimate time series has reached decadal resolution (Sarnthein et al., 2002; Voelker, 2002).

It is difficult to increase the number of reservoir-age reconstructions because three parameters are necessary but not all of them are available anywhere and anytime:

1. The surface ocean  $^{14}\text{C}$  concentration.
2. An absolute age from an alternative dating method.
3. The atmospheric  $^{14}\text{C}$  concentration which is not derived from marine samples

Holocene reconstructions can be obtained from any sample that is dated by two independent methods, e.g. corals that can be dated with  $^{14}\text{C}$  and with U/Th to obtain the calendar age, while the atmospheric  $^{14}\text{C}$  concentration is constrained by dendrochronology. For Pleistocene reconstructions coeval volcanic ash layers in terrestrial soils, marine sediments and/or ice cores have been used at a few locations (e.g. Siani et al., 2001).

Besides reconstructions, there have also been many attempts to calculate  $^{14}\text{C}$  with numerical models, but only very few have focused on reservoir ages, such as Butzin et al. (2005), who modeled reservoir ages for the Last Glacial Maximum (LGM). Temporal variations have been modeled for the last  $\sim 10$  kyr BP, but only global mean values were simulated using box models (Stuiver and Braziunas, 1993; Hughen et al., 2004a). How past circulation

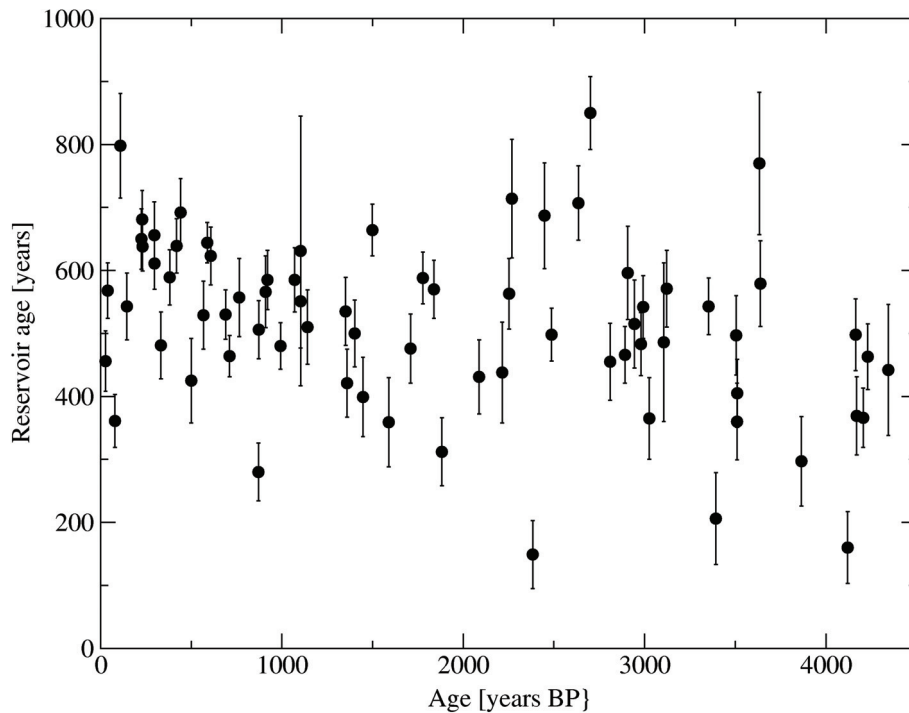


**Figure 1.2:** Reconstructed reservoir-age variations and the  $1\sigma$  error based on the data by Eiríksson et al. (2004).

changes might have contributed to the spatial reservoir-age variability has been modeled by prescribing a fresh-water perturbation to the model (Delaygue et al., 2003). At present spatially and temporally differentiated reservoir-age variations for the late Quaternary have not been modeled.

As described, reservoir ages vary in longitude, latitude and time, but they also change with depth. In this respect the term reservoir age is also used below the surface layer. The depth-dependence is important because some organisms used for  $^{14}\text{C}$  dating are distributed along a wider depth range; for instance, planktonic foraminifera live and calcify (thus incorporate  $^{14}\text{C}$ ) between 0 and 250 m depth (e.g. Carstens et al., 1997; Simstich et al., 2003). The  $^{14}\text{C}$  concentration decreases with depth (Fig. 1.3). On average, there is a  $\sim 150$  year age difference in the global mean values of the upper 250 m of the water column. This depth trend is independent of the fact that global mean reservoir age of  $\sim 560$  years in the GLODAP dataset (Key et al., 2004) exceeds the previously estimated value of  $\sim 400$  years (e.g. Stuiver et al., 1998).

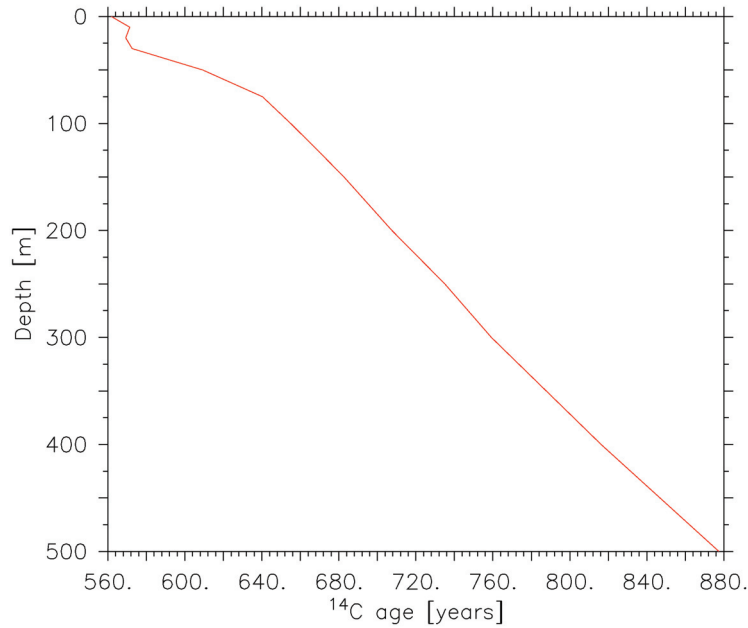


**Figure 1.3:** Global mean  $^{14}\text{C}$  age depth profile for the upper 500 m of the ocean; based on the GLODAP database (Key et al., 2004).

Although all the aforementioned uncertainties influence marine  $^{14}\text{C}$  dating, mostly a constant, PD surface marine reservoir age of a location next to the area of interest is used. Constant reservoir ages have even been applied if a main purpose of the measurements was the production of an  $^{14}\text{C}$  calibration curve (e.g. Hughen et al., 2006) because an alternative is lacking..

### 1.3 Objectives and strategy

The objective of the present work is to model spatially differentiated reservoir-age variations during the late Quaternary to provide reservoir-age estimates for  $^{14}\text{C}$  dating of marine samples. The results should resolve uncertainties caused by previous assumptions and answer the following questions:

- When and why did marine reservoir-age variations occur during the past 45 kyr and which amplitude did they have?

- How did the spatial reservoir-age distribution change during this period and is the assumption valid that reservoir-ages variations mainly occur in high latitudes and can be neglected in low latitudes?
- Can the model results be used to improve the reservoir-age correction when marine samples are dated using the  $^{14}\text{C}$  method?

In order to answer these questions, radiocarbon is included as a tracer in a three dimensional climate model (Chap. 2) which is forced by two different datasets of atmospheric  $^{14}\text{C}$  reconstructions, the  $^{14}\text{C}$  production rate and  $\Delta^{14}\text{C}_{atm}$  (Chap. 3). The calculated reservoir ages are accessible via the internet (Chap. 4).

Differences between the LGM and the PD Atlantic meridional overturning circulation are still ambiguous (e.g. Weber et al., 2007). Radiocarbon is a proxy which has the potential to assess this and other ocean-circulation changes. The  $^{14}\text{C}$ -age difference between surface and deep ocean, which is reconstructed from benthic and planktonic foraminifera (B-P method) is widely used to draw conclusions on past ocean-circulation changes, but it is influenced by variations of atmospheric  $\Delta^{14}\text{C}$ . An alternative technique to avoid this source of error is the so-called projection age method (Adkins and Boyle, 1997). Potential uncertainties in this method, such as the estimate of a constant reservoir age, leave questions open:

- Which of the two methods, B-P or projection-age, is more robust regarding  $\Delta^{14}\text{C}_{atm}$  variations?
- Is the reliability of these methods dependent on regional differences?
- Do specific temporal  $\Delta^{14}\text{C}_{atm}$  variations influence methods differently?
- Is there potential to improve the methods?

The second objective of this study is to answer these questions by analyzing the uncertainties of these two methods at different locations and for different scenarios of atmospheric  $^{14}\text{C}$  changes (Chap. 5).





# Chapter 2

## Radiocarbon and the UVic ESCM

### 2.1 The UVic ESCM

The basis for the reservoir age and the projection-age calculations is the University of Victoria Earth System Climate Model (UVic ESCM; Weaver et al., 2001) in version 2.7, update level 3. In the employed configuration it is a global model that consists of an ocean, atmosphere and sea-ice model. The Modular Ocean Model (version 2) is a three-dimensional primitive equation ocean general circulation model (Pacanowski, 1995). This model is coupled to a two-dimensional energy-moisture balance model of the atmosphere with a formulation of the vertically-integrated thermodynamic energy (Fanning and Weaver, 1996). One major simplification is that prognostic equations for momentum conservation are replaced by specified wind data. The second simplification is the parametrization of atmospheric heat and moisture transport by diffusion, although moisture is also advected by the prescribed wind field.

The dynamic-thermodynamic sea-ice model (Bitz et al., 2001) includes a simple zero layer formulation of Semtner (1976) and lateral growth and melt parametrization (Hibler, 1979). Ice dynamics use the elastic viscous plastic rheology (Hunke and Dukowicz, 1997).

The horizontal resolution of all components in this model of intermediate complexity is  $3.6^\circ$  in longitude and  $1.8^\circ$  in latitude. The ocean has 19 levels of irregular depth, which increase from 50m at the surface to 500 m at the deepest levels (Weaver et al., 2001). Variations in solar insolation over a year at the top of the atmosphere drive the model.

The wind stress at the ocean surface is prescribed from a monthly climatology, the so-called NCEP/NCAR 40-year reanalysis project. This reanalysis consists of land surface, ship, weather balloon, aircraft and satellite data of the years 1957–1996 C.E., which have been merged to a long-term mean (Kalnay et al., 1996).

In the Arctic Ocean the convergence of longitudes limits length of the calculation time steps of the ocean model. To avoid this problem the option of a rotated grid has been chosen. This rotates the North Pole to (40°W, 78°N) a location in Greenland (Pacanowski, 1995) and enabled us to extend the time step for the tracer and density calculations from 108,000 to 216,000 seconds to increase the calculation speed of the model.

Sub-gridscale mixing in the ocean is included following the Gent and McWilliams (1990) parametrization for mixing associated with mesoscale eddies, in which diffusion occurs along and across isopycnals. Along-isopycnal and isopycnal-thickness diffusivity are both set to  $0.4 \times 10^7 \text{ cm}^2 \text{ s}^{-1}$ . A vertical diffusion profile, increasing from  $\kappa_v = 0.3 \text{ cm}^2 \text{ s}^{-1}$  in the thermocline to  $1.3 \text{ cm}^2 \text{ s}^{-1}$  in the deep ocean (Bryan and Lewis, 1979) is used as a background diffusion.

## 2.2 Radiocarbon in the model

Radiocarbon is added to the ocean part of the model as a passive tracer, following the guidelines of the Ocean Carbon Modeling Intercomparison Project (OCMIP-2, Orr et al., 2000):

$$F_{air-sea} = K_w ({}^{14}C_{sat} - {}^{14}C_{surf})$$

with

$${}^{14}C_{sat} = \alpha C \cdot pCO_2 \cdot (P/P_0) \cdot R_{std},$$

$$K_w = (1 - f_{ice}) (a \cdot u^2) (Sc/660)^{\frac{1}{2}},$$

and

$$Sc = 2073.1 - 125.62 \cdot SST + 3.63 \cdot SST^2 - 0.043 \cdot SST^3$$

where  $F_{air-sea}$  is the flux of  ${}^{14}\text{C}$  from the atmosphere to the ocean,  $K_w$  is  $\text{CO}_2$  gas transfer velocity,  ${}^{14}C_{sat}$  and  ${}^{14}C_{surf}$  are the  ${}^{14}\text{C}$  concentrations in the atmosphere and surface ocean respectively,  $\alpha C$  is the carbon solubility for water-vapor saturated air  $\left[ \frac{\text{mol}}{\text{m}^3 \cdot \mu\text{atm}} \right]$  (Weiss

and Price, 1980),  $pCO_2$  is partial pressure of  $CO_2$  in the atmosphere,  $P$  is local sea-level air pressure,  $P_0$  is the mean sea-level air pressure of 1013,25 hPa,  $R_{std}$  is the standard ratio of  $^{14}C/^{12}C$  (Sect. 1.1),  $f_{ice}$  is the modeled fraction of sea-ice coverage (height >1 cm),  $a$  is a constant to adjust the global flux,  $u^2$  is the windspeed  $[\frac{m}{s}]$  and  $Sc$  is sea-surface temperature (SST[K]) dependent Schmidt number.

Gas exchange with the atmosphere depends on the atmosphere-to-surface ocean  $^{14}C$  gradient, windspeed, sea-ice cover and sea-surface temperature. In the ocean the radiocarbon tracer is transported via diffusion and advection like all the other tracers (e.g. temperature, salinity). A sink is added to account for the radiocarbon decay with the true half-life of 5730 years.

The atmosphere is treated as one global well-mixed box with respect to  $^{14}C$  because the atmospheric mixing time between both hemispheres for  $^{14}C$  is of the order of a few years and splitting the atmosphere into troposphere and stratosphere has only an influence on variations shorter than 20 years (Siegenthaler et al., 1980). Both periods are much shorter than the timescale of interest. The terrestrial biosphere has an effect if forcing variations are on timescales from a few decades to some centuries (Siegenthaler et al., 1980). As this work concentrates on even longer variations, the terrestrial biosphere is also not taken into account, which makes the model more efficient.

Generally such a calculation needs all carbon isotopes ( $^{12}C$ ,  $^{13}C$  and  $^{14}C$ ) and biota to account for all fractionation processes. For efficiency reasons, approximate equations have been developed and validated that allow to model an abiotic ocean with one tracer for  $^{14}C$ , if the fractionation corrected  $\Delta^{14}C$  is of interest and not  $\delta^{14}C$  (Orr, 2002).

## 2.3 Model tuning

The model has to be tuned to fit the observed ocean circulation and the  $^{14}C$  distribution at present and in the past.

### 2.3.1 Present-day ocean circulation

In a first step, the modeled and the observed ocean circulation are compared. The model is adjusted to PD parameters such as solar radiation and land-ice distribution of the year 1950 C.E., monthly mean wind from reanalysis data of the 20<sup>th</sup> century (Kalnay et al., 1996) and a pre-industrial atmospheric CO<sub>2</sub> content of 280 parts per million of volume (ppmv). At these settings, the North Atlantic Deep Water (NADW) formation and the export of North Atlantic water at 30°S agree with observations of Talley et al. (2003), but there is hardly any Antarctic Bottom Water (AABW) formation is simulated.

Modification of the oceanic diffusivity coefficients are tested to increase AABW production in the model. Originally, Gent-McWilliams (GM) diffusivity and the “along isoneutral diffusion coefficient” are both set to  $4 \cdot 10^6$ , in agreement with Griffies (2004), who pointed out that there are no strong arguments to use different diffusivities. In contrast, Pacanowski and Griffies (2000) reported that most researchers would suggest to set the GM diffusivity between  $\frac{1}{2}$  and  $\frac{1}{4}$  of the isoneutral diffusion coefficient. This suggested reduction of the GM diffusivity does not cause a significant AABW-formation increase when introduced to the model. The creation of the suggested ratio by increasing the isoneutral diffusion coefficient does not have a strong impact up to tripling the value. Four times higher isoneutral diffusion finally leads to a small AABW-production increase without severe changes in NADW, but still far below the observed strength (Talley et al., 2003). On the other hand, a GM-diffusivity increase causes a reduction of NADW formation. As all these modifications of the diffusivity did not lead to an significant AABW formation, both diffusion coefficients are set to the standard value of  $4 \cdot 10^6$ .

One major simplification of the atmosphere part of the UVic ESCM is the parametrization of atmospheric moisture transport by diffusion (Weaver et al., 2001). The scaling of this diffusion is another option to influence deep-water formation (Saenko and Weaver, 2003). A reduction of the latitudinal moisture transport leads to less fresh-water input in high latitudes and to increased deep-water formation, whereas an increased moisture transport leads to more fresh-water input in high latitudes and reduced deep-water formation. In the standard configuration of the UVic ESCM this relationship is used by prescribing more moisture diffusion in the southern than in the northern hemisphere to form enough deep water in the North Atlantic to match observations. A reduction of the southern hemisphere moisture diffusion to 60% of the original value results in a maximum meridional

overturning in the North Atlantic of 20 Sverdrup ( $Sv = \frac{10^6 m^3}{s}$ ) and an export of NADW at 30°S of 14 Sv. AABW formation increases to 4 Sv and reaches up to 30°N in the deep Atlantic (Fig. 2.1a). These water mass movements agree well with observations (Talley et al., 2003; Lynch-Stieglitz et al., 2007). The circumpolar current reaches 90-100 Sv, which is also in agreement with measurements (Orsi et al., 1995).

### 2.3.2 Radiocarbon distribution

After tuning the general water mass circulation, the carbon cycle including  $^{14}C$  needs to be validated, with the ocean-atmosphere  $CO_2$  flux as a key parameter to adjust. According to Orr et al. (2000), the global mean  $CO_2$  flux from the atmosphere to the ocean should be set to the value of  $0.061 \frac{mol}{m^2 yr \mu atm}$  (Broecker et al., 1986) based on the Geochemical Ocean Section Study (GEOSECS) that was obtained between 1972 and 1977. In the appropriately adjusted model this  $CO_2$  flux appears to be overestimated, when it is compared to the results of the GLObal Ocean Data Analysis Project (GLODAP, Key et al., 2004); a data set, compiled from high-quality oceanographic measurements from the 1980s and 1990s, mainly from the World Ocean Circulation Experiment (WOCE), the Joint Global Ocean Flux Study (JGOFS) and the Ocean Atmosphere Carbon Exchange Study (OACES), which increased the number of  $^{14}C$  measurements by about one order of magnitude.

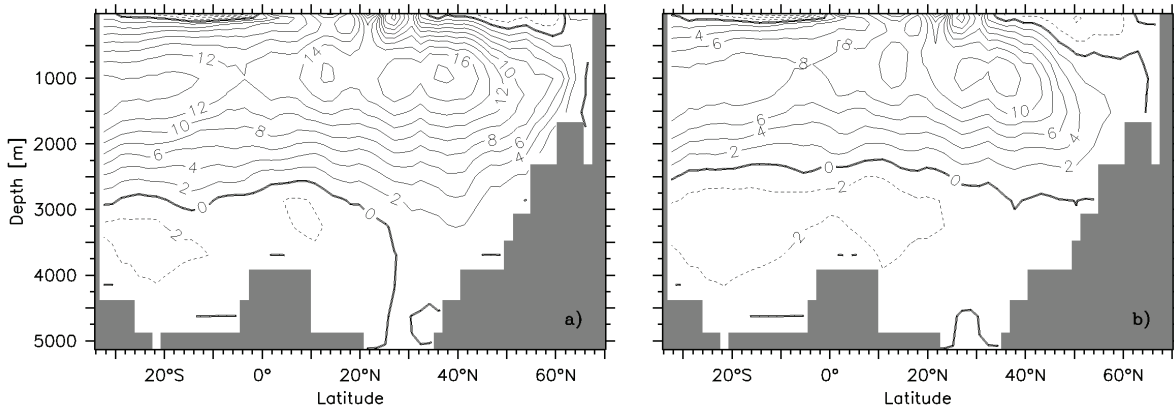


**Figure 2.1:** a) Atlantic Ocean meridional streamfunction [Sv] of the model simulation with PD forcing and in b) with LGM forcing. With LGM-like boundary conditions the AMOC is reduced by approximately one third and shallower such that AABW can reach further north at the bottom of the ocean.

The best match of the UVic ESCM results and the GLODAP dataset can be reached by reducing the global gas transfer velocity (piston velocity) to 80% of the previously calculated value. Sweeney et al. (2007) reported a similar overestimation of the gas-exchange rate and give two possible factors as an explanation. First, the estimates for bomb  $^{14}\text{C}$  in the ocean based on the GEOSECS data (Broecker et al., 1985; Broecker et al., 1995) were too large, as proven by Heshaimer et al. (1994); Joos (1994); Key et al. (2004); Peacock (2004); Naegler et al. (2006). Second, air-sea gas exchange parameterizations neglected spatial and temporal variations in the  $^{14}\text{C}$  concentration difference between atmosphere and ocean (Sweeney et al., 2007). Consequently, the model is adjusted to match the results of GLODAP (Key et al., 2004) applying the discussed piston velocity reduction. After 10 kyr of calculation time  $^{14}\text{C}$  is in equilibrium in the model ocean. This equilibrium state is used to initialize the time transient simulation of atmospheric  $^{14}\text{C}$  variations.

### 2.3.3 Last glacial maximum ocean circulation

Model experiments suggest that the strength of the Atlantic meridional overturning circulation (AMOC) influences marine reservoir ages (e.g. Delaygue et al., 2003; Muscheler et al., 2004; Butzin et al., 2005). In order to analyze the influence of circulation changes on the reservoir-age distribution, an experiment with LGM-like boundary conditions is set up because the ocean-circulation pattern is assumed to have differed from PD one during this period (e.g. Lynch-Stieglitz et al., 2007). To achieve a different circulation state of the ocean, the solar forcing of 21 kyr BP is prescribed to account for the difference in incoming radiation and their influence on the temperature and ice distribution. The atmospheric  $\text{CO}_2$  concentration is reduced to 200 ppmv (Raynaud et al., 1993). Land-ice reconstructions for 21 kyr BP are used to account for the increased albedo. The included continental ice-sheet reconstruction ICE-4G (Peltier, 1994) in the UVic ESCM is replaced by the revised reconstruction ICE-5G (v1.2) (Peltier, 2004).

The  $\text{CO}_2$  reduction, LGM solar forcing and LGM land-ice distribution lead to a 30% reduced Atlantic deep-water formation and a weaker and shallower overturning cell (Fig. 2.1b), which is consistent with reconstructions of the nutrient distribution, the Protactinium/Thorium isotopes ratio and most other circulation tracers (Lynch-Stieglitz et al., 2007; McManus et al., 2004; Schmittner et al., 2002; Meissner et al., 2003; Marchal et al., 2000).

It is widely accepted and supported by reconstructions of African dust and pollen movements (e.g. Stuut et al., 2002; Shi et al., 2001) that the wind speed increased during glacials when the temperature gradient between low and high latitudes increased (Marshall et al., 1993; Wunsch, 2003b). To account for the difference in the wind, momentum flux/wind stress, surface wind speed and mean wind for the advective moisture transport for PD in the UVic ESCM are substituted by estimates for the LGM from the high resolution Community Climate System Model (CCSM, Version 3) included in the Paleo Model Intercomparison Project (PMIP2, Braconnot et al., 2007).

In the CCSM the increased wind stress causes a stronger Gulf Stream, although this does not result in increased sea-surface temperatures (SST) in the northern North Atlantic, probably because more sea ice is transported with the East Greenland and Labrador Current. At the subtropical front the melting ice leads to a cooling and freshening of the sea surface and to a decrease in salinity, which finally led to a reduction of deep-water formation by  $\sim 30\%$ . The increased wind strengthens the Gulf Stream in the coarse resolution UVic ESCM as well, but no sea-ice is transported to the deep-water formation sites of the North Atlantic. Consequently, the salinities in the northern North Atlantic increase, which causes more deep-water formation with this model compared to the CCSM.

As reservoir ages should be simulated in agreement with reconstructions that mostly indicate less North Atlantic deep-water formation, another strategy is followed. The UVic ESCM is tuned to NCEP/NCAR wind fields, which differ from the calculated CCSM wind for PD. Hence, the model is forced by the original NCEP/NCAR wind field for PD to which anomalies between PD and LGM wind taken from the CCSM are added. This wind stress increases the NADW formation for the LGM once more to a value similar to the PD simulation.

The dynamical wind feedback approximation (Weaver et al., 2001) is an alternative option in the UVic ESCM to consider changes in the wind fields. Its application also leads to an intensification of the wind under LGM boundary conditions, but again forces increased deep-water production.

Another possible mechanism to reduce NADW formation is an artificial freshwater perturbation in the northern North Atlantic. It can be argued that this is necessary because the resolution of the model prohibits a transport of sea ice from the Arctic Ocean along the coast of Greenland, which finally melts close to the deep-water formation areas as seen

in the CCSM and comparable to the “freshwater bypass” of Ganopolski and Rahmstorf (2001). If this is introduced into the model and the artificial freshwater input is compensated in the Arctic Ocean, the desired deep-water formation decline cannot be observed, only if the freshwater input is compensated globally, which would be difficult to argue for.

In summary for the LGM-like experiment, the glacial reduction in NADW-formation rate and shallowing of the AMOC cell cannot be obtained with stronger glacial wind stress and advective moisture transport in this version of the UVic ESCM. The PD wind is assumed to have in general only little implications on the results, as the consequences of increased wind are contradictory. Stronger wind cause more sea-ice in the CCSM model, which reduces atmosphere-ocean gas exchange, whereas stronger wind itself increase the gas exchange (Sect. 2.2). The combination of LGM insolation, atmospheric  $\text{CO}_2$  content and land-ice topography causes a reduction of the maximal meridional overturning in the Atlantic from 21 to 14 Sv (Fig. 3.5). Accordingly, to analyse the influence of a significantly differing ocean circulation which is in agreement with reconstructions (e.g. Lynch-Stieglitz et al., 2007), the PD wind fields will be prescribed for the LGM-like simulation. The same forcing strategy was used by Meissner et al. (2003) in their LGM simulation with an earlier version of the UVic ESCM.

## 2.4 Model validation

In addition to model the PD  $^{14}\text{C}$  distribution in the ocean, it is necessary to enable the model to calculate oceanic  $^{14}\text{C}$  variations as a response to atmospheric  $^{14}\text{C}$  production-rate changes. In the following chapters, the term “production rate” refers to the atmospheric  $^{14}\text{C}$  production rate.

The model is forced with the  $^{14}\text{C}$  production rate in an experiment, where the well observed artificial  $^{14}\text{C}$  production during nuclear-weapon tests in the second half of the 20<sup>th</sup> century is simulated. Estimates for the nuclear-bomb strength are taken from Hesshaimer et al. (1994). The  $\Delta^{14}\text{C}_{\text{atm}}$  measurements used for comparison are spatially weighted global means based on regional data of Hua and Barbetti (2004). The model is initialized with the PD equilibrium state described in the last section, which is corrected for the Suess-effect, the reduction of the  $^{14}\text{C}/^{12}\text{C}$  ratio, caused by the anthropogenic burning of  $^{14}\text{C}$  free fossil fuels since  $\sim 1850$  C.E.



The UVic ESCM is able to predict temporal  $\Delta^{14}\text{C}$  variations in the atmosphere which are in agreement with observations (Fig. 2.2). Leads and lags in the curves of modeled and observed  $\Delta^{14}\text{C}$  do not exceed a year. Responsible for these little differences is probably the model's atmosphere configuration, which is not divided into stratosphere and troposphere.  $^{14}\text{C}$  is mainly generated in the stratosphere while measurements are from the troposphere. Another reason might be the averaging of observational data to a global mean, because most nuclear weapons  $^{14}\text{C}$  was injected into the northern hemisphere (Hua and Barbetti, 2004) and it took about one year until injected  $^{14}\text{C}$  became measurable in the other hemisphere.

In the model, the  $^{14}\text{C}_{\text{atm}}$  decrease after the atmospheric peak of the year 1965 is slightly less steep than the observations suggest. The absence of a terrestrial biosphere in the model is most likely responsible for this behaviour, because it buffers the  $\Delta^{14}\text{C}_{\text{atm}}$  changes on timescales of decades to a few centuries. Nevertheless, the atmospheric response at interannual to decadal timescale appears realistic, implying that the model ocean takes up the same amount of  $^{14}\text{C}$  as real ocean.

There are two ways to check the distribution of bomb radiocarbon within the ocean. The first one is a comparison of  $\Delta^{14}\text{C}$  snapshots at many locations, for instance between the ocean  $\Delta^{14}\text{C}$  from the GLODAP dataset and the model. The comparison is hampered

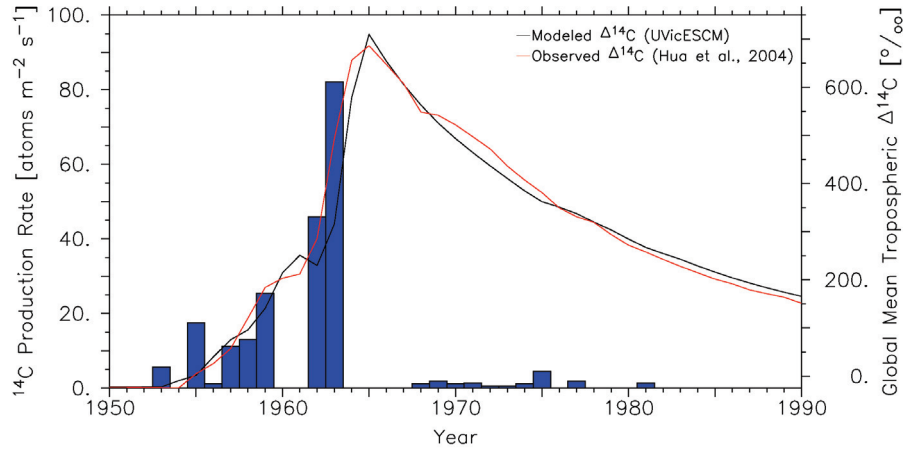


**Figure 2.2:** Observed and modeled  $\Delta^{14}\text{C}_{\text{atm}}$  due to nuclear weapon tests. The blue bars represent the  $^{14}\text{C}$  production which was caused by nuclear weapon tests (Hesshaimer et al., 1994). The red curve shows the observed and globally averaged  $\Delta^{14}\text{C}_{\text{atm}}$  (Hua and Barbetti, 2004), while the black curve is the response of the model to the production-rate forcing.

because measurements were taken over a 20 year period, i.e. the rapidly varying  $^{14}\text{C}$  signal is not resolved globally. Thus, only single measurements could be compared, which makes this approach very unreliable. The second strategy is a comparison of the model's temporal response with a time series of reconstructed  $\Delta^{14}\text{C}$ . Following this strategy the reconstructions of surface-ocean corals (Druffel, 1989) and deep-sea corals (Eltgroth et al., in prep.) are compared. At the surface the model slightly underestimates the  $\Delta^{14}\text{C}$  measured in corals (Fig. 2.3 and Fig. 2.4a). One reason could be that most models, including the UVic ESCM, are too diffusive. Thus, the radiocarbon is transported into the subsurface ocean faster than in reality. An alternative explanation is that the well-stratified region, where the corals were actually sampled, is not resolved by the too coarse resolution of the model or that this region is spatially shifted by a few degrees. This is supported by the fact that at a location  $10^\circ$  south and  $4^\circ$  east the observed  $\Delta^{14}\text{C}$  is also predicted by the model (Fig. 2.3).

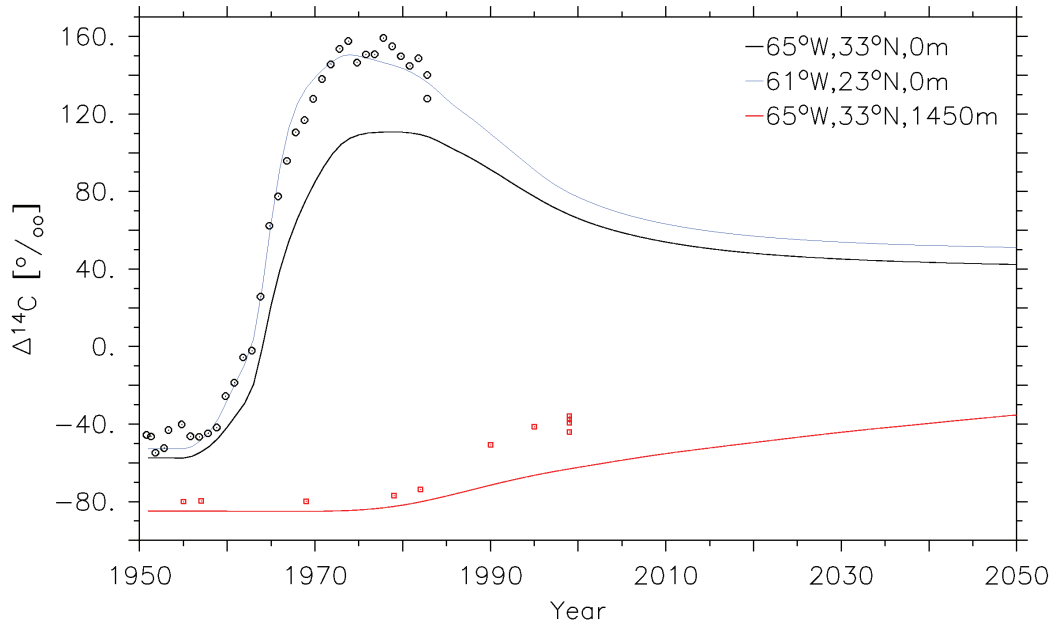


**Figure 2.3:** Modeled and reconstructed  $\Delta^{14}\text{C}$  close to Bermuda ( $33^\circ\text{N}$ ,  $65^\circ\text{W}$ ). The red squares are the deep-sea coral measurements at 1450m depth (Eltgroth et al., in prep.), the black circles are shallow-water coral measurements (Druffel, 1989), the black and red curves are model results at the same location and depth and the blue curve is the model output at the ocean surface at  $23^\circ\text{N}$ ,  $61^\circ\text{W}$ .

The bomb  $^{14}\text{C}$  reaches the depth of 1450 m, where the deep-sea coral grew, mainly by horizontal advection in the simulated time period. This can be seen in the  $\Delta^{14}\text{C}$  plume that follows the Atlantic deep western boundary current (Fig. 2.4b). In regions not influenced by the NADW no bomb  $^{14}\text{C}$  signal is simulated at this depth suggesting that vertical diffusion does not carry the  $^{14}\text{C}$  to this depth. The  $^{14}\text{C}$  increase at depth in the model is seen at the same time as in the observations ( $\sim 1980$  C.E.), due to the advection, but it increases from 1980 to 2000 C.E. only by  $\sim 15\text{‰}$  instead of the  $\sim 40\text{‰}$  measured in the coral data. Advection in the model seems to be too slow, given that the observed  $^{14}\text{C}$  concentrations are finally reached with a time lag of  $\sim 20$  years. Despite the time lag, the concentrations in the bomb experiment seem to peak and level close to observation. The aforementioned good agreement in the equilibrium run might be the result of a slightly overestimated diffusion and an underestimated advection in the model.

Natural variation of atmospheric  $^{14}\text{C}$  in the late Quaternary occurred on longer timescales and with a smaller amplitude than in the extreme case of nuclear weapon tests. In our model setup the response of oceanic  $^{14}\text{C}$  at centennial and millennial timescales is assumed to work better than on a decadal timescale due to a smaller influence of the terrestrial

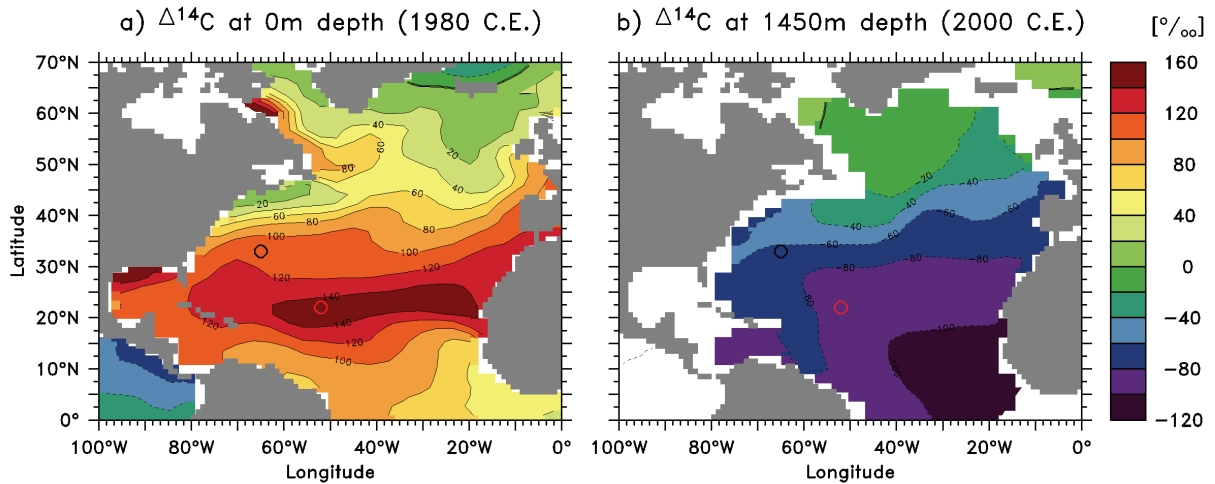


**Figure 2.4:** Modeled  $\Delta^{14}\text{C}$  in the North Atlantic. a) At the surface ocean for the year 1980 C.E. when the  $^{14}\text{C}$  concentration reached its maximum. b) At 1450 m depth for the year 2000 C.E. when most recent deep coral measurements were made. The coral sampling location near Bermuda (33° N, 65° W) is indicated by the black circle; the model location where maximum observed  $\Delta^{14}\text{C}$  concentrations were observed in the surface ocean (23° N, 61° W) is marked with a red circle.

biosphere and also because the ocean is closer to equilibrium, without the strong gradients between surface and deep ocean  $\Delta^{14}\text{C}$ . Overall, the model ocean is believed to take up nearly the same amount of  $^{14}\text{C}$  as the real ocean and it is expected that the model responses realistically to the  $\Delta^{14}\text{C}_{atm}$  variations of the time period between 50 kyr BP and 1950 C.E.

# Chapter 3

## Variations of marine reservoir ages modeled for the last 45,000 years

In this chapter the marine radiocarbon reservoir-age variations are modeled, which occurred due to atmospheric  $^{14}\text{C}$  concentration changes. In principle two possibilities exist to model marine  $^{14}\text{C}$  variations. One approach is to analyze the oceanic  $^{14}\text{C}$  changes due to the model forcing with the atmospheric  $^{14}\text{C}$  production rate. Alternatively, reconstructed atmospheric  $\Delta^{14}\text{C}$  can be used. Both forcings are applied and will be compared. The  $^{14}\text{C}$  production-rate forcing is discussed first in Sect. 3.1, the  $\Delta^{14}\text{C}_{atm}$  forcing follows in Sect. 3.2.

### 3.1 $^{14}\text{C}$ production-rate forcing

Cosmic nuclide production in the Earth's atmosphere on millennial timescale and the strength of the geomagnetic field are highly correlated (Laj et al., 1996). The weaker the geomagnetic field, the more cosmic rays enter the atmosphere and the more  $^{14}\text{C}$  is produced, as it can be seen for instance during the geomagnetic low  $\sim 40$  kyr BP, the so-called “Laschamp event” (Beer et al., 2002).

High-resolution datasets of geomagnetic intensity have been reconstructed for the entire period of radiocarbon dating (Valet et al., 2005; Laj et al., 2004). The GLObal PaleoIntensity Stack (GLOPIS-75, Laj et al., 2004) which is based on a stack of 24 marine

paleointensity records, is used here. All cores in GLOPIS-75 are tuned to the Greenland Ice Sheet Project 2 (GISP2) age model (Meese et al., 1994). For dating purposes it should be noted here that the GISP2 age might not be exactly a true calendar age in all cases. Modified age scales have been published, namely SFCP04 (Shackleton et al., 2004) and GICC05 (Andersen et al., 2006) and they deviate by up to 2000 years at specific time periods.

The  $^{14}\text{C}$  production rate can be calculated from the geomagnetic intensity and ranges between 0.75 and 2.2 times the PD value of  $2.02 \frac{\text{atoms}}{\text{cm}^2 \text{ s}}$  during the past 75 kyr (Fig. 3.1 Masarik and Beer, 1999).

Solar radiation has low energy (1–1000 MeV) and consists mainly of photons (98%), which are insufficient to produce relevant amounts of  $^{14}\text{C}$  isotopes (Masarik and Beer, 1999). Instead, magnetic fields of the solar wind act as a shield and protect the Earth from cosmic rays additionally to the geomagnetic field (Bard et al., 1997). Solar radiation variations occur with a decadal to centennial periodicity such as the 11 yr Schwalbe cycle, the 80 yr Gleissberg cycle and the 205 yr DeVries cycle.

Solar-activity variations reconstructed for the past 9300 years indicate a constant radiation in the long-term mean during the Holocene, although the variations in this period exceeded

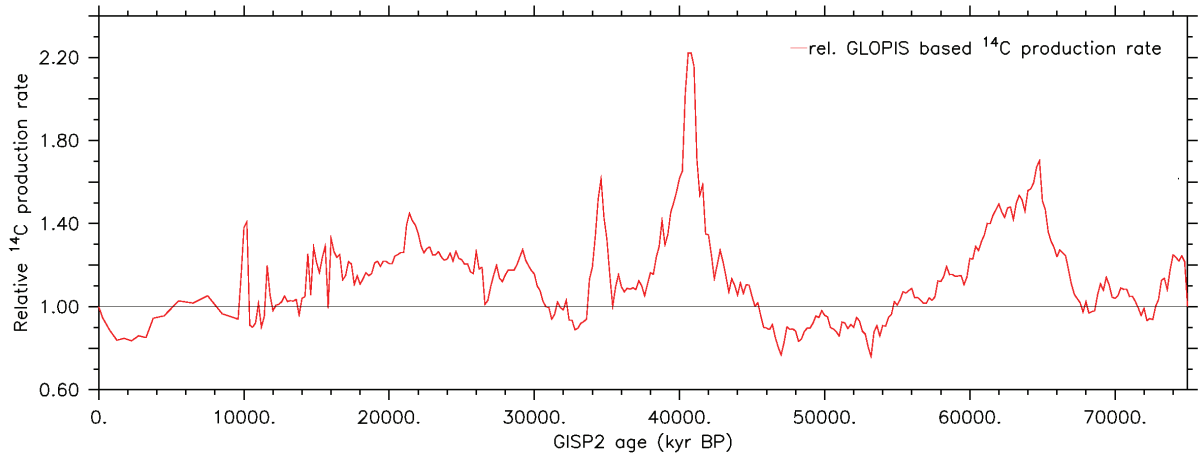


**Figure 3.1:** Relative  $^{14}\text{C}$  production rate ( $1=\text{PD}$ ) based on the geomagnetic intensity (GLOPIS-75 Laj et al., 2004) and the conversion into a  $^{14}\text{C}$  production rate following Masarik and Beer (1999).

the instrumentally measured ones of the last 50 years (Vonmoos et al., 2006). For the last glacial and the deglaciation the solar activity is also believed to have been constant in the long-term mean, but especially when the geomagnetic field is weak, low solar activity can cause a non-linear  $^{14}\text{C}$  production-rate increase (Fig. 3.2). As solar variations have only been reconstructed for the Holocene, a mean solar activity of 550 MeV is assumed in the calculation of the  $^{14}\text{C}$  production-rate from GLOPIS-75.

Galactic cosmic rays consist mainly (87%) of protons. These heavy particles have enough energy (10 MeV–100 GeV) to cause the generation of  $^{14}\text{C}$  in the atmosphere (Masarik and Beer, 1999). The cosmic ray flux is believed to be very stable as long as there is no supernova explosion within 33 light-years to Earth. The influence of the only reported supernova in this time period, called Geminig, on the Antarctic  $^{10}\text{Be}$  record has been analyzed (Ellis et al., 1996). They could not be completely exclude possible links but claim such links would be very unlikely. Hence, the approach to calculate the  $^{14}\text{C}$  production rate from the geomagnetic intensity alone seems to be reasonable.

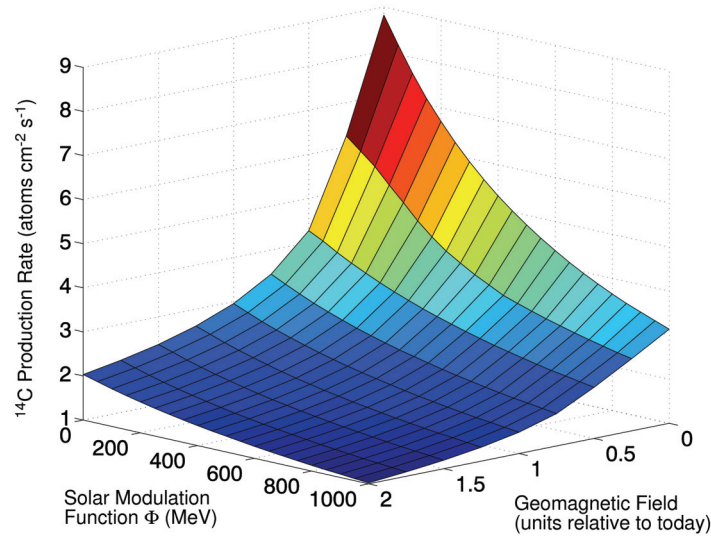


**Figure 3.2:** Dependence of the  $^{14}\text{C}$  production rate on the solar activity and on the intensity of the geomagnetic field (J. Beer, unpubl., pers. comm.).

### 3.1.1 Model experiment

In order to model the reservoir-age variations in the ocean, the equilibrium  $^{14}\text{C}$  production rate is diagnosed from the control experiment. It is equal to the steady-state net flux of  $^{14}\text{C}$  from the atmosphere into the ocean and amounts to  $1.18 \frac{\text{atoms}}{\text{cm}^2 \text{ s}}$ . This production rate lies below the global mean of  $2.02 \frac{\text{atoms}}{\text{cm}^2 \text{ s}}$  (Masarik and Beer, 1999) because the model does not include all carbon reservoirs on Earth, it is limited to the abiotic ocean. The production rate is similar to previous modeling results of  $1.31 \frac{\text{atoms}}{\text{cm}^2 \text{ s}}$  (Meissner et al., 2003), considering that the previously overestimated carbon exchange flux was still assumed there (Sect. 2.3). The equilibrium production rate is then multiplied by the relative production rate, in which PD is equal to one.

The response time of the climate system to production-rate variations is long due to the decay time of  $^{14}\text{C}$  (Siegenthaler et al., 1980). An impulse of 5x the PD production rate over a period of 10 years is simulated using the UVic ESCM (Fig. 3.3). 5,000 years after the impulse,  $\Delta^{14}\text{C}_{\text{atm}}$  is still significantly above the initial level of 0‰. Hence, the model

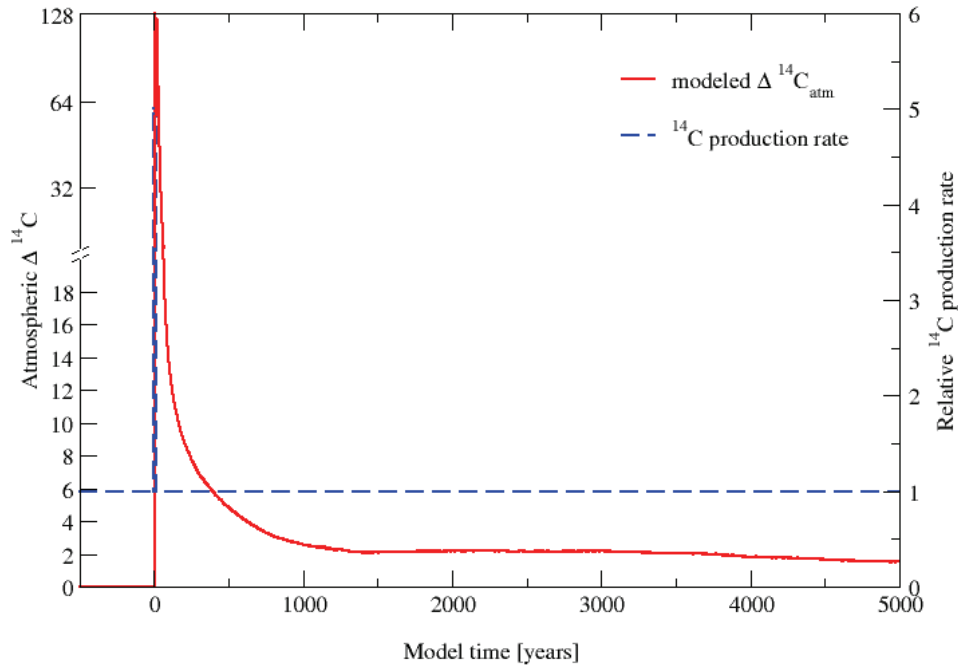


**Figure 3.3:** Modeled  $\Delta^{14}\text{C}_{\text{atm}}$  response of the UVic ESCM to a  $^{14}\text{C}$  production-rate increase of 5x the PD value over 10 years.



is forced by the  $^{14}\text{C}$  production rate starting at 75 kyr BP with the intention to produce reliable data from 45 kyr BP onwards.

The influence of carbon-cycle changes, such as reduced oceanic deep-water production that are tested by applying LGM-like boundary conditions, will be discussed later (Sect. 3.2).

### 3.1.2 Results

The modeled atmospheric  $\Delta^{14}\text{C}$  history agrees with reconstructions for the Holocene. Larger differences of up to  $\sim 75\text{‰}$  occur in the Younger Dryas. During the deglaciation the curves depart more and more from each other. Finally for the last glacial the model predicts up to  $300\text{‰}$   $\Delta^{14}\text{C}_{\text{atm}}$  instead of the reconstructed values of more than twice that number (Fig. 3.4).

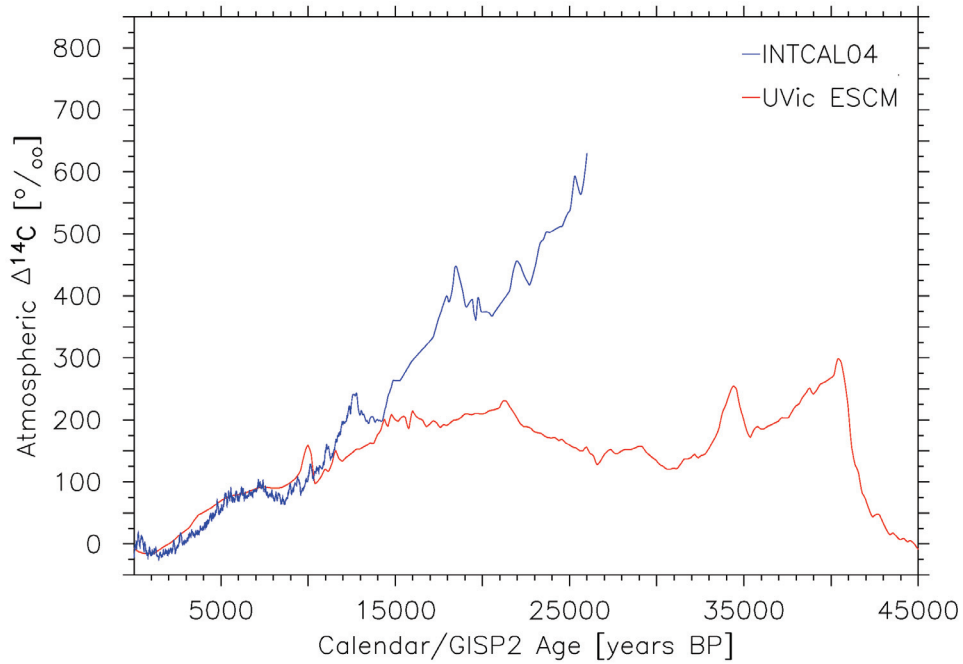


**Figure 3.4:** Reconstructed (INTCAL04) and modeled (UVic ESCM)  $\Delta^{14}\text{C}_{\text{atm}}$  variation in the atmosphere during the past 45 kyr. The data agrees in the Holocene but modeled  $\Delta^{14}\text{C}_{\text{atm}}$  only reaches  $\sim 300\text{‰}$  in the last glacial while reconstructions show values twice as high.

### 3.1.3 Discussion

So far, box models have not been able to reproduce reconstructed  $\Delta^{14}\text{C}_{atm}$  values for the last glacial exceeding 500‰ using geomagnetic data based  $^{14}\text{C}$  production rates alone (Beck et al., 2001; Laj et al., 2000, 2002; Hughen et al., 2004b). More complex box models simulated even lower  $\Delta^{14}\text{C}$  in the atmosphere than simple box models as shown in the comparison between a 17-box and 4-box model (Laj et al., 2002). The UVic ESCM confirms the results of the simple box models and only reaches up to  $\sim 300\text{‰}$   $\Delta^{14}\text{C}_{atm}$ .

Simulated  $\Delta^{14}\text{C}_{atm}$  shows less high frequency variations, probably because of the missing solar variations or the temporal resolution of the forcing data, but in general the agreement of model results and reconstructions for the Holocene (Reimer et al., 2004) is good. It suggests that the model works well with the  $^{14}\text{C}$  production rate forcing. The larger offset in the Pleistocene is supposed to be a result of changes in carbon-reservoir sizes (e.g. Marchitto et al., 2007). Major changes in the carbon cycle are necessary, to reach the observed  $\Delta^{14}\text{C}_{atm}$  values. One possible explanation would be a glacial deep-ocean carbon reservoir that is well isolated from the atmosphere and stores radiocarbon-depleted waters (Marchitto et al., 2007). Recent model simulations forced by LGM boundary conditions or freshwater discharges into the northern North Atlantic only suggest an increase of  $\Delta^{14}\text{C}_{atm}$  by  $\sim 70\text{‰}$  due to reduced deep-water formation (Marchal et al., 1999; Delaygue et al., 2003). How the reconstructed level of  $\Delta^{14}\text{C}_{atm}$  in the last glacial can be explained remains an open question.

The  $^{14}\text{C}$  production rate can alternatively be reconstructed from  $^{10}\text{Be}$  data (Muscheler et al., 2004). This stable nuclide is built in the atmosphere in a way comparable to  $^{14}\text{C}$  but  $^{10}\text{Be}$  quickly attaches to aerosols and is removed from the atmosphere within 1–2 years by precipitation. Records of the  $^{10}\text{Be}$  production rate are preserved in the ice sheets of Greenland and Antarctica. Their advantage is that they are not influenced by changes in the complex carbon cycle. The disadvantages are a climatic component from ice accumulation that needs to be removed and a possible dipolar component. Radiocarbon production rates derived from  $^{10}\text{Be}$  agree well with the geomagnetic-based ones in the Holocene, but show differences of up to 20% in the Pleistocene (Muscheler et al., 2005). This seems to be caused, at least partly, by dating inaccuracy. Box model experiments forced with a  $^{10}\text{Be}$  based  $^{14}\text{C}$  production rate also calculate only up to  $300\text{‰}$   $\Delta^{14}\text{C}_{atm}$  for the last glacial (Muscheler et al., 2004). Hence, it is very likely that changes in the carbon

cycle are responsible for the underestimation of  $\Delta^{14}\text{C}_{atm}$  and the  $^{10}\text{Be}$  approach has no advantage over the GLOPIS-75 based production-rate estimate.

However, production-rate changes remain a major cause for  $\Delta^{14}\text{C}_{atm}$  variations. Superimposed on them will be carbon cycle changes which produce additional variability. Reservoir-age variations simulated with the production-rate forcing will be discussed in Sect. 3.3.

### 3.1.4 Conclusions

If the model is forced by the the production-rate, which causes only a part of the reconstructed  $\Delta^{14}\text{C}_{atm}$  variations, maybe the amplitude and certainly the frequency of reservoir-age variations is underestimated. To exclude this source of uncertainty, the GLOPIS-75 based production-rate forcing is rejected in favour of the for the  $\Delta^{14}\text{C}_{atm}$  forcing, which is presented in the next chapter. However, a comparison of both methods will follow in Section 3.3.



## 3.2 Modeling variations of marine reservoir ages during the last 45,000 years

Jörg Franke<sup>1</sup>, André Paul<sup>1,2</sup> and Michael Schulz<sup>1,2</sup>

<sup>1</sup>Department of Geosciences, University of Bremen, Germany.

<sup>2</sup>MARUM - Center for Marine Environmental Sciences, Bremen, Germany.

Accepted for online review in “Climate of the Past”.

### 3.2.1 Abstract

When dating marine samples with  $^{14}C$ , the reservoir-age effect is usually assumed to be constant, although atmospheric  $^{14}C$  production-rate and ocean-circulation changes cause temporal and spatial reservoir-age variations. These lead to dating errors, which can limit the interpretation of cause and effect in paleoclimate data. We used a global ocean circulation model forced by transient atmospheric  $\Delta^{14}C$  variations to calculate reservoir ages for the last 45,000 years for a present day-like and a last glacial maximum-like ocean circulation. A  $\sim 30\%$  reduced Atlantic meridional overturning circulation leads to increased reservoir ages by up to  $\sim 500$  years in high latitudes. Temporal variations are proportional to the absolute value of the reservoir age; regions with large reservoir age also show large variation. Temporal variations range between  $\sim 300$  years in parts of the subtropics and  $\sim 1000$  years in the Southern Ocean. For tropical regions, which are generally assumed to have nearly stable reservoir ages, the model suggests variations of several hundred years.

### 3.2.2 Introduction

Late Quaternary sediments are frequently dated by means of their radiocarbon ( $^{14}C$ ) content.  $^{14}C$  originates in the atmosphere, where cosmic rays generate free neutrons that can react with nitrogen to produce  $^{14}C$  (Masarik and Beer, 1999). After exchange with the other carbon reservoirs most of the radiocarbon is stored in the ocean, where it decays. The finite exchange flux between the reservoirs causes the radiocarbon age of marine sample always to be higher than that of a coeval atmospheric sample (Stuiver and Braziunas,

1993). This age difference is known as “reservoir age” and has to be taken into account in the conversion from radiocarbon age to calendar age.

Present-day (PD) reservoir ages average globally at about 400 years (e.g. Hughen et al., 2004a). Regional reservoir-age anomalies for the time before nuclear weapon tests are mainly known from sites along coastlines (Reimer and Reimer, 2001). Accordingly  $^{14}\text{C}$  dates are mostly corrected for a local but constant PD reservoir age instead of the global mean. Temporal reservoir-age variations in contrast are hardly considered when marine samples are dated, because they could only be scarcely reconstructed for limited time periods and at a few locations (Southon et al., 1990; Bard et al., 1994; Austin et al., 1995; Burr et al., 1998; Sikes et al., 2000; Siani et al., 2001; Waelbroeck et al., 2001; Keigwin and Schlegel, 2002; Kovanen and Easterbrook, 2002; Eiriksson et al., 2004; Bard and Rostek, 2005; Fairbanks et al., 2005; Bondevik et al., 2006; Schimmelmann et al., 2006; Hughen et al., 2006). These reconstructions suggest that reservoir-age changes of several hundred years occurred in the late Quaternary. Errors of such a magnitude might lead to misinterpretations of cause and effect in paleoclimate time series.

Changes in the geomagnetic field, which directly influences the atmospheric  $^{14}\text{C}$  production rate are considered to be the main reason for reservoir-age variations (Laj et al., 1996). Model experiments suggest that the strength of the Atlantic meridional overturning circulation (AMOC) also significantly influences atmospheric  $\Delta^{14}\text{C}$  ( $\Delta^{14}\text{C}_{atm}$ ) and subsequently reservoir ages, too (Delaygue et al., 2003; Muscheler et al., 2004). Running a spatially explicit ocean circulation model forced by changes in atmospheric  $^{14}\text{C}$  offers the opportunity to assess a major part of reservoirs-age variability, that is induced by  $^{14}\text{C}$  production-rate changes.

### 3.2.3 Model setup

The reservoir-age calculation was done using a global model of intermediate complexity, the University of Victoria Earth System Climate Model (UVic ESCM) in version 2.7 (Weaver et al., 2001). It consists of a three-dimensional ocean general circulation model (Modular Ocean Model, version 2, Pacanowski (1995)), coupled to a two-dimensional energy-moisture balance model of the atmosphere (Fanning and Weaver, 1996) and a dynamic-thermodynamic sea-ice model (Bitz et al., 2001). The horizontal resolution of all compo-

nents is  $3.6^\circ$  in longitude and  $1.8^\circ$  in latitude. The ocean has 19 levels of irregular depth, increasing from 50 m at the surface to 500 m at the deepest levels (Weaver et al., 2001). It is driven by variations in solar insolation over a year at the top of the atmosphere. The wind stress at the ocean surface is prescribed from a monthly climatology (Kalnay et al., 1996). We used the option of a rotated grid to avoid convergence of the meridians towards the North Pole. Sub-gridscale mixing is included following the Gent and McWilliams (1990) parametrization for mixing associated with mesoscale eddies. Vertical diffusion is increasing from  $0.3 \text{ cm}^2 \text{ s}^{-1}$  in the thermocline to  $1.3 \text{ cm}^2 \text{ s}^{-1}$  in the deep ocean (Bryan and Lewis, 1979).

To evaluate if the model simulates PD ocean circulation right, a control experiment was set up, using PD parameters as a solar radiation and land-ice distribution of the year 1950 Common Era (C.E.), monthly mean winds from reanalysis data of the 20<sup>th</sup> century (Kalnay et al., 1996) and a pre-industrial atmospheric  $\text{CO}_2$  content of 280 ppmv. In this configuration the model shows a maximum North Atlantic overturning of 20 Sv and a southward export of North Atlantic Deep Water (NADW) at  $30^\circ \text{ S}$  of 14 Sv (Fig. 3.5a). Antarctic Bottom Water (AABW) reaches up to  $30^\circ \text{ N}$ . All these values agree fairly well with calculations based on observational data (Talley et al., 2003). Finally a circumpolar current of around 100 Sv is comparable with observations compiled by Orsi et al. (1995).

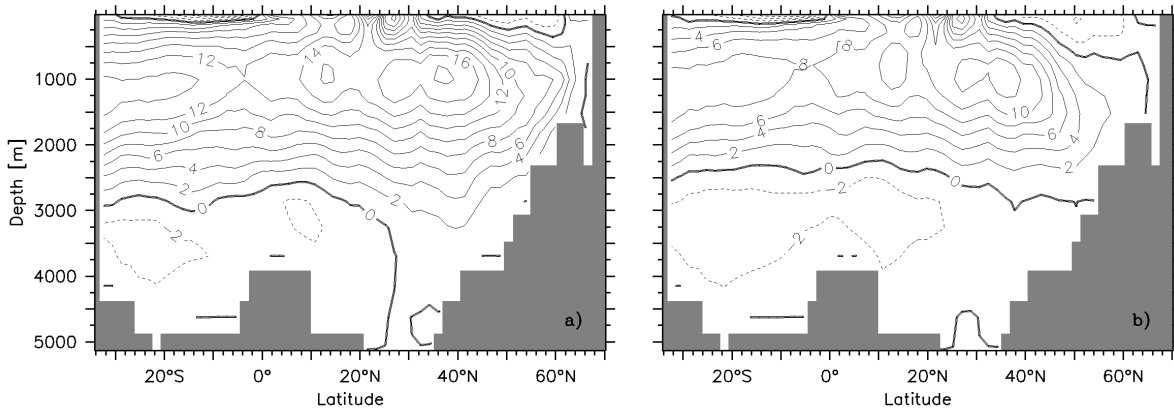


**Figure 3.5:** a) Atlantic Ocean meridional streamfunction [Sv] of the model simulation with PD forcing and in b) with LGM forcing. With LGM-like boundary conditions the AMOC is reduced by approximately one third and shallower such that AABW can reach further north at the bottom of the ocean.

In the ocean part of the model, radiocarbon was included as a passive tracer following the guidelines of the Ocean Carbon Modeling Intercomparison Project (OCMIP-2, Orr et al., 2000):

$$F_{air-sea} = K_w ({}^{14}C_{sat} - {}^{14}C_{surf})$$

with

$${}^{14}C_{sat} = \alpha C \cdot pCO_2 \cdot (P/P_0) \cdot R_{std},$$

$$K_w = (1 - f_{ice}) (a \cdot u^2) (Sc/660)^{\frac{1}{2}},$$

and

$$Sc = 2073.1 - 125.62 \cdot SST + 3.63 \cdot SST^2 - 0.043 \cdot SST^3$$

where  $F_{air-sea}$  is the flux of  ${}^{14}C$  from the atmosphere to the ocean,  $K_w$  is  $CO_2$  gas transfer velocity,  ${}^{14}C_{sat}$  and  ${}^{14}C_{surf}$  are the  ${}^{14}C$  concentrations in the atmosphere and surface ocean respectively,  $\alpha C$  is the carbon solubility for water-vapor saturated air  $\left[ \frac{mol}{m^3 \cdot \mu atm} \right]$ ,  $pCO_2$  is partial pressure of  $CO_2$  in the atmosphere,  $P$  is local sea level air pressure,  $P_0$  is the mean sea-level air pressure of 1013,25 hPa,  $R_{std}$  is the normalized ratio of  ${}^{14}C/{}^{12}C$ ,  $f_{ice}$  is the modeled fraction of sea-ice coverage (height > 1 cm),  $a$  is a constant to adjust the global flux,  $u^2$  is windspeed in  $\left[ \frac{m}{s} \right]$  and  $Sc$  is sea-surface temperature (SST[K]) dependent Schmidt number.

The gas exchange with the atmosphere depends on the atmosphere to surface-ocean  ${}^{14}C$  gradient, windspeed, sea-ice cover and sea-surface temperature. In the ocean the radiocarbon tracer is transported via diffusion and advection like all the other tracers (e.g. temperature, salinity). A sink has been added to account for the radiocarbon decay with the true half-life of 5730 years.

The atmosphere is treated as one well-mixed box with respect to  ${}^{14}C$  because the atmospheric mixing time for  ${}^{14}C$  is on the order of some years, which is much shorter than the timescale of interest. Splitting the atmosphere into troposphere and stratosphere is not necessary, because this would only have an influence on variations at timescales shorter than 20 years (Siegenthaler et al., 1980). The terrestrial biosphere has an effect if forcing variations are on timescales from a few decades to some centuries (Siegenthaler et al., 1980). As we concentrated on even longer variations, the terrestrial biosphere is also not taken into account, to make the model more efficient.



### 3.2.4 Experiments and model forcing

#### Control run and model evaluation

In the control experiment  $\Delta^{14}C_{atm}$  is held constant at 0‰, which is defined as the pre-industrial  $^{14}C / ^{12}C$ -ratio of the year 1950 C.E. To evaluate the model, we compared the oceanic  $^{14}C$  distribution with the global carbon climatology (Key et al., 2004). This dataset includes the radiocarbon measurements at the time of sampling as well as calculated estimates for natural background and bomb-produced  $^{14}C$ . The gas exchange of the model was reduced by  $\sim 20\%$  compared to OCMIP recommendations (Orr et al., 2000), which is in agreement with recent calculations (Sweeney et al., 2007).

#### Atmospheric $\Delta^{14}C$ variations in a bomb $^{14}C$ experiment

Since our main interest is to simulate temporal reservoirs-age variations, the model response to  $^{14}C$  production-rate changes needs to be verified. This can be achieved in an experiment, which is forced by the well-known radiocarbon production due to the test of nuclear weapons during the second half of the 20<sup>th</sup> century. Estimates for the nuclear bomb strength were taken from Hesshaimer et al. (1994). The model was started from the the Suess-effect corrected PD equilibrium state described in the last section and was run for 40 years. The  $\Delta^{14}C_{atm}$  measurements used for comparison are spatially weighted global means based on regional data of Hua and Barbetti (2004).

#### Influence of different ocean circulation states

To study the influence of different ocean circulation states on the  $^{14}C$  distribution, the model was forced by LGM-like boundary conditions: insolation and land ice distribution were set to 21 kyr BP and the atmospheric  $CO_2$  concentration was reduced to 200 ppmv (Tab. 1). Using these parameters the Atlantic Meridional Overturning Circulation (AMOC) became weaker by roughly one third and it became shallower, such that AABW could penetrate further northward in the deep Atlantic (Fig. 3.5). This weaker and shallower overturning cell is consistent with the glacial nutrient distribution, Pa/Th and most other circulation tracers (Schmittner et al., 2002; Meissner et al., 2003; McManus et al., 2004;

Lynch-Stieglitz et al., 2007). To assess the influence of this different circulation on the reservoir ages we used the PD wind fields following Meissner et al. (2003).

### Atmospheric $\Delta^{14}\text{C}$ forcing

To study past changes in oceanic  $^{14}\text{C}$  content, we prescribed the temporal  $\Delta^{14}\text{C}$  evolution based on reconstructions. For this we used the INTCAL04 dataset (Reimer et al., 2004) up to 25 kyr BP. Between 25 and 50 kyr BP we used the reconstructions by Fairbanks et al. (2005) and Hughen et al. (2006) because they could remove some of the uncertainties that caused disagreement in earlier reconstructions (e.g. Voelker et al., 1998; Bard et al., 1998; Goslar et al., 2000; Kitagawa and Plicht, 2000; Beck et al., 2001; Hughen et al., 2004b). The  $\Delta^{14}\text{C}_{\text{atm}}$  model-forcing dataset was constructed by interpolating an error weighted spline (Williams and Kelley, 2007) through all the reconstructed data (Fig. 3.6).

The long time period needed to reach an equilibrium between atmospheric and oceanic  $^{14}\text{C}$  concentrations requires a model spin-up time of several thousand years (Siegenthaler et al., 1980). As  $\Delta^{14}\text{C}_{\text{atm}}$  reconstructions do not exist prior to 50 kyr BP, we spun up the model from 75 kyr BP using a  $^{14}\text{C}$  production rate, calculated after (after Masarik and Beer, 1999) from a global paleomagnetic intensity stack (GLOPIS, Laj et al., 2004). At 50 kyr BP the forcing was switched to the interpolated  $\Delta^{14}\text{C}$  spline. This change of forcings adds some uncertainty to the initial oceanic  $^{14}\text{C}$  level, beside the possibility of a different ocean circulation state.

**Table 3.1:** *Forcing of different reservoir-age simulations*

	PD	LGM
Insolation	1950 C.E.	21 kyr BP
Land ice	1950 C.E.	21 kyr BP
		ICE-5G <sup>a</sup>
CO <sub>2</sub>	280 ppmv	200 ppmv
Windfields	recent NCEP/NCAR	recent NCEP/NCAR
	Reanalysis <sup>b</sup>	Reanalysis <sup>b</sup>

<sup>a</sup>Peltier (2004)

<sup>b</sup>Kalnay et al. (1996)

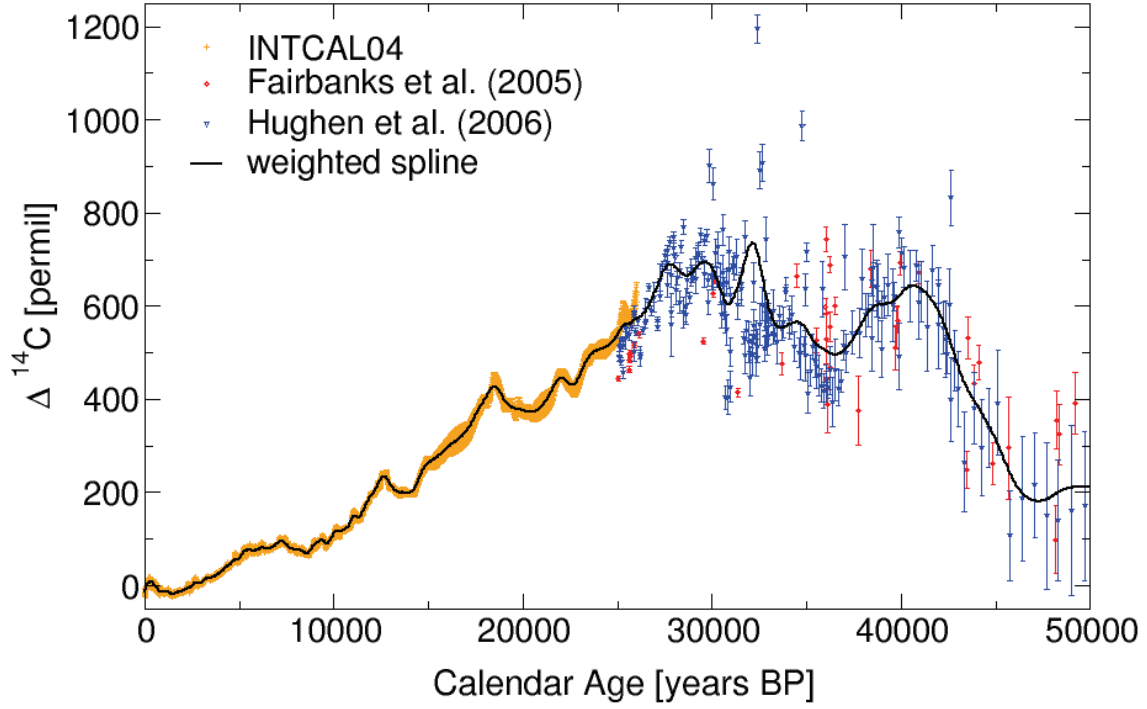


**Figure 3.6:** *INTCAL04  $\Delta^{14}C_{atm}$  and its  $1\sigma$  error estimate (Reimer et al., 2004, orange), coral data (Fairbanks et al., 2005, red) and Cariaco Basin sediment data (Hughen et al., 2006, blue). A spline function (black) was interpolated through the data weighted by the  $1\sigma$  error of all the reconstructed values.*

### 3.2.5 Results

#### Control run and bomb experiment

The modeled  $\Delta^{14}C$  distribution agrees with the pre-nuclear GLObal Ocean Data Analysis Project (GLODAP, Key et al., 2004) estimate mostly within  $\pm 10\text{‰}$  (Fig. 3.7). Only in upwelling areas the model predicts too negative  $\Delta^{14}C$  values. In the equilibrium experiment the global mean surface ocean  $\Delta^{14}C$  is  $-61\text{‰}$  close to the bomb  $^{14}C$  corrected GLODAP estimate of  $-65\text{‰}$ .

Forced by the  $^{14}C$  production-rate changes due to nuclear weapon testing, the model is able to predict temporal  $\Delta^{14}C_{atm}$  variations in good agreement with observations (Fig. 3.8).

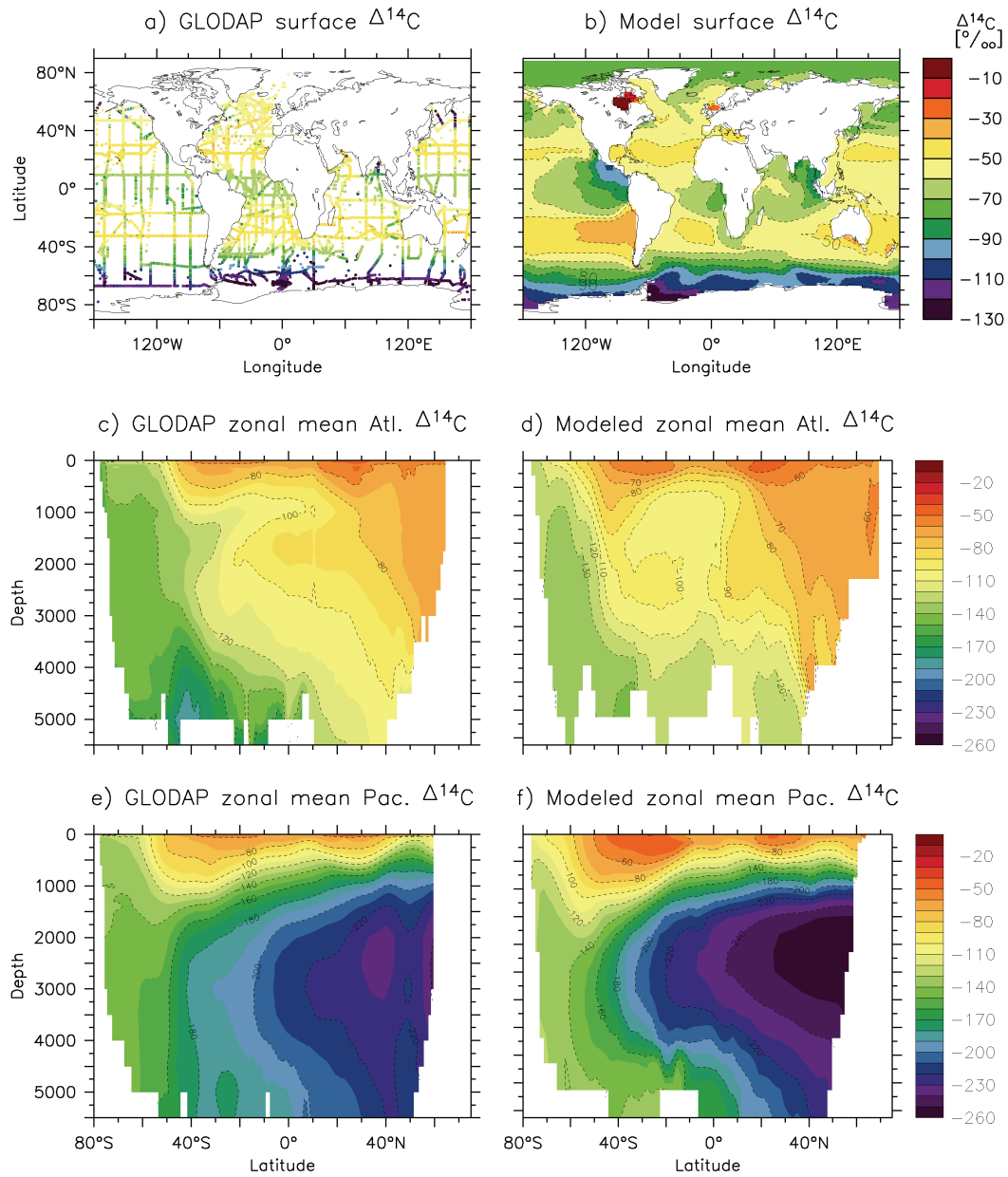


**Figure 3.7:** Model/data comparison: a) Surface ocean background  $\Delta^{14}\text{C}$  (measured value minus calculated bomb fraction) from the GLODAP carbon data compilation (Key et al., 2004). b) Surface ocean  $\Delta^{14}\text{C}$  in the UVic ESCM PD control run with constant  $\Delta^{14}\text{C} = 0\text{‰}$ . c) Interpolated zonal mean Atlantic  $\Delta^{14}\text{C}$  depth profile from the GLODAP dataset; d) modeled Atlantic; e) GLODAP zonal mean profile for the Pacific and f) the modeled Pacific.

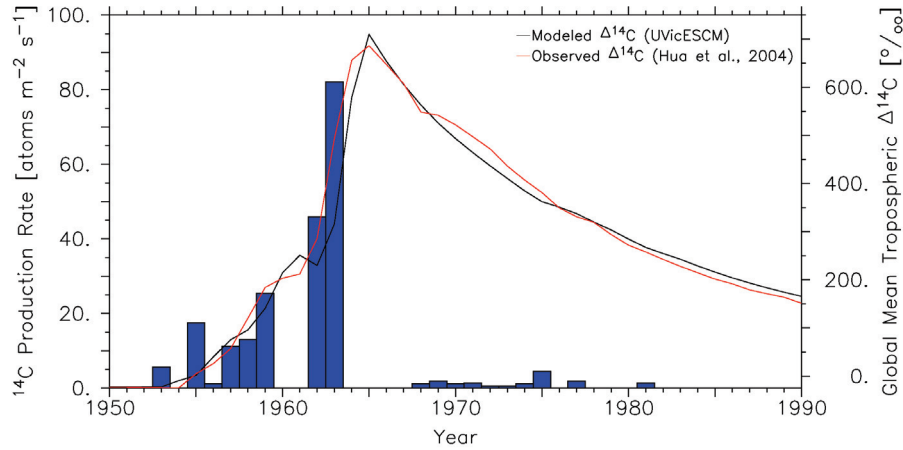


**Figure 3.8:** Observed and modeled  $\Delta^{14}C_{atm}$  in response to nuclear weapon tests. The blue bars represent the  $^{14}C$  production which was caused by nuclear weapon tests (Hesshaimer et al., 1994). The red curve shows the observed and globally averaged  $\Delta^{14}C_{atm}$  (Hua and Barbetti, 2004), while the black curve is the response of the model to the production-rate forcing.

### Time slices

We ran two simulations for the different circulation states of the ocean, both with the same time-dependent  $\Delta^{14}C_{atm}$  forcing. Three time slices of this simulation are plotted in Fig. 3.9. One for the “Laschamp” event 41 kyr BP, which is important in relationship to the radiocarbon history because the geomagnetic field collapsed almost completely, resulting in a high  $^{14}C$  production (Laj et al., 2000). The LGM was chosen as a second time slice because of its paleoclimatic importance, and finally PD for comparison.

The PD reservoir ages, reached at the end of the transient experiment for a modern ocean circulation (Fig. 3.9a), are slightly smaller than in the equilibrium experiment because  $\Delta^{14}C_{atm}$  had a decreasing trend over the last centuries before this snapshot was taken. Nevertheless the reservoir-age estimates agree with present day observation of 400–500 years in the northern North Atlantic, 300–400 years in the subtropical oceans and up to 1000 years close to Antarctica. For an AMOC reduced by  $\sim 30\%$ , the model suggests larger reservoir ages than with a modern circulation, reaching values of 400–1400 years (Fig. 3.9b).

The LGM falls in a time period of decreasing  $\Delta^{14}C_{atm}$ . If the circulation would have been like today the model predicts reservoir ages to be below present day values, ranging from 200 years in the subtropical ocean up to 900 years close to Antarctica (Fig. 3.9c).

The reduced AMOC leads to increased reservoir ages reaching from 300 to 1200 years (Fig. 3.9d).

During the Laschamp event and its high  $^{14}\text{C}$  production rate the model suggests globally increased reservoir ages of 400–1400 years if the circulation would have been like today (Fig. 3.9e) and of 500–1800 years in case of the reduced AMOC (Fig. 3.9f).

### Temporal reservoir-age variations

The amplitude of the modeled temporal reservoir-age variations over the last 45 kyr varies spatially. This is shown for the simulation with PD boundary conditions (Fig. 3.10). The amplitude of temporal variations with LGM boundary conditions is very similar, only shifted to higher reservoir-ages. The smallest changes occur in some subtropical regions but even there the range of temporal variation is rarely below 300 years. In the northern North Atlantic these variation are larger and reach up to 700 years. Largest reservoir-age variations were modeled for the Southern Ocean where they could exceed 1000 years. Reservoir-age increases coincide with  $\Delta^{14}\text{C}_{atm}$  increases and the other way around.

### Reduced Atlantic meridional overturning circulation

To analyze the influence of circulation change induced reservoir-age differences separated from the temporal  $\Delta^{14}\text{C}_{atm}$  variations, the control experiment with the PD circulation is compared with an experiment of constant  $\Delta^{14}\text{C}_{atm}$  and LGM-like boundary conditions. In the LGM-like simulation  $\Delta^{14}\text{C}_{atm}$  was set to zero instead of the reconstructed LGM value to allow for a direct comparison of the results.

In an equilibrium state, reservoir-ages increase globally with the LGM forcing (Fig. 3.11). The circulation induced differences stay small at around 100–200 years in the subtropical and tropical regions with strong stratification and slow diffusive mixing of deep water into the surface. Largest anomalies of 250–400 years could be seen in the Southern Ocean and even up to 500 years in the Arctic Ocean, probably a result of increased sea-ice coverage that limits the gas exchange.

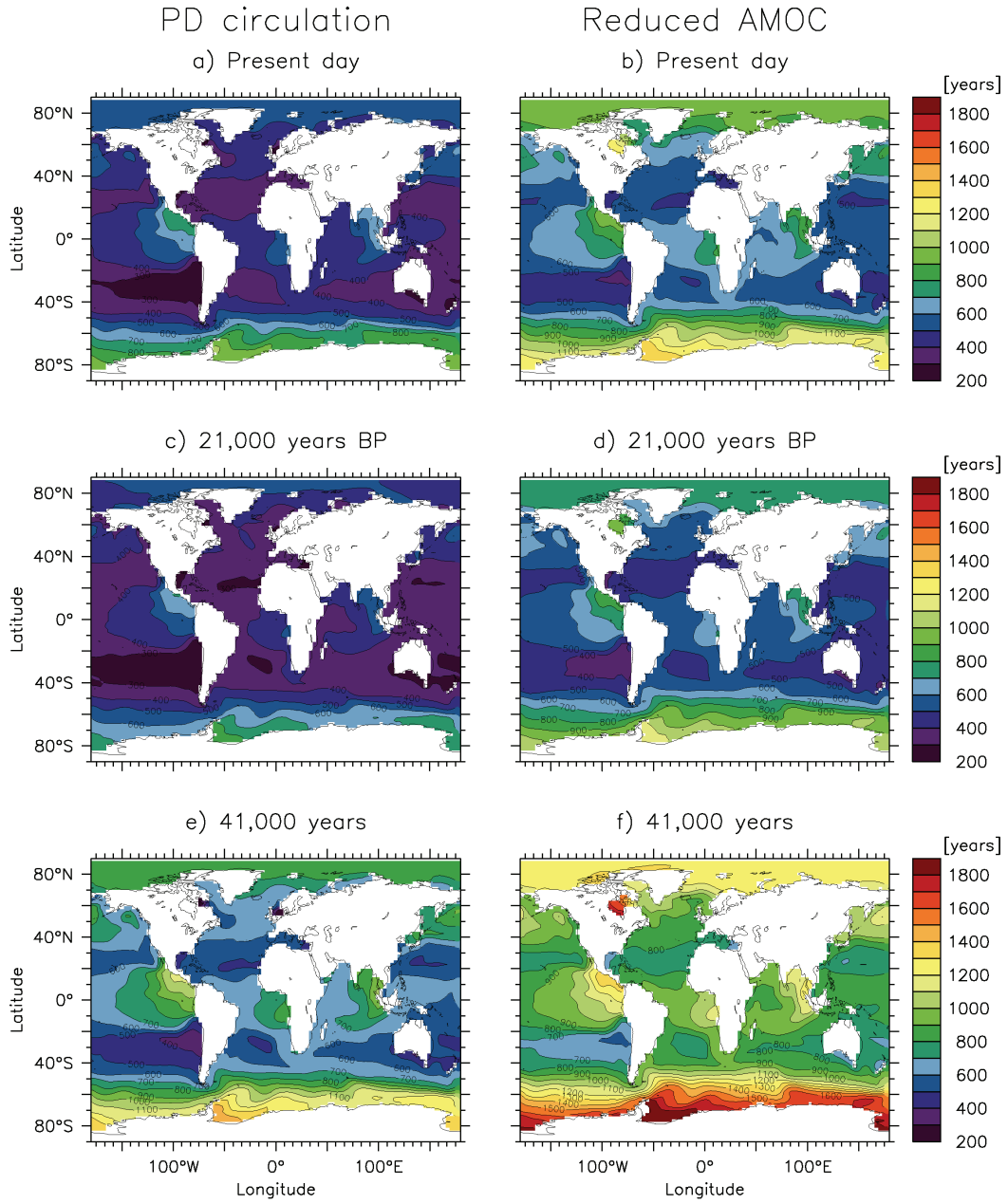


**Figure 3.9:** Modeled reservoir ages for selected time slices, for PD (a and b), the LGM 21 kyr BP (c and d) and for the “Laschamp” event 41 kyr BP (e and f), when the geomagnetic field broke down nearly completely, resulting in a high  $^{14}C$  production. The figures a, c and e on the left hand site were generated from the simulation with PD forcing, b), d) and f) on the right hand site with the reduced AMOC under LGM boundary conditions.

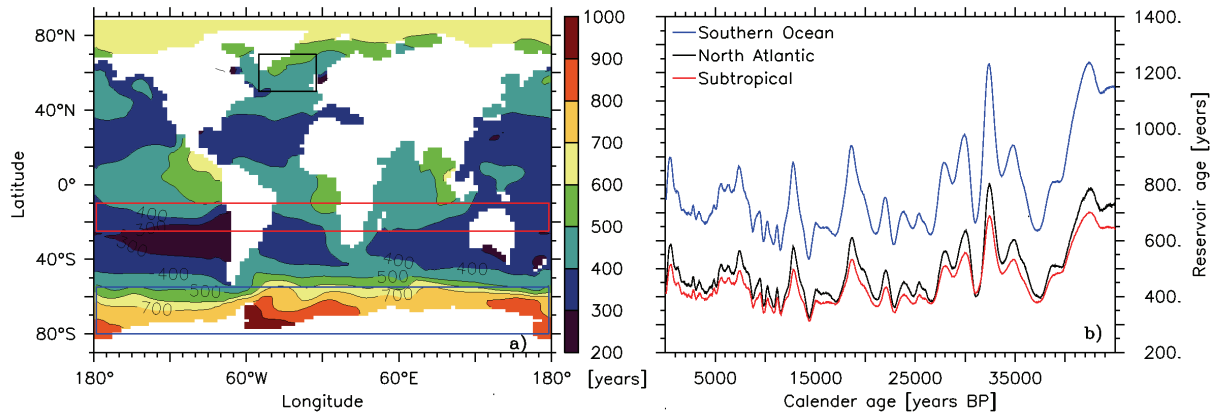


**Figure 3.10:** Modeled range of reservoir-age variations over the time period from 45 kyr BP to PD in a). In b) the regional mean reservoir-age variations are plotted for the areas indicated by equally colored rectangles in a).

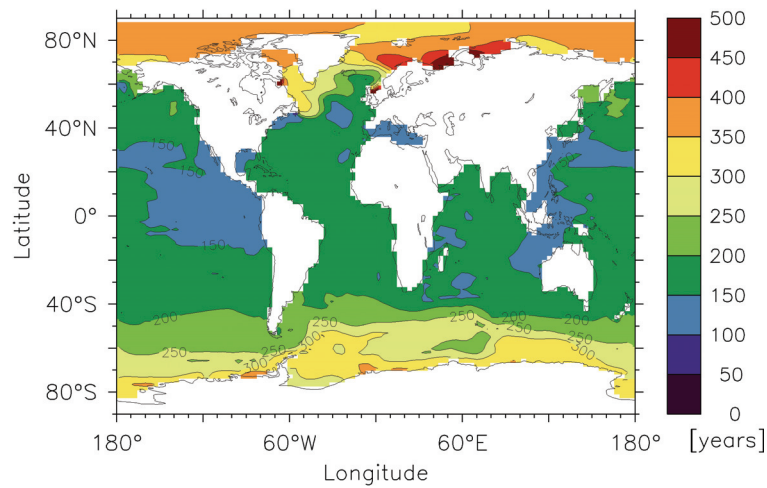


**Figure 3.11:** Anomaly map of the equilibrium reservoir age modeled with reduced AMOC minus reservoir age simulated with present day AMOC.



### 3.2.6 Discussion

#### Atmospheric $^{14}C$ forcing

In principle there exist two possibilities to model atmospheric  $^{14}C$  variations. One approach would be the forcing of the model with a  $^{14}C$  production rate, the other option is  $\Delta^{14}C_{atm}$  reconstructions. The  $^{14}C$  production-rate variations can be calculated based on reconstructions of geomagnetic intensity (e.g. Valet et al., 2005; Laj et al., 2004) or  $^{10}Be$  (Muscheler et al., 2004) using the method of Masarik and Beer (1999).

So far, no model has been able to reproduce the reconstructed  $\Delta^{14}C$  values of far above 500 ‰ in the atmosphere during the last glacial, using  $^{14}C$  production rates alone (Beck et al., 2001; Laj et al., 2000, 2002; Hughen et al., 2004b; Muscheler et al., 2004). More complex models showed even lower  $\Delta^{14}C$  values in the atmosphere than simple models as it could be seen in the difference between a 17-box and a 4-box model (Laj et al., 2002). Forced with the  $^{14}C$  production rate, based on the global paleointensity stack (Laj et al., 2004), the UVic ESCM confirms the results of the box models used in other studies before and only simulates up to  $\sim 300$  ‰. To reach the observed  $\Delta^{14}C_{atm}$  values, which are approximately twice as large, major changes in the carbon cycle are required. One possible explanation would be a glacial deep-ocean carbon reservoir that is well isolated from the atmosphere and stores radiocarbon depleted waters (Marchitto et al., 2007).

Generally the absolute  $\Delta^{14}C_{atm}$  value is irrelevant for the reservoir age, as it can be seen in Fig. 3.10, in which glacial reservoir ages vary around the same level as ages in the Holocene, although  $\Delta^{14}C_{atm}$  was a few hundred permil higher. Instead, the rate of  $\Delta^{14}C_{atm}$  change is the essential factor. Hence, modeled reservoir-age variation do not have to differ in magnitude between the  $^{14}C$  production rate and the  $\Delta^{14}C_{atm}$  forcing, as long as production-rate increase and AMOC reduction do not occur at the same time. Still major reservoir-age changes would stay unconsidered because the production rate can only explain half of the overall variability.

The  $\Delta^{14}C$  forcing has the advantage that the variations, which were not caused by atmospheric  $^{14}C$  production-rate changes also appear in the simulated reservoir ages. Measurement uncertainties in the  $^{14}C$  reconstructions could be reduced, so the large scatter between different datasets decreased over the last years. Nevertheless the reconstructions before 12.4 kyr BP still do not agree with each other completely (Fairbanks et al., 2005;

Hughen et al., 2006), e.g. because the calibration to an age scale is often associated with some uncertainties or because an unknown reservoir age has to be assumed for marine samples. To convert the marine  $\Delta^{14}\text{C}$  values from corals and sediments to an atmospheric value, constant reservoir ages have been applied, as no reservoir-age variation estimates exist for the low latitudes in the last glacial or the deglaciation.

If we assume reservoir-age variation in (sub)tropics, a temporally increased reservoir age implies that the reconstructed  $\Delta^{14}\text{C}_{atm}$  is underestimated compared to the value calculated with a constant reservoir age. If the real reservoir age is smaller than the constant one,  $\Delta^{14}\text{C}_{atm}$  is overestimated. This together might cause modeled reservoir-age variations to be underestimated because reservoir-age increases coincide with  $\Delta^{14}\text{C}$  increases and the other way around (see section 3.2.5).

Based on the bomb experiment we think that the  $\Delta^{14}\text{C}_{atm}$  forcing can be treated comparable to a  $^{14}\text{C}$  production-rate forcing in the model. Simulating long-term variations, there will always be enough time for the ocean to equilibrate with the atmosphere within the gas exchange rate limitations.

The disadvantage of the  $\Delta^{14}\text{C}_{atm}$  forcing is that any  $\Delta^{14}\text{C}_{atm}$  increase acts as if it was caused by a production-rate increase. This may lead to artifacts in deep-water formation areas during times of reduced deep-water production, since the coupling of the surface layer to the deep ocean remains unchanged. In these cases our modeled reservoir-age variations will be slightly underestimated again.

### Reservoir-age variations

The comparably large oceanic carbon reservoir responds to atmospheric  $\Delta^{14}\text{C}$  changes with a time lag due to limited gas exchange. A  $\Delta^{14}\text{C}_{atm}$  increase leads to a larger atmosphere-ocean  $^{14}\text{C}$  difference and accordingly to a reservoir-age increase, because the ocean cannot react fast enough, e.g. around 41 kyr BP (Fig. 3.10). As soon as  $\Delta^{14}\text{C}_{atm}$  stops rising or is reduced, the reservoir ages decrease again. The opposite is true when  $\Delta^{14}\text{C}_{atm}$  declines, e.g. around 15 kyr BP.

Changes in reservoir ages occur globally nearly simultaneous because the fast varying and well mixed atmosphere is the key driver (Fig. 3.10). In contrast, the amplitude of the reservoir-age variations differs at any location. Regions of large reservoir ages are as well

areas of large reservoir-age variations, like the Southern Ocean with more than 1000 years of PD surface  $^{14}C$  age and also variations of more than 1000 years (Fig. 3.9 and 3.10). In a period of a  $\Delta^{14}C_{atm}$  increase the radiocarbon content of the atmosphere increases while the radiocarbon depleted water that wells up from the deep ocean, was once at the sea surface, when atmospheric  $\Delta^{14}C$  was much lower. This causes the  $^{14}C$  gradient between atmosphere and ocean to be larger than caused by the limited gas exchange alone. In the opposite case of a  $\Delta^{14}C_{atm}$  decrease, upwelling water was in contact with an atmosphere of higher  $\Delta^{14}C$  which leads to small reservoir ages.

In case of reservoir-age changes that are not caused by  $^{14}C$  production-rate variation, the simulated reservoir-age change is correct, but not the level, at which the reservoir ages remain after that first change. Box models suggested that more deep-water production will transport more radiocarbon into the deep ocean and finally decrease atmospheric  $\Delta^{14}C$ . In contrast, a reduced AMOC will lead to a lower  $^{14}C$  transport into the deep ocean and to increased atmospheric  $\Delta^{14}C$  (Beck et al., 2001; Laj et al., 2002; Hughen et al., 2004b). The observed global reservoir-age increase in our simulation with a reduced AMOC agrees with this finding (Fig. 3.11). Temporally stable reservoir-age shifts can be initiated by changes in the carbon-reservoir sizes. A  $\Delta^{14}C_{atm}$  increase in the model forcing, increases the atmosphere-ocean  $^{14}C$  difference in the first moment as well, but because of the constant deep-water formation, the ocean starts to take up more  $^{14}C$ , too. This decreases the reservoir ages again in the model, while they would remain larger in reality as long as the carbon reservoirs stay in a different state, like in the simulation with LGM boundary conditions.

Reservoir ages of more than 2000 years were reconstructed in the northern North Atlantic (Bard et al., 1994; Sarnthein et al., 2001; Waelbroeck et al., 2001) and close to New Zealand (Sikes et al., 2000). Further evidence for such large reservoir-age variations comes from  $^{14}C$ -plateau matching, which also suggests reservoir ages of 2000 years and more in the early deglaciation after the LGM (Sarnthein et al., 2007). If we add up the modeled temporal variations of up to 1000 years, variations subsequent to the reduced AMOC of up to 500 years or even more in case of a complete deep-water formation shutdown and including the underestimated effects mentioned in section 3.2.6, reservoir-ages variations of above 2000 years, appear to be reasonable in some regions. From the model simulation we would expect such large variations only in the Southern Ocean but not in the northern North Atlantic.

Modeled reservoir-age variation are not limited to high latitudes, they reach up to a few hundred years in tropical oceans, which were believed to be nearly stable (Hughen et al., 2004a). This has implications for the dating of atmospheric samples, because it adds some uncertainty to all  $^{14}\text{C}$  calibration curves, which assume a constant reservoir age prior to 12.4 kyr BP.

### **Potential of modeled reservoir ages**

In contrast to reservoir-age reconstructions, estimates from an ocean circulation model are available at every location, time and also at different depth levels. The depth is an important factor because reconstructions are often based on foraminifera that calcified between sea surface and 250 m depth (Simstich et al., 2003; Schiebel and Hemleben, 2005). The reservoir age of a species living at 250 m depth can severely differ from the surface reservoir age. This occurs especially in the North Pacific where reservoir ages at 250 m depth are up to 500 years larger than at the ocean surface. Model results suggest that it is also important to consider the living depth of a species before correcting for the reservoir age in other regions.

### **Comparison of modeled and reconstructed reservoir ages for the Younger Dryas**

Finally the reliability of modeled reservoir ages should be checked by a comparison with reconstructions. For this purpose the North Atlantic is the best covered region. For the time period from the Bølling to the Preboreal reservoir ages were reconstructed from co-existing marine and terrestrial material (Björck et al., 1998; Bondevik et al., 1999, 2006), from volcanic ash layers (Bard et al., 1994; Austin et al., 1995) and from corals (Cao et al., 2007).

The reconstructions show large scatter and have large error bars, which nearly cover the whole range of variations, e.g. reservoir ages from Norway at nearly the same time between 13.7 and 13.8 kyr BP show  $\sim 400$  years difference (Fig. 3.12). Nevertheless there is a trend from PD-like reservoir ages around 400 years in the Bølling, over an increase in the Allerød to the Younger Dryas reservoir ages of circa 600 years and finally a decrease towards a PD value in the Preboreal again. The model predicts the Bølling reservoir age, the increase

in the Allerød and the PD-like values in the Preboreal very well in the run with the PD circulation. Only during the Younger Dryas ( $\sim 12.9\text{--}11.6$  kyr BP) the modeled reservoir ages remain below the reconstructed values and they start to decrease too quickly after reaching a maximum at the beginning of the Younger Dryas. It is thought that the cause of this reservoir-age increase was a slowdown of the AMOC during the Younger Dryas (e.g. McManus et al., 2004). In the model simulation with reduced AMOC, the predictions for Younger Dryas reach or even exceed the reconstructions. The fact that reservoir ages decrease too early with the PD forcing demonstrates that a  $\Delta^{14}C_{atm}$  model forcing changes reservoir ages temporally like atmospheric  $^{14}C$  production-rate variations, but it can only generate the initial peak of a carbon reservoir-size change induced reservoir-age variation. The correct interpretation and consideration of ocean circulation changes is therefore essential, when simulated reservoir ages should be applied for an age correction of marine samples.

A compilation of reconstructions from different locations might create the wrong impression that reservoir ages should be the same everywhere. Indeed, the existence of local differences can hardly be seen in the scatter of the data but simulation results clearly show a  $\sim 50$  year reservoir-age difference between Norway and Orphans Knoll (Fig. 3.12). The modeled reservoir ages for Sweden differ largely between the simulated AMOC states. That highlights that a reduction of the AMOC always increases the reservoir ages but by spatially different amounts.

The comparison of modeling results and reconstructions shows that our model can simulate the reservoir-age variation induced by changes in  $\Delta^{14}C_{atm}$  in the correct order of magnitude. It is difficult to determine the quality of the model results due to the large scatter in the reconstructions.

### 3.2.7 Conclusions

Our ocean general circulation model confirms the results of previous box-model experiments that geomagnetic variations alone appear to be insufficient to explain reconstructed atmospheric  $^{14}C$  variations in the last glacial and the deglaciation.

Simulations of past reservoir-age variations, using a  $\Delta^{14}C_{atm}$  forcing, emphasize the need to make a temporal, spatial and depth depended reservoir-age correction when marine

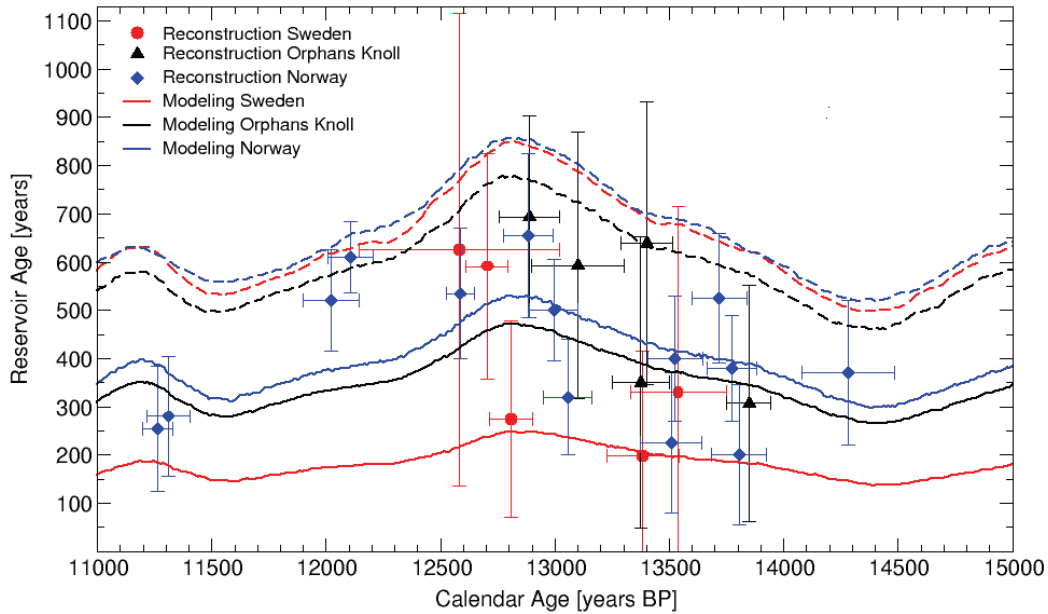


**Figure 3.12:** Reconstructed and modeled reservoir ages from the Bølling/Allerød over the Younger Dryas to the Preboreal: The symbols represent the reconstructed reservoir ages for three regions in the northern North Atlantic, Sweden (Björck et al., 1998), Norway (Bondevik et al., 1999, 2006) and Orphans Knoll (Cao et al., 2007). The modeled mean reservoir ages at the sample locations are plotted for the PD circulation (solid curve) and for the reduced AMOC simulation (dashed curve).

samples are dated with the radiocarbon method. The model suggests reservoir-age variations of several hundred years within some centuries due to  $^{14}\text{C}$  production-rate and ocean-circulation changes. The modeled reservoir-age variations are not limited to high latitudes and can reach up to a few hundred years in tropical oceans. This has implications for  $^{14}\text{C}$  calibration curves, which are mainly based on coral data and a constant reservoir age.

For regions and time periods where no reservoir-age variation can be reconstructed, the model results will be a useful tool to estimate reservoir ages for any marine sample. Modeled reservoir ages are available online ([www.reservoirage.uni-bremen.de](http://www.reservoirage.uni-bremen.de)).

### 3.3 Comparison of $\Delta^{14}\text{C}$ and $^{14}\text{C}$ production-rate forcings

In the previous sections (Sect. 3.1 and 3.2) the different options to force the model were described. The  $\Delta^{14}\text{C}$  forcing has been preferred because the model could not reach the reconstructed  $\Delta^{14}\text{C}$  values in the atmosphere using the  $^{14}\text{C}$  production-rate forcing and because it would hence lack all reservoir-age variations induced by carbon-reservoir changes. The model simulation forced with the GLOPIS-75 based  $^{14}\text{C}$  production-rate forcing is here compared to the  $\Delta^{14}\text{C}$  forcing to assess which reservoir-age variations are circulation induced and if a  $^{14}\text{C}$  production-rate forcing results in underestimated reservoir ages because modeled absolute  $\Delta^{14}\text{C}_{atm}$  values are too small.

#### 3.3.1 Results

The modeled atmospheric  $\Delta^{14}\text{C}$  begins to increase at 45 kyr BP from a level that is  $\sim 300\%$  smaller than the reconstructions (Fig. 3.13a). However, the variation with a peak at  $\sim 41$  kyr BP has a similar amplitude. The following  $\Delta^{14}\text{C}$  decrease as well as the increase at  $\sim 35$  kyr BP are both similar in the model results and in the reconstructions. In contrast the  $\Delta^{14}\text{C}$  peaks between  $\sim 32$  and 26 kyr BP as well as the decreasing  $\Delta^{14}\text{C}$  trend between  $\sim 26$  and 15 kyr BP including another peak at  $\sim 18$  kyr BP only exist in the spline through the reconstructions. From  $\sim 15$  to 10 kyr BP both curves run nearly parallel except for an increase in the reconstructions at  $\sim 12.5$  kyr BP and one in the modeled  $\Delta^{14}\text{C}$  at  $\sim 10$  kyr BP. In the Holocene both curves finally match well.

Although atmospheric  $\Delta^{14}\text{C}$  is significantly larger in the reconstructions between 45 and 15 kyr BP, the global mean reservoir ages vary in the same range and by a similar amplitude (red and black curve in Fig. 3.13b). Differences are that the peak at  $\sim 41$  kyr BP is more pronounced using the production-rate forcing, a variation at  $\sim 32$  kyr BP only exists when the  $\Delta^{14}\text{C}$  forcing is applied and generally smaller but more variable reservoir ages are modeled between  $\sim 28$  and 10 kyr BP using the  $\Delta^{14}\text{C}$  forcing.

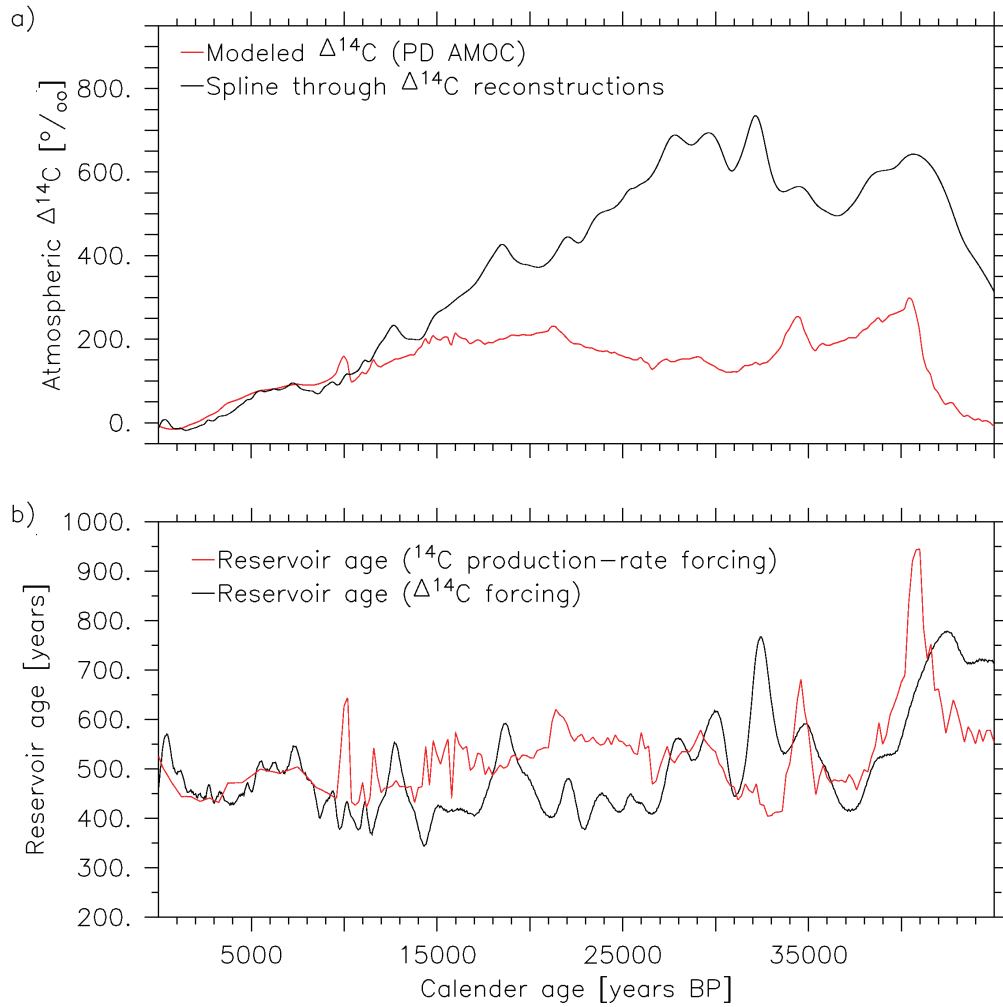


**Figure 3.13:** a) Comparison of the simulated  $\Delta^{14}\text{C}_{\text{atm}}$  when the model is forced by the  $^{14}\text{C}$  production rate (red) and by the spline that has been interpolated through  $\Delta^{14}\text{C}_{\text{atm}}$  reconstructions (black). In both cases PD-like boundary conditions are prescribed. b) Comparison of the modeled global mean surface reservoir ages, using the  $^{14}\text{C}$  production-rate forcing (red) and the  $\Delta^{14}\text{C}_{\text{atm}}$  forcing (black).



### 3.3.2 Discussion

The most distinct  $\Delta^{14}\text{C}_{atm}$  increase occurs around 41 kyr BP during the so-called “Laschamp event”, when the geomagnetic field broke down nearly completely causing a high production of  $^{14}\text{C}$  in the atmosphere. The reconstructions of  $\Delta^{14}\text{C}_{atm}$  and the modeled  $\Delta^{14}\text{C}_{atm}$  using  $^{14}\text{C}$  production-rate forcing diverge by  $\sim 300\text{‰}$  because they start at a different initial level, but the amplitude of  $\sim 300\text{‰}$  is nearly the same (Fig. 3.13a). The peaks also match in time in both curves as well as the following  $\Delta^{14}\text{C}_{atm}$  decreases. This indicates that the  $\Delta^{14}\text{C}_{atm}$  increase is completely caused by the production-rate increase.

Although the modeled reservoir ages vary in the same range, they differ significantly from each other (Fig. 3.13b). The amplitude of the variations initiated by the  $^{14}\text{C}$  production-rate forcing is significantly higher than that with the  $\Delta^{14}\text{C}_{atm}$  forcing. Unexpected is the temporal lag of more than 1000 years. The cause for both differences is the same, the steepness of the  $\Delta^{14}\text{C}_{atm}$  or production-rate increase is the important factor influencing the amplitude of the reservoir-age changes and the initial  $\Delta^{14}\text{C}_{atm}$  level is not decisive. First the production-rate curve increases more steeply causing the higher amplitude. Second the slope of the  $\Delta^{14}\text{C}_{atm}$ -forcing curve shows a decrease in steepness earlier than the production-rate curve as a result of smoothed spline through the reconstructions. This causes the observed time lag, although both  $\Delta^{14}\text{C}_{atm}$  curves have their peak at the same time. In this case of a pure production-rate signal, the production-rate forcing might result in more reliable reservoir-age variations although the different initial level suggests other sizes of the carbon reservoirs than at present. Another factor causing time lags can be a difference in the age models. The GLOPIS-75 data set has been tuned to the GISP-2 ice core (Laj et al., 2004), the Cariaco Basin sediment data to the Hulu cave speleothem  $\delta^{18}\text{O}$  record (Hughen et al., 2006) and corals were dated with U/Th (Fairbanks et al., 2005). In case of the Laschamp event this seems to be a minor error source because the peaks of the modeled  $\Delta^{14}\text{C}_{atm}$  and spline occur with a time lag of only  $\sim 150$  years.

Some peaks of high atmospheric  $\Delta^{14}\text{C}$  have been interpreted as results of a reduced deep-water formation after freshwater inputs by melting icebergs in the North Atlantic (e.g. Hughen et al., 2004b). A reservoir-age variation connected to a possible reduction of North Atlantic deep-water formation at Heinrich event 4 ( $\sim 38$  kyr BP, Hemming, 2004) cannot be found in the  $\Delta^{14}\text{C}_{atm}$  reconstruction. The only temporally close  $\Delta^{14}\text{C}_{atm}$  increase at 38.7 kyr BP coincides with a  $^{14}\text{C}$  production rate increase.

The subsequent  $\Delta^{14}\text{C}_{atm}$  increase occurs at  $\sim 35$  kyr BP in both curves (Fig. 3.13a). This again reflects variations in production rate as a cause. As this variation is smaller and shorter in time, the time lag of the reservoir-age variation between both forcings is also much smaller than at 41 kyr BP.

At  $\sim 32$  kyr BP the interpolated spline through the  $\Delta^{14}\text{C}_{atm}$  reconstructions shows a distinct peak which causes a coeval reservoir-age variation of the same magnitude as the Laschamp event. There is no change in geomagnetic intensity at this time and no Heinrich event reported. The peak seems to be an artifact of the spline interpolation in a period of large data scatter (Fig. 3.6). Hence, the reservoir ages modeled with the production-rate forcing are more reliable between 33.5 and 31 kyr BP.

The  $\Delta^{14}\text{C}_{atm}$  increase at  $\sim 30$  kyr BP might be related to an Atlantic deep-water formation decrease due to freshwater input at Heinrich event 3 ( $\sim 31$  kyr BP, Hemming, 2004), but contemporaneously there is a production-rate increase. Therefore and especially if the previous  $\Delta^{14}\text{C}_{atm}$  peak is just an interpolation artifact, the reservoir-age variation might be underestimated using both model forcings.

The following  $\Delta^{14}\text{C}_{atm}$  variations at around 28 and 22 kyr BP are less pronounced in the production-rate forced model experiment than in the reconstructions, but all create similar reservoir-age variations by their rate of  $^{14}\text{C}$  increase. The spline interpolation is again the reason why reservoir ages vary a few hundred years earlier with the  $\Delta^{14}\text{C}_{atm}$  forcing.

Since  $\sim 27$  kyr BP the general  $\Delta^{14}\text{C}_{atm}$  trend is decreasing, while it is slightly increasing between 32 and 21 kyr BP, constant between 21 and 15 kyr BP and finally also decreasing since 15 kyr BP when the model is forced by the production-rate. The trend in the reconstructions leads generally to lower reservoir ages. The global mean values are approximately 400 years between 27 and 15 kyr BP when the model is forced by  $\Delta^{14}\text{C}_{atm}$  instead of 500 to 550 years when the model is forced by the  $^{14}\text{C}$  production rate. The good agreement between production-rate forcing and  $\Delta^{14}\text{C}_{atm}$  in the Holocene suggests that the model predicts  $\Delta^{14}\text{C}_{atm}$  well as long as there are no major changes in the carbon cycle. Thus, deglacial and glacial differences between reconstructions and the model have to be a result of changes in the carbon cycle. As the decreasing  $\Delta^{14}\text{C}_{atm}$  trend at the end of the last glacial and during the deglaciation cannot be modeled with the production-rate forcing, the reservoir ages using the  $\Delta^{14}\text{C}_{atm}$  forcing are more reliable for the last 27 kyr BP, although the trend is handled in the model calculation as if it would be a  $^{14}\text{C}$

production-rate change, as the real cause is not fully understood.

Heinrich event 2 ( $\sim 24$  kyr BP, Hemming, 2004) seems to be hidden behind the steeply decreasing  $\Delta^{14}\text{C}_{atm}$  trend. A slightly reduced decrease is visible in the  $\Delta^{14}\text{C}_{atm}$  reconstructions leading to small reservoir-age variations in the simulation with the  $\Delta^{14}\text{C}_{atm}$  forcing.

High  $\Delta^{14}\text{C}_{atm}$  values around 18 kyr BP coincide with the Heinrich event 1, at which fresh-water was released from melting icebergs in the North Atlantic Ocean (e.g. Hughen et al., 2004b). Another peak occurred at the time of the Younger Dryas around 12.5 kyr BP, when again a reduced North Atlantic deep-water formation was reported (e.g. Berger, 1990; Broecker, 2006). It has been shown in Sect. 3.2 that the model, forced by temporal  $\Delta^{14}\text{C}$  variations, can predict the initial reservoir-age increase, which is impossible using the production-rate forcing. In case of a reservoir-age increase due to another factor than the production rate, simulated reservoir ages will not be correctly predicted after the initial reservoir-age increase. If a reduced AMOC is the cause for the reservoir-age variation, the corresponding model simulation (Sect. 3.2.5) can help to estimate the reservoir-age change.

The model predicts a  $\Delta^{14}\text{C}_{atm}$  peak around 10 kyr BP due to changes in the geomagnetic field. This cannot be derived from the  $\Delta^{14}\text{C}_{atm}$  reconstructions, which depend on the relatively precise tree-ring calibrations in this period. In this sense the  $\Delta^{14}\text{C}_{atm}$  reconstructions are assumed to be more reliable for forcing the model in this time period.

In the Holocene both data sets nearly agree and result in the similar reservoir-age variations. The resolution and accuracy of the atmospheric  $\Delta^{14}\text{C}$  in this period is higher than of the GLOPIS-75 data set, although the spline is interpolated through the data. This makes the reservoir ages modeled using the  $\Delta^{14}\text{C}$  forcing preferable once more.

### Effect of the spline interpolation

In the last section it has been discussed that the interpolation of the spline causes a time lag in the simulated reservoir ages and that  $\Delta^{14}\text{C}_{atm}$  variation is an interpolation artifact. In order to assess more effects of the interpolation, reservoir ages are additionally simulated for the last deglaciation and the Holocene using the original INTCAL04 dataset (Reimer et al., 2004).

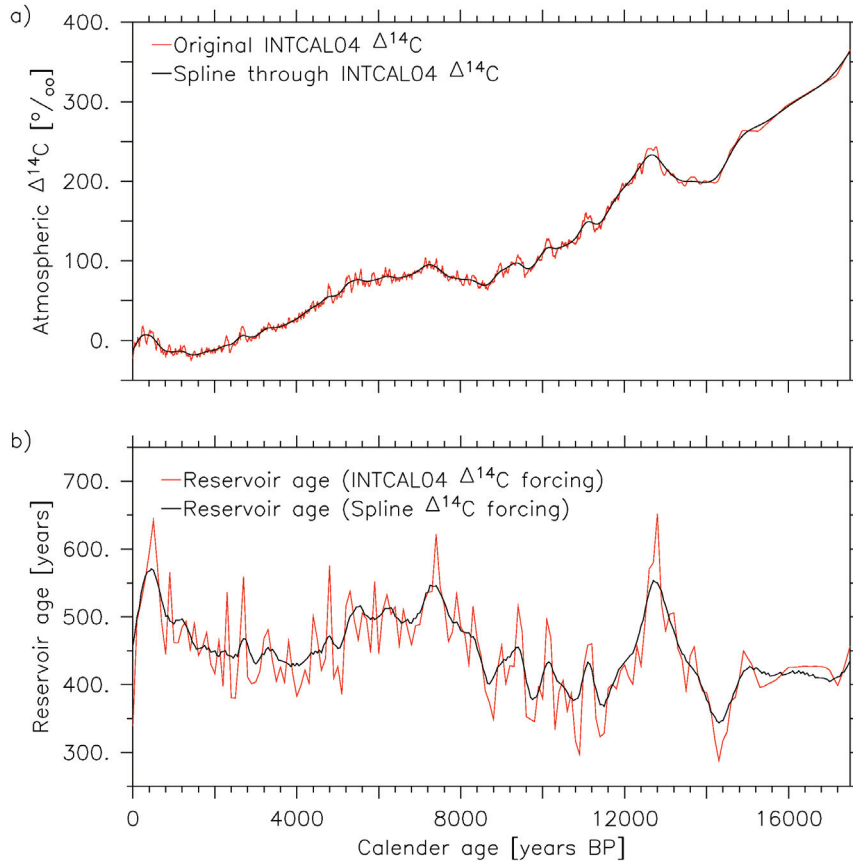


**Figure 3.14:** a) Comparison of the original INTCAL04  $\Delta^{14}C_{atm}$  data (red, Reimer et al., 2004) with the spline that has been interpolated through  $\Delta^{14}C_{atm}$  reconstructions (black). b) Comparison of the modeled global mean reservoir ages, using the original INTCAL04 data (red) and the interpolated spline (black) as a model forcing.

Forcing the model by the original INTCAL04 dataset instead of the smoothed spline through the INTCAL04 data leads to same major reservoir-age variations and does not introduce time lags of more than 10 years in the time period between 18 kyr BP and PD. However, it adds high frequency variations lasting between a few years and a few decades during the past  $\sim 12$  kyr, the period in which the atmospheric  $\Delta^{14}\text{C}$  could be reconstructed with high resolution. Here the original INTCAL04 forcing increases the positive and negative reservoir-age extrema by up to 80 years compared to the spline forcing (Fig. 3.14). This effect was already indicated when the  $^{14}\text{C}$  production-rate forcing caused a larger reservoir-age variation than the  $\Delta^{14}\text{C}$  forcing at the Laschamp event. Before 12 kyr BP

where  $\Delta^{14}\text{C}_{atm}$  has been reconstructed from marine data, high frequency  $\Delta^{14}\text{C}_{atm}$  variations are unknown as the atmosphere-ocean gas exchange smoothed atmospheric changes. Thus, the influence of the spline interpolation on the simulated reservoir ages is mostly neglectable and does not exceed a few decades.

Consequently, the interpolation of the spline leads to a slight underestimation of the frequency and amplitude of reservoir-age variations during the entire simulation period, but only in the Holocene reconstructions exist that allow to force the model with this accuracy and resolution. Time lags of several hundred years in the reservoir ages simulated by different forcings occur only between 35 and 45 kyr BP.

### 3.3.3 Conclusions

By comparing the modeled reservoir ages using a  $\Delta^{14}\text{C}_{atm}$  and a  $^{14}\text{C}$  production-rate forcing it is shown that both can initiate reservoir-age variations of the similar magnitude. Between 27 and 50 kyr BP the production-rate forcing is assumed to have less uncertainties because (i) most  $\Delta^{14}\text{C}_{atm}$  variations seem to be related to production-rate changes, (ii) Heinrich event 3 and 4 seem to have little influence on  $\Delta^{14}\text{C}_{atm}$  reconstructions and (iii) there is no obvious bias caused by the spline interpolation. Still one has to be aware that all errors in the forcing data propagate into the modeled reservoir ages. The  $^{14}\text{C}$  production-rate forcing has been calibrated to the GISP-2 age scale and consequently the modeled reservoir ages are tied to this age model, instead of absolute calendar ages.

For the time period from 27 kyr BP to PD the reservoir-age variations, modeled with the  $\Delta^{14}\text{C}_{atm}$  forcing, seem to be more reliable because the general decreasing trend of atmospheric  $\Delta^{14}\text{C}$  is considered as well as major changes in the carbon cycle that occurred for instance in the Heinrich event 1 or the Younger Dryas. In this period the age scale causes less problems because the reconstructions agree better but there are still uncertainties when the  $\Delta^{14}\text{C}_{atm}$  was calculated from marine data and not from tree rings. For past  $\sim 12$  kyr the INTCAL04  $\Delta^{14}\text{C}_{atm}$  forcing without an interpolation can further increase the resolution of the simulated reservoir-age variations.

The fact that the model predicts Holocene  $\Delta^{14}\text{C}_{atm}$  variations well when it is forced by the  $^{14}\text{C}$  production rate and that the predictions have an offset in the Pleistocene suggests that the carbon-reservoir sizes, most probably the large oceanic reservoir, differed during the last glacial severely from the PD situation.

# Chapter 4

## The reservoir-age database

The modeled reservoir ages are stored in a database, which is accessible through the world wide web (WWW) and an easy to operate user interface. Reservoir ages are available for geographical regions at a specific calendar and  $^{14}\text{C}$  age, as temporal variation at a specific location and for different depth levels.

### 4.1 The Live Access Server

The “Live Access Server” (LAS, <http://ferret.pmel.noaa.gov/Ferret/LAS/>) is especially designed for such geo-scientific data sets in the climate model output format “NetCDF” (Network Common Data Form). The architecture of LAS is modular and has three levels (Fig.4.1): (i) the user interface shown in the browser to make requests to the database, (ii) a so-called “business logic” which transfers the request into commands for the back end application “Ferret”, which (iii) accesses the database and generates the requested plot or table. Ferret is an interactive software to visualize and analyze oceanographic and meteorological data of up to four dimensions (<http://ferret.pmel.noaa.gov/Ferret/>).

The recent version of LAS (1.0 Armstrong) that is installed on the webserver <http://www.reservoirage.uni-bremen.de> is programmed in Java and mainly configured via XML files. A detailed description about the installation and configuration of LAS including the reservoir age modeling results can be found in the Appendix.

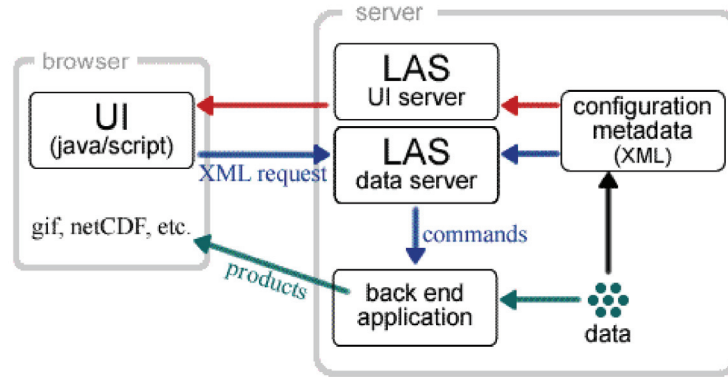


**Figure 4.1:** Modular architecture of the Live Access Server. Source: [http://ferret.pmel.noaa.gov/Ferret/LAS/Documentation/intro\\_to\\_LAS.htm](http://ferret.pmel.noaa.gov/Ferret/LAS/Documentation/intro_to_LAS.htm).

## 4.2 Time axis

The model is forced by data which is on a calendar-age scale or in case of the production-rate forcing on the GISP2-age scale, but also handled as if it would be a calendar-age scale. Accordingly the modeled reservoir ages also refer to the calendar-age scale. This original model output is uploaded to LAS to present simulated reservoir-age variations over time.

In practice the user will mostly obtain a  $^{14}\text{C}$  age for the sample from the laboratory which needs to be corrected for the reservoir effect. Afterwards the corrected  $^{14}\text{C}$  age can finally be transformed to a calendar age using an atmospheric calibration curve. To allow for a search of reservoir ages corresponding to a  $^{14}\text{C}$  age, the data has to be transformed from the calendar-age time axis to a  $^{14}\text{C}$ -age time axis (Fig. 4.2). This procedure is impaired by  $^{14}\text{C}$  plateaus, periods in time where the  $^{14}\text{C}$  concentration shows little variation. In these periods more than one calendar and reservoir age refer to the same  $^{14}\text{C}$  age. The  $^{14}\text{C}$  plateaus are less pronounced in the model ocean than in reconstructions because the model is just forced by variations in the atmospheric  $^{14}\text{C}$  concentration and not by transient changes in the ocean circulation. Hence,  $^{14}\text{C}$  plateaus in the marine  $\Delta^{14}\text{C}$  evolution do not span more than a few decades which keeps the range of possible calendar ages that refer to a  $^{14}\text{C}$  age within a limit of 40 years and the range of reservoir ages within a limit of 30 years. These values are extrema, the mean deviation in these plateaus is 10 years for the calendar ages and  $\sim 1$  year for the reservoir ages. In consideration of the small possible



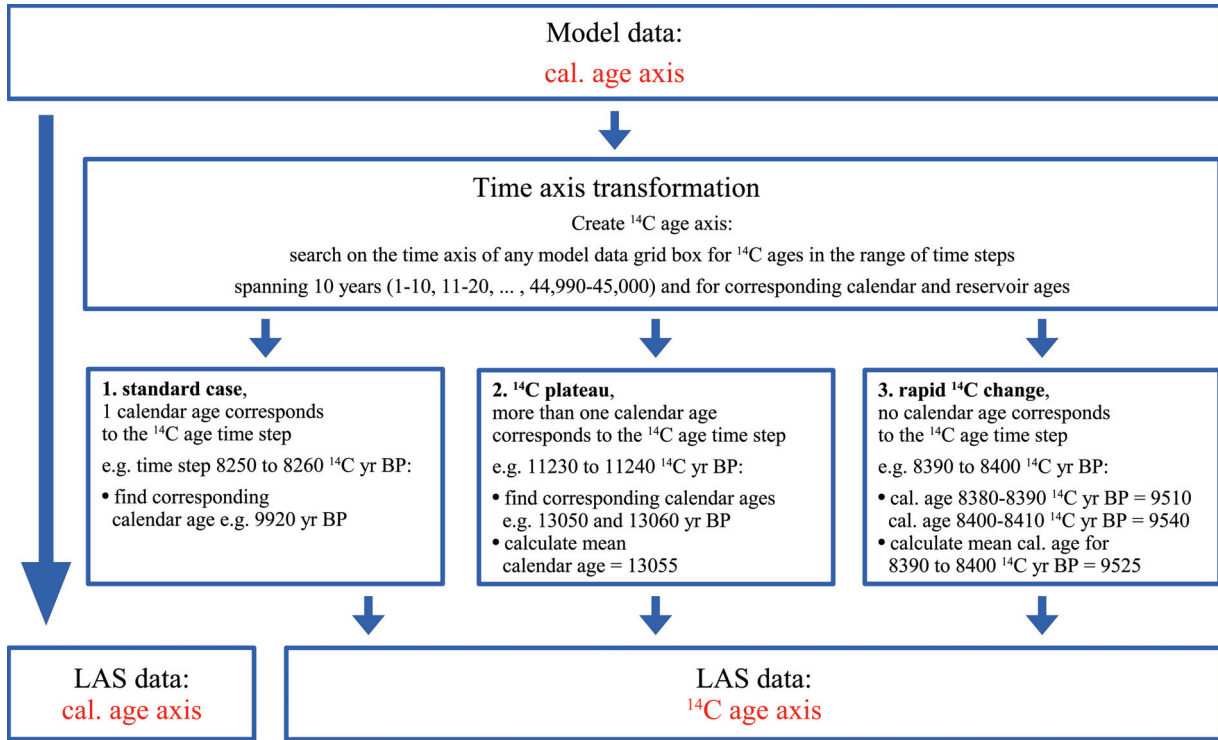


**Figure 4.2:** Procedure of time-axis conversion.

error, the arithmetic means of the calendar-age and reservoir-age values referring to a <sup>14</sup>C age are stored in the database if a <sup>14</sup>C plateaus made it necessary.

On the other hand a few <sup>14</sup>C ages do not refer to any calendar and reservoir age because they are missed when a fast <sup>14</sup>C-age change occurs while only 10-yearly mean values are generated by the model. In these cases a linear interpolation between the temporally next data points is done to offer a dataset without gaps.

All <sup>14</sup>C age in the database are calculated applying the “true” half-life of radiocarbon. Conventional <sup>14</sup>C ages calculated with the “Libby” half-life need to be corrected before using the database.

$$^{14}C_{true\ age} = 1.03 \cdot ^{14}C_{conv.\ age}$$

### 4.3 Reservoir-age request

A data request to get simulated reservoir ages from of the database (<http://www.reservoirage.uni-bremen.de/las/servlets/dataset>) can be made with the LAS UI (Live Access Server User Interface). The request itself is separated in a three step structure:

1. Datasets:

Available NetCDF files for different forcings and time axes are listed in this menu.

2. Variables:

Variables from the dataset, selected in step 1, need to be chosen in the second step.

3. Constraints:

In the last step the request has to be specified in detail (Fig. 4.3).

- (a) A view type has to be selected, e.g. “Longitude-Latitude” for a map at one specific depth level or “Time series” to see changes at one specific location.
- (b) The output format has to be selected depending on the data request. For two dimensional maps and depth profiles, the most common and tested output format is a “color plot”, for time series it is a “line plot”. Of course, the raw data can also be saved as NetCDF or ASCII file.
- (c) Regions or locations of interest can be selected from a dropdown menu or via left mouse clicks on the map or by entering coordinates directly.
- (d) The time or time period of interest has to be given in years BP.
- (e) A depth level has to be selected. The value is the mean depth in meters of any of the 19 depth levels of the model.
- (f) To modify the graphical output, additional options can be selected.
- (g) Finally, output from the database will be generated after transmitting the request by selecting the “next” button (Fig. 4.4 and 4.5).

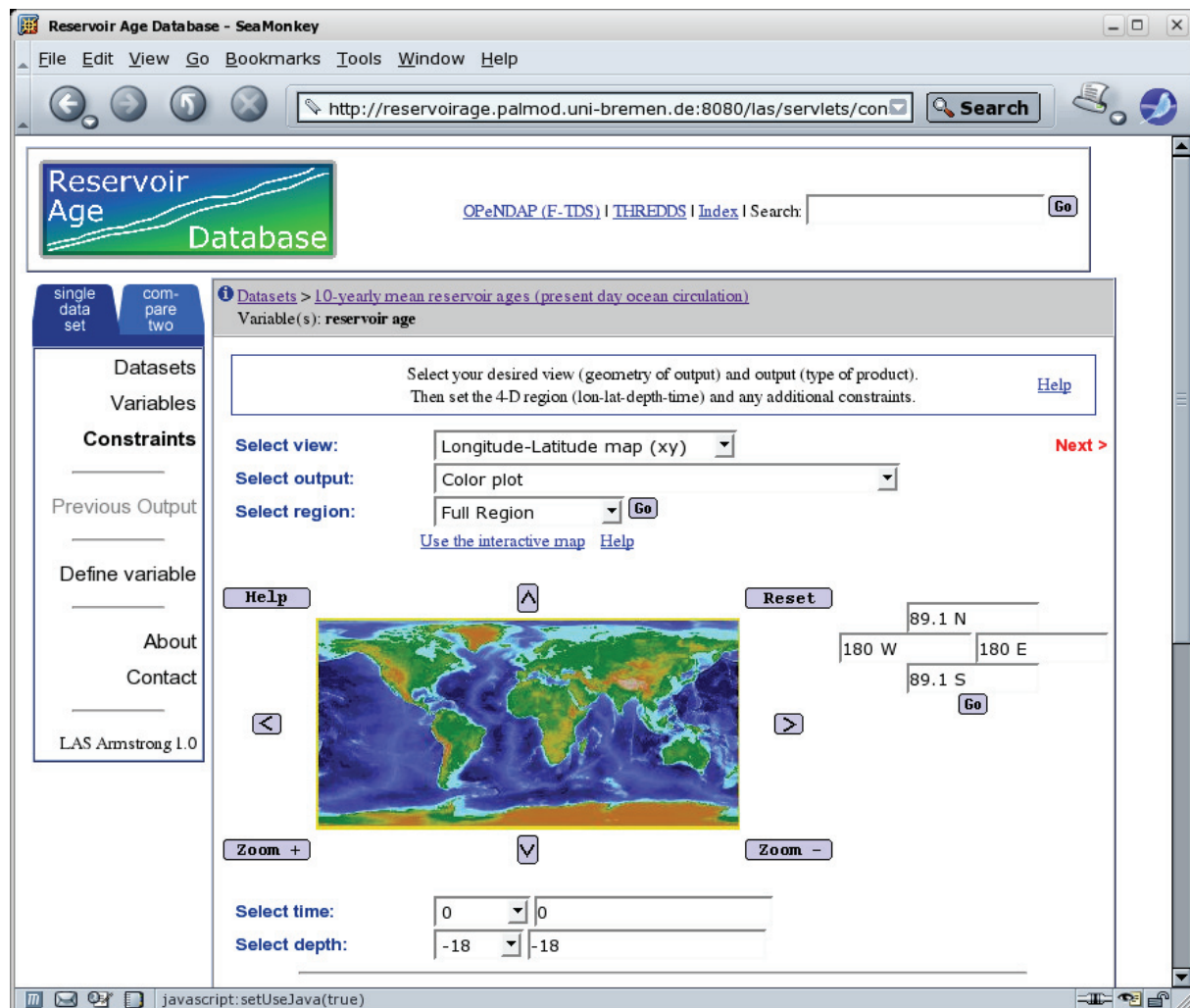


Figure 4.3: Screenshot from the “Constraints” webpage of LAS.

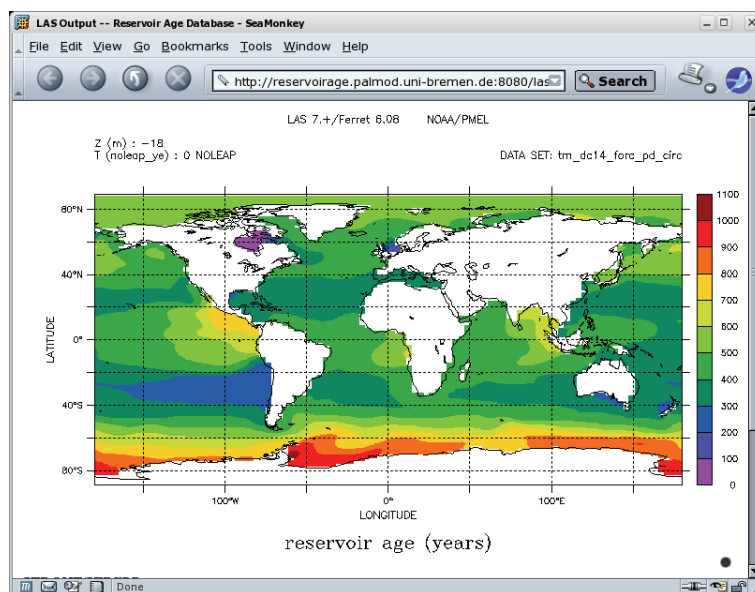


Figure 4.4: Screenshot from the output of a reservoir-age map request.

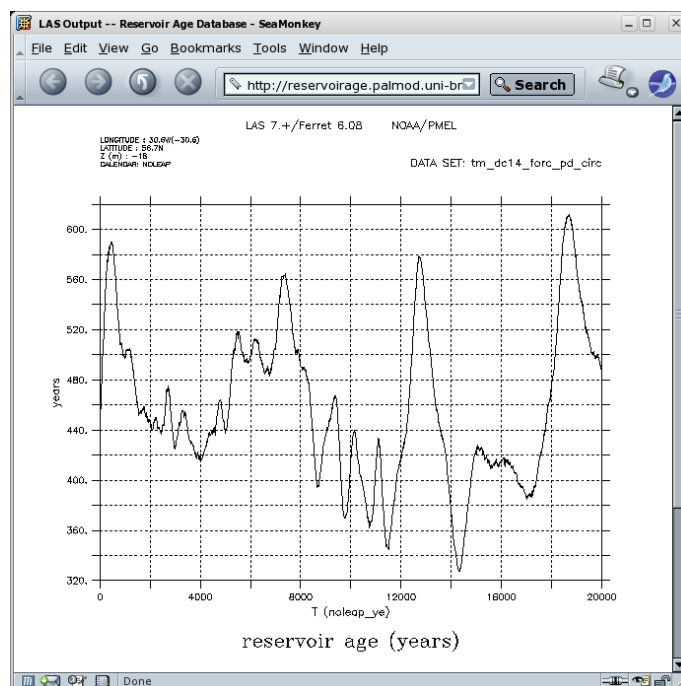


Figure 4.5: Screenshot from the output of a reservoir-age time series request.

## Chapter 5

# Assessing the ability of the $^{14}\text{C}$ projection-age method to constrain the circulation of the past in a 3D ocean model

**Jörg Franke**<sup>1</sup>, Michael Schulz<sup>1,2</sup>, André Paul<sup>1,2</sup> and Jess F. Adkins<sup>3</sup>

<sup>1</sup>Department of Geosciences, University of Bremen, Germany.

<sup>2</sup>MARUM - Center for Marine Environmental Sciences, Bremen, Germany.

<sup>3</sup>Division of Geological and Planetary Sciences, California Institute of Technology, Pasadena, California, USA.

Submitted to “Geochemistry, Geophysics, Geosystems”.

### 5.1 Abstract

Radiocarbon differences between benthic and planktonic foraminifera (B-P ages) or radiocarbon projection ages (Adkins and Boyle, 1997) are frequently used to determine changes of the past ocean-circulation rate. A global 3D-ocean circulation model is used to study, which method is less influenced by atmospheric  $\Delta^{14}\text{C}$  variations. Three factors cause uncertainties, first the long equilibration time of the ocean subsequent to atmospheric  $\Delta^{14}\text{C}$

changes. Second, different mixing processes in the ocean, which cause an ocean response of smaller amplitude than the atmospheric forcing and third, the unknown source region of subsurface waters as well as their temporal reservoir-age variations.

The model suggests that B-P ages and projection ages have lower uncertainties the closer they are to deep-water formation zones. In the North Atlantic the B-P age method is less influenced by  $\Delta^{14}\text{C}_{atm}$  variations than the projection-age method. Projections ages vary less in the Pacific as long as atmospheric  $\Delta^{14}\text{C}$  decreases linearly. A more irregular atmospheric  $\Delta^{14}\text{C}$  evolution leads to age variations of similar magnitude with both methods. Based on the model experiment, we suggest a potential improvement of the projection-age method.

## 5.2 Introduction

Past ocean circulation changes are a matter of active research (Lynch-Stieglitz et al., 2007). Many proxies have been developed over the last several years to draw conclusions how ocean circulation rate differed from today, e.g. sortable silt (McCave et al., 1995) or Pa/Th (McManus et al., 2004). Still, one of the most frequently used methods remains the determination of past ocean-circulation rate from  $^{14}\text{C}$  differences between planktonic and benthic foraminifera at the same depth in a sediment core (Broecker et al., 1988; Shackleton et al., 1988; Duplessy et al., 1989). One potential error in the benthic-to-planktonic age difference (B-P age), often called top-to-bottom age, is the temporal change of atmospheric  $\Delta^{14}\text{C}$  ( $\Delta^{14}\text{C}_{atm}$ ) such as the irregular decrease of more than 300 ‰ during the last deglaciation. These  $\Delta^{14}\text{C}_{atm}$  variations will be visible in the surface ocean within a few months but it will take hundreds of years until the signal reaches some parts of the deep ocean.

To eliminate this source of error, Adkins and Boyle (1997) introduced a method which takes this circulation induced time lag into account. Three parameters are needed for the correction. First a calendar age estimate that can be derived from parallel U/Th dating in deep-sea corals or, less accurately, from reservoir effect corrected and calibrated  $^{14}\text{C}$  measurements in planktonic foraminifera. In addition, estimates of deep-water  $\Delta^{14}\text{C}$  and atmospheric  $\Delta^{14}\text{C}$  are required. Starting from deep sea  $\Delta^{14}\text{C}$  at a given calendar age,  $^{14}\text{C}$  decay is calculated backwards through time (projection). After a specific amount of “re-

verse” decay time the  $\Delta^{14}\text{C}$  value of the sample reaches the  $\Delta^{14}\text{C}$  level of the atmosphere. The corresponding difference between calendar age of the deep-sea sample and calendar age of intersection with the atmospheric curve finally should be corrected for the constant reservoir age of the source region to give the so-called “projection age”.

The projection-age method was applied for instance to the deep North Atlantic (Adkins et al., 1998), the northwest Pacific (Ahagon et al., 2003) and the western North Atlantic (Keigwin and Schlegel, 2002). However several uncertainties mentioned by Adkins and Boyle (1997) were never fully quantified or eliminated. The projection-age method was developed in a idealized and purely advective model that assumed direct atmosphere-ocean surface exchange without any reservoir-age effect. The deep ocean receives the water from the surface after a certain amount of time (ventilation age) using a closed system decay approach (no mixing of different water masses). Thus, the deep ocean  $\Delta^{14}\text{C}$  curve nearly mimicked the atmospheric curve with a time lag of the ventilation age (Fig. 1 in Adkins and Boyle, 1997).

Uncertainties in the projection-age method arise from mixing processes in the ocean and the reservoir age which varied spatially and temporally in the past (e.g. Bondevik et al., 2006; Hughen et al., 2006; Schimmelmann et al., 2006). The correction for the reservoir age is difficult because variations have only been reconstructed for a few locations and because of the largely unknown source region where water was subducted in the past. Another problem arises from the fact that atmospheric  $\Delta^{14}\text{C}$  variations can result from ocean-circulation changes and not only from production-rate changes (Adkins and Boyle, 1997). This has been shown e.g. for the Younger Dryas (Bondevik et al., 2006) and would result in an overestimation of both B-P and projection ages (Adkins and Boyle, 1997).

We use a coupled atmosphere-ocean circulation model to investigate the relationships between ventilation, B-P, and projection ages. The goal is to provide a guideline to which method works best at a given location, to highlight advantages and disadvantages of the methods, and to explore potential improvements of the projection-age method.

### 5.3 Model description and simulation setup

To test the projection-age concept we used the global scale UVic ESCM (University of Victoria Earth System Climate Model, Weaver et al. (2001)) in version 2.7. It consists

of a three-dimensional ocean general circulation model (Modular Ocean Model, version 2, Pacanowski (1995)) coupled to a two-dimensional energy-moisture balance model of the atmosphere (Fanning and Weaver, 1996) and a dynamic-thermodynamic sea ice model (Bitz et al., 2001). The horizontal resolution of all compartments is  $3.6^\circ$  in longitude and  $1.8^\circ$  in latitude, while the ocean has 19 levels of irregular depth, increasing from 50 m at the surface to 500 m at the deepest levels (Weaver et al., 2001; Meissner et al., 2003). It is driven by variations in solar insolation over a year at the top of the atmosphere. The wind stress at the ocean surface is prescribed from a monthly climatology (Kalnay et al., 1996). We used the option of a rotated grid in the North Atlantic Ocean to avoid convergence of the meridians at  $90^\circ\text{N}$ . Sub-gridscale mixing is included following the Gent and McWilliams (1990) parametrization for mixing associated with mesoscale eddies. Vertical diffusion is increasing from the surface to the deep ocean (Bryan and Lewis, 1979).

Radiocarbon was included as an additional tracer following the guidelines of the Ocean Carbon Modeling Intercomparison Project (OCMIP-2 Orr et al., 2000) in the ocean part of the model. The gas exchange with the atmosphere depends on the gradient between the atmosphere and the surface ocean, windspeed, sea-ice coverage and sea surface temperature. In the ocean the tracer is transported via diffusion and advection. A sink has been added to account for the  $^{14}\text{C}$  decay with a half-life of 5730 years. The atmosphere is treated with respect to  $^{14}\text{C}$  as one well mixed box. This assumption is justified because we investigate variations of centennial to millennial timescale while the atmospheric mixing time for  $^{14}\text{C}$  is on the order of some years.

The time elapsed since seawater was last exposed to the atmosphere is referred to as “age” in tracer oceanography (England, 1995). As a reference for comparison of  $^{14}\text{C}$  age with the ocean ventilation age we added a so-called ideal age tracer (Williams et al., 1995; England, 1995) to the model. Each time when the ideal age tracer reaches the ocean surface layer in the model it is reset to zero, assuming that it was exposed to the atmosphere when it made its way into the turbulent mixed surface layer. Below the surface layer the tracer ages, while transported and mixed like all other tracers.

We ran two simulations for different atmospheric  $\Delta^{14}\text{C}$  forcings using pre-industrial present day (PIPD) boundary conditions (insolation and land-ice for the year 1950 common era (C.E.) and an atmospheric  $\text{CO}_2$  content of 280 ppmv). The first simulation was the control



run with a constant  $\Delta^{14}\text{C}_{atm}$  of 0‰. It should assess the model ability to calculate the present day radiocarbon distribution in the ocean using modern boundary condition and highlight discrepancies between the different methods.

In the second experiment  $\Delta^{14}\text{C}_{atm}$  is linearly decreased over 5000 years from 0 to -100‰ (Fig. 5.3, model year 10,000–5000) as in Adkins and Boyle (1997). This generally decreasing trend in  $\Delta^{14}\text{C}_{atm}$  has been reconstructed for the last deglaciation (Reimer et al., 2004), but of course it was not as gradual and also not monotonic. Reconstructions show plateaus of constant  $\Delta^{14}\text{C}_{atm}$  as well as  $\Delta^{14}\text{C}_{atm}$  increases, e.g. in the Younger Dryas. To get one step closer to such conditions, we simulated what would happen if the  $\Delta^{14}\text{C}_{atm}$  increases for an interval of 1000 years by 20‰ and then decreases again afterwards linearly over 4000 years to -160‰ (Fig. 5.3, model year 5000–0). The entire 10,000 year long simulation was started from the control run and its steady state  $\Delta^{14}\text{C}$  in the atmosphere. In both experiments circulation induced  $\Delta^{14}\text{C}_{atm}$  changes were not simulated.

The “age” terms we use here are defined as follows. The reservoir age is the age difference between the atmosphere and the surface ocean (e.g. Cao et al., 2007). It is influenced by the gas exchange between atmosphere and ocean and the ocean circulation and mixing because upwelling  $^{14}\text{C}$  depleted water mixes with surface water. By definition the Suess effect corrected  $^{14}\text{C}$  age of the atmosphere in the year 1950 C.E. is zero (Keeling, 1979). This means the  $^{14}\text{C}$  age of the surface ocean layer is the same as the reservoir age in the control run where a value 0‰ has been set for the atmosphere. The reservoir age belonging to a subsurface water parcel depends on the location where it last had contact with the atmosphere. Because this location is often unknown, especially far away from deep-water formation zones, one can choose a local value, the global low latitude value of 400 years or a best-guess value for the appropriate sinking region. Although the projection-age method was never intended to use a spatially varying value that included low latitude upwelling regions, we use the local reservoir age to correct the model results for a better comparison with B-P ages. We call this “local reservoir age” while the “real reservoir age” would be the one in which the path of the water since it became subducted would be considered. The ventilation age is defined after Thiele and Sarmiento (1990) as the time elapsed since the water parcel left the surface ocean and contact with the atmosphere (“ideal age”).

It should be noted that the difference between a benthic and planktonic  $^{14}\text{C}$  age are based on the true half-life which is  $\sim 3\%$  larger than the Libby half-life.

## 5.4 Results

### 5.4.1 Control run

The different methods to estimate circulation age are compared for constant  $\Delta^{14}\text{C}_{atm}$  ( $= 0\text{‰}$ ) forcing (Fig. 5.1). A 3000 m depth level was chosen to show the ocean ventilation pattern uninfluenced by the bottom topography and above the calcite compensation depth in the Pacific (Berger, 1977). The B-P ages (Fig. 5.1c) are of similar magnitude as the ventilation ages (Fig. 5.1a) at a global scale. Anomalies of B-P ages to ideal ages in the Atlantic reach up to  $\sim 200$  years. In the Pacific they are up to twice as high (Fig. 5.2a).

To calculate the projection ages, the reservoir age of the source region is needed. If the local reservoir age would be assumed, projection ages would be nearly the same as B-P ages as long as  $\Delta^{14}\text{C}_{atm}$  is constant (Fig. 5.1c). In regions where surface  $^{14}\text{C}$  ages are strongly influenced by the upwelling of old water, the local reservoir age would contradict the original idea of projection ages. An estimate of how projection ages in these regions should look like are shown in Fig. 5.1d in which a global mean reservoir age of 400 years has been used for correction.

The projection age without reservoir-age correction which is identical to the  $^{14}\text{C}$  age at depth (Fig. 5.1b) shows a similar pattern than that of the ideal ages. Obviously the missing reservoir-age correction results in greater differences to the ideal ages than B-P ages. The necessary reservoir age correction can be assessed in the model, as long as  $\Delta^{14}\text{C}_{atm}$  is constant, from the difference plot of ideal age and the  $^{14}\text{C}$  age (Fig. 5.2b). The maximum offset of  $\sim 700$  years can again be found in the deep Pacific.

### 5.4.2 Experiment with decreasing atmospheric $\Delta^{14}\text{C}$

An experiment of linearly decreasing  $\Delta^{14}\text{C}_{atm}$  was used by Adkins and Boyle (1997) to show the advantage of the projection-age method. We simulate a comparable scenario from model year 10,000 to 5000 (Phase 1 in Fig. 5.3 and 5.4). The response of the ocean to the atmospheric forcing is shown at two locations in the northern Atlantic (Fig. 5.3a) and northern Pacific (Fig. 5.3b) at 3000 m depth. At most other oceanic locations the  $\Delta^{14}\text{C}$ -evolution curves fall somewhere in between these two extremes, only the initial oceanic  $\Delta^{14}\text{C}$  values, the time lag and the smoothing of the deep ocean  $\Delta^{14}\text{C}$ -curve varies between

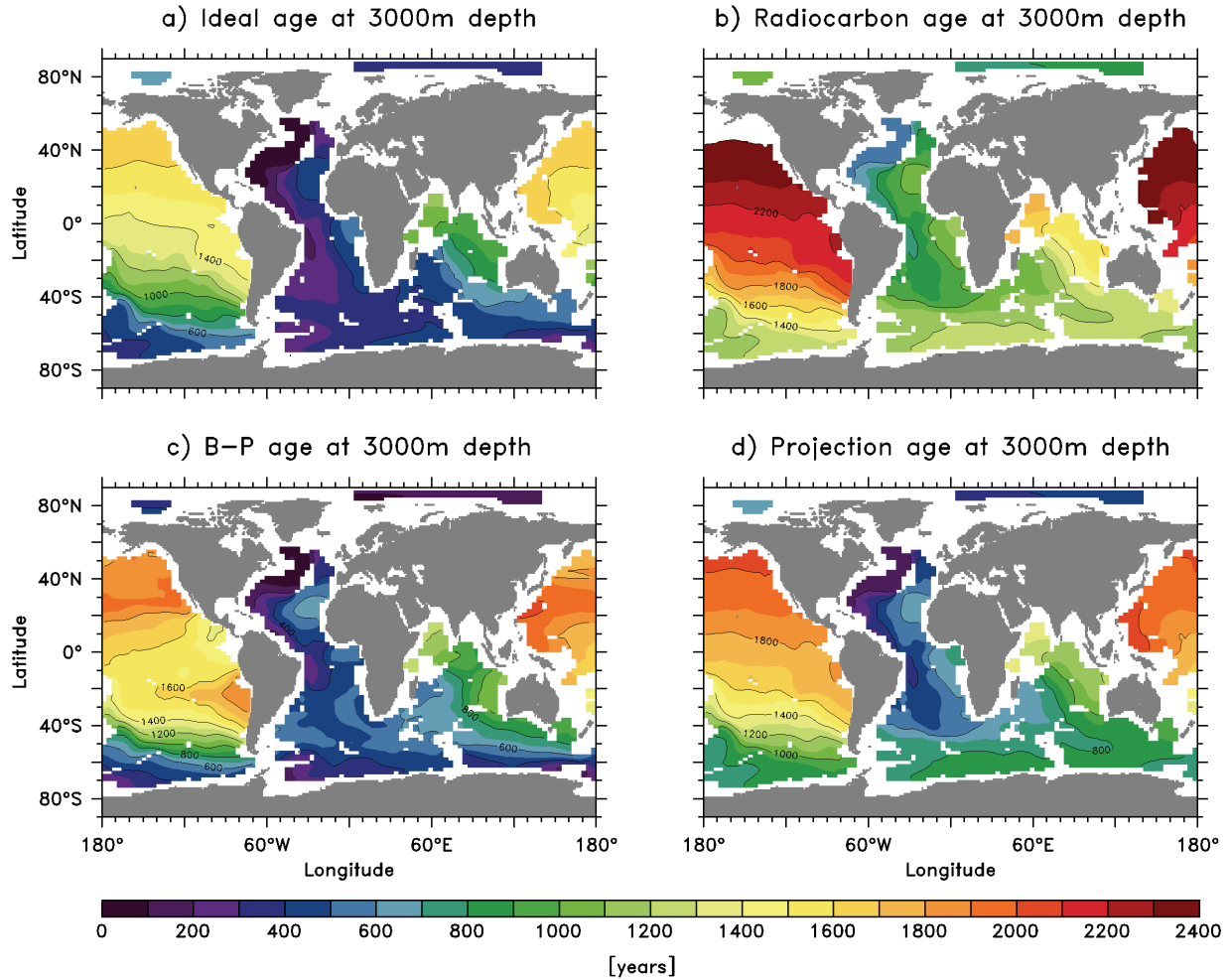


**Figure 5.1:** Maps from the simulation with constant  $\Delta^{14}C_{atm}$  and PD boundary condition at 3000 m depth. a) Modeled ideal/ventilation ages are calculated with a tracer that is always set to zero in the surface ocean layer of the model. b) Radiocarbon ages showing how projection ages without reservoir age correction would look like. They have the same pattern as the ideal ages in a) and indicate the difficulty to correct for the real reservoir-age effect. c) Conventional B-P ages, in this simulation nearly equal to the projection ages if they would also be corrected for a local surface reservoir age. d) Projection ages corrected for a global mean reservoir age 400 years.

locations. Noteworthy is the response of the deep ocean at the beginning of the  $\Delta^{14}C$  decrease. In the Atlantic it runs nearly parallel to the atmosphere, while in the Pacific, there is no sharp bend in the deep ocean  $\Delta^{14}C$ -curve. Instead it is a smoothed curve which reduces the difference between subsurface ocean and the atmospheric/surface ocean  $\Delta^{14}C$ . The way projection ages are calculated is indicated by the colored arrows (Fig. 5.3). Note that when comparing the temporal evolution curves in Fig. 5.4 all curves are referenced

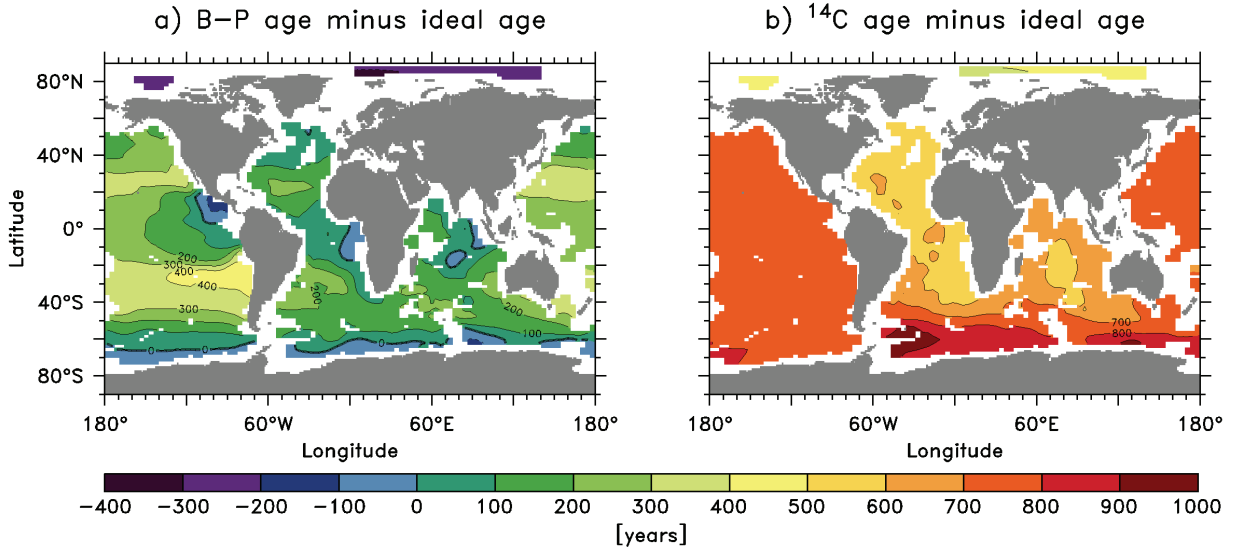


**Figure 5.2:** Anomaly maps for the control run. a) Difference between B-P ages (Fig. 5.1c) and ideal ages (Fig. 5.1a). b) Anomaly of  $^{14}\text{C}$  ages (Fig. 5.1b) to ideal ages (Fig. 5.1a). Here, the anomalies indicate the reservoir age for which the projection ages need to be corrected to show the ventilation age in case of constant  $\Delta^{14}\text{C}_{\text{atm}}$ .

to the time in the modeled deep ocean  $\Delta^{14}\text{C}$  where the projection started. As predicted and explained by Adkins and Boyle (1997) for the simplified scenario of a closed-system decay, B-P ages are generally decreasing when atmospheric  $\Delta^{14}\text{C}$  is decreasing (Fig. 5.4, model year 10,000 to 5000). B-P ages always drifts, although the circulation is constant. The drift in the northern Atlantic location is only very small after the initial shift to a lower reservoir age, while a faster B-P age drift continues in the Pacific as long as  $\Delta^{14}\text{C}_{\text{atm}}$  decreases linearly.

Original projection ages are calculated by finding the intersection of the  $^{14}\text{C}$ -decay trajectory with the atmospheric  $\Delta^{14}\text{C}$ -evolution curve (indicated by the red arrows in Fig. 5.3) and a subsequent correction for a constant reservoir age (dashed red arrows in Fig. 5.3). Because of the offset between surface ocean and atmospheric  $\Delta^{14}\text{C}$ , the decay trajectory intersects with an atmospheric  $\Delta^{14}\text{C}$  level too far back in time. At the beginning of the experiment the projection curve “catches” the flat part of the atmospheric curve while the deep-sea curve is already decreasing. The consequence is an increasing projection age at the beginning of the experiment at both locations before it slowly decreases back to the equilibrium value (Fig. 5.4).

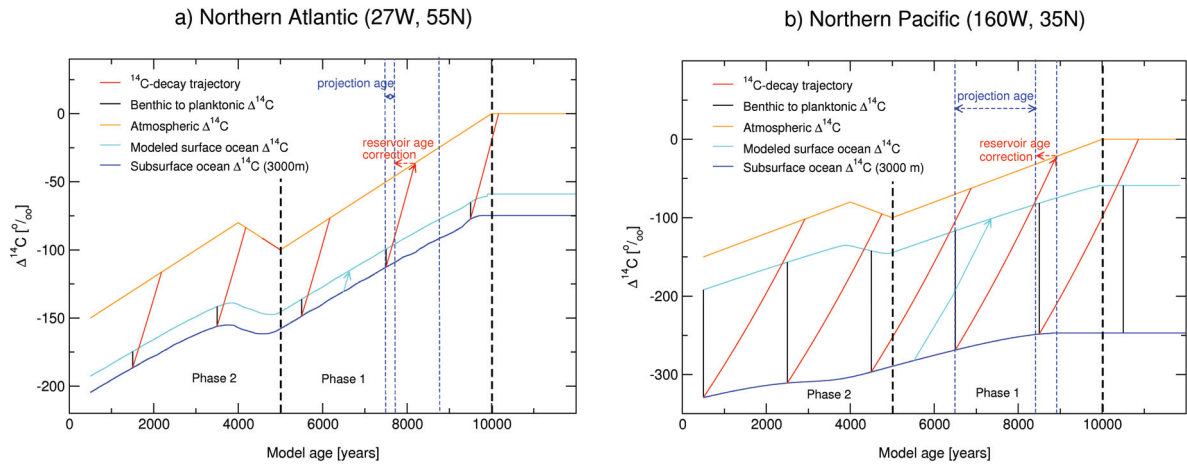


**Figure 5.3:** Response of the ocean to the  $\Delta^{14}\text{C}_{\text{atm}}$  forcing at two locations: a) the Atlantic: 27W, 55N and b) Pacific: 160W, 35N. The cyan curves show the fast response of the models surface ocean layer to the atmospheric forcing (orange curve). The blue curves below demonstrates the slow response of the deep ocean at 3000 m depth due to ocean circulation and mixing. The original projection ages are calculated by finding the intersection of the  $^{14}\text{C}$ -decay trajectory (red curve/arrow) with the orange atmospheric curve and a subsequent reservoir age correction (red dashed arrows). The projection age varies significantly if the  $^{14}\text{C}$ -decay trajectory to the intersection with the modeled surface ocean  $\Delta^{14}\text{C}$  is chosen (cyan arrow), instead of the atmospheric curve.

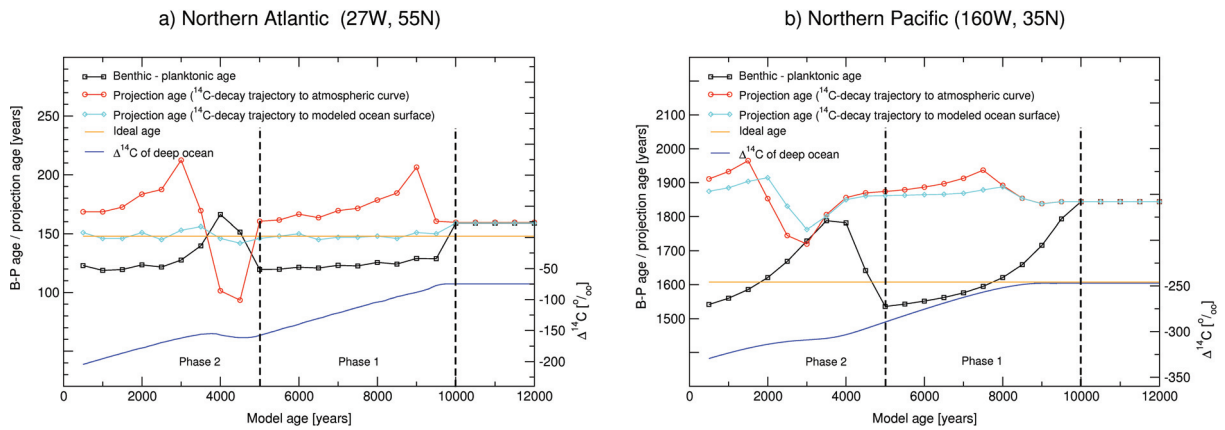


**Figure 5.4:** Temporal changes in the B-P ages and different ways to calculate projection ages, as they were indicated by the black lines and colored arrows in Fig. 5.3. All curves are referenced to the modeled deep ocean  $\Delta^{14}\text{C}_{\text{atm}}$  (blue curve). Changes in B-P ages are plotted in black, original projection ages (intersection of  $^{14}\text{C}$ -decay trajectory with atmospheric curve and subsequent reservoir age correction) in red and alternative projection ages (intersection of  $^{14}\text{C}$ -decay trajectory with modeled surface ocean curve) in cyan.

Additionally projection ages have been calculated by finding the intersection with the modeled surface ocean  $\Delta^{14}\text{C}$  curve (cyan curve in Fig. 5.3) at the same location. At the Atlantic location the curve is similar to the one of the B-P ages. Projection ages decrease when  $\Delta^{14}\text{C}_{atm}$  starts to decrease, but the amplitude of the variations is smaller than in the B-P ages (Fig. 5.4a). In contrast, the projection-age curve in the Pacific is similar to the original projection age method, but again the amplitude of the variations is smaller (Fig. 5.4b).

After 5000 years of linear  $\Delta^{14}\text{C}_{atm}$  decrease, B-P ages are  $\sim 50$  years too old in the North Atlantic and by more than 300 years in the North Pacific, compared to the ones from the control run and still have a decreasing trend. Projection ages shortly increased by  $\sim 50$  years in the North Atlantic and by  $\sim 100$  years in the North Pacific, but afterwards they returned to the constant equilibrium value again (Fig. 5.4).

Pacific projection ages are older than the ideal age and on the same level as B-P ages because of the reservoir age choice. Altogether it can be noticed that both methods show age variations, which are smaller in the Atlantic and larger in the Pacific.

### 5.4.3 Experiment with 1000-year long atmospheric $\Delta^{14}\text{C}$ increase

The atmospheric  $\Delta^{14}\text{C}$  increase between model year 5000 and 6000 (Phase 2 in Fig. 5.3 and 5.4) can be seen in the deep Atlantic ocean only slightly smoothed and with a small time lag with respect to the atmospheric forcing (Fig. 5.3b). In contrast, this atmospheric  $\Delta^{14}\text{C}$  peak hardly exists in the deep Pacific  $\Delta^{14}\text{C}$  evolution anymore. There is only a very little effect of reduced  $\Delta^{14}\text{C}$  decrease visible (Fig. 5.3a). Thus both, projection and B-P ages vary significantly over time.

The evolution of surface ocean and atmospheric  $\Delta^{14}\text{C}$  is also not parallel. This can be seen in the difference between the model surface  $\Delta^{14}\text{C}$  (cyan curve in Fig. 5.3) and the atmospheric  $\Delta^{14}\text{C}$  (orange curve in Fig. 5.3), indicating that reservoir ages vary rapidly in our simulation. The global mean reservoir age varies similar to the one in the northern North Atlantic region by more than 100 years caused by atmospheric  $^{14}\text{C}$  changes. The reservoir age in the Southern Ocean region shows higher variability by more than 200 years (Fig. 5.5).

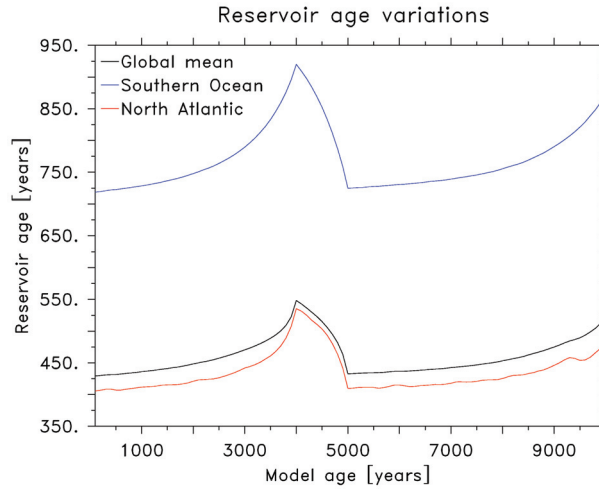


**Figure 5.5:** Global and local reservoir age variations due to atmospheric  $\Delta^{14}\text{C}$  variations: The global mean reservoir age (black curve) decreases by nearly 100 years in the 5000 years of linear  $\Delta^{14}\text{C}_{\text{atm}}$  decrease (model year 10,000–5000). When atmospheric  $\Delta^{14}\text{C}$  increases by 20‰, the reservoir age increases rapidly by over 100 years. Corresponding to the final  $\Delta^{14}\text{C}_{\text{atm}}$  decrease, reservoir-ages decrease again nearly as rapidly as they increased. These rapid variations occur due to the slow response of the huge oceanic reservoir to changes in the comparable small atmospheric reservoir. In the northern North Atlantic the reservoir age variations are only slightly larger than the global mean (red curve). A much higher variability of more than 200 years reservoir-age change occurs in the Southern ocean (blue curve).

Comparing projection and B-P ages, errors are shifted in time if the deep sea point is used as a reference (Fig. 5.4). Projection ages fall by  $\sim 50$  years in the Atlantic as  $\Delta^{14}\text{C}_{\text{atm}}$  increases over 1000 years. Coeval to the atmospheric  $\Delta^{14}\text{C}$  decrease they rapidly increase by more than 100 years. Afterwards they slowly return to the equilibrium level. In the Pacific the reaction is similar but has more than twice the amplitude and is shifted in time.

B-P ages increase just by  $\sim 50$  years in the Atlantic and then slowly return to the constant value they had in linear  $\Delta^{14}\text{C}_{\text{atm}}$  decrease experiment. In the Pacific B-P ages increase by  $\sim 300$  years before they start their decreasing trend again.

## 5.5 Discussion

### 5.5.1 Control run

Differences between projection/B-P age and ideal/ventilation age are caused by two factors. First deep-water parcels are not simply a translation of local surface waters, or surface waters with a global mean reservoir age, to the deep ocean. Accordingly, neither the difference between the surface and subsurface  $^{14}\text{C}$  ages nor the assumption of 400 years can eliminate the true reservoir-age effect. To arrive at a true ventilation age, the reservoir-age correction would have to be made for the region, at which the subsurface water parcel had its last contact with the atmosphere. For the deep northern Pacific this might be the Southern Ocean with its reservoir age of several hundred years. The greater the difference between local reservoir age (or 400 years) and true reservoir age, the larger the offset between B-P/projection age and ideal/ventilation age will be. This is the reason why the ideal age is close to the projection/B-P age in the Atlantic (Fig. 5.4a) and much smaller in the Pacific (Fig. 5.4b) where the applied reservoir-age correction is smaller than the real one of the source region.

The second factor is that  $^{14}\text{C}$  decays exponentially while at the same time water parcels which started to decay at different times and with different initial  $^{14}\text{C}$  concentrations are continuously mixed. Nonlinearity makes it impossible to eliminate this source of error. The more mixing between water masses of different ages occurs, the larger this error will be. Generally we expect more of this mixing to take place far away from deep-water production areas and only a little mixing close to them. In reality, we always find a combined effect of reservoir age and mixing errors that can hardly be separated.

The comparison of  $^{14}\text{C}$  age (Fig. 5.1b) with the ideal age (Fig. 5.1a) offers the opportunity to calculate the real offset between these ages. In the deep Atlantic, below 2000 m depth, there is a minimum age offset of around 500 years (Fig. 5.6b). This is the result of North Atlantic deep-water formation, where the surface water has a reservoir age of approximately  $\sim 400$  years and then entrains older local deep waters during sinking (Adkins and Boyle, 1999). Where ideal ages are larger, some locations line up at an offset of 750 years, which we interpret as an indication of a Southern Ocean source. Most locations that are not close to the deep-water formation areas, fall in between these two offsets and represent a mixing of the sources.



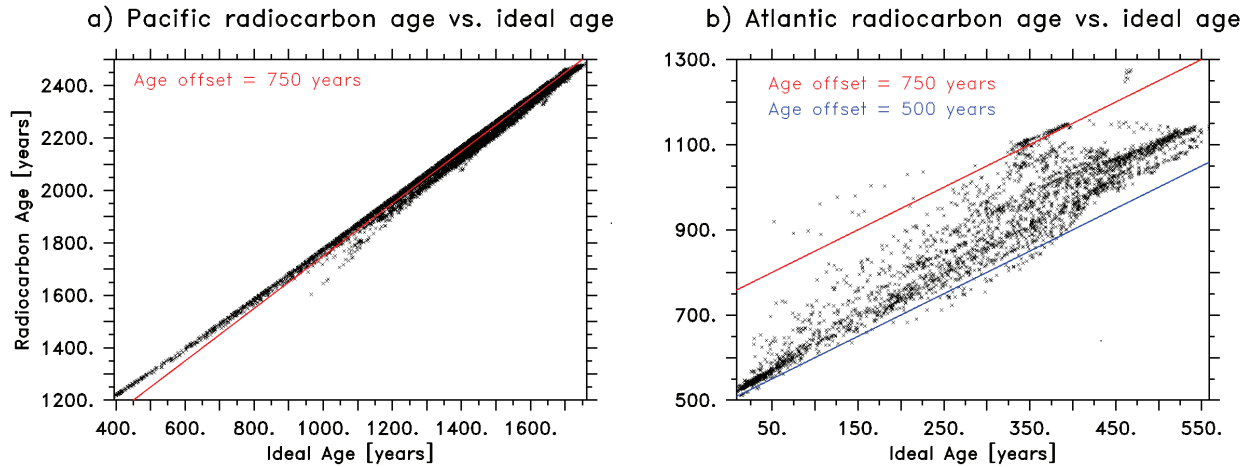


**Figure 5.6:** The points mark the offset between  $^{14}\text{C}$  age and ideal age in Pacific (a) and the Atlantic (b) below 2000 m depth. The age offset of around 500 years in (b) especially at low ideal ages is the result of North Atlantic deep-water formation. At higher ideal ages some locations line up at an offset of 750 years indicating a Southern Ocean source. Most locations, which are not close to the deep-water formation areas, fall in between these two offsets and represent a mixing of the sources. In the whole deep Pacific the offset is nearly the same, about 750 years. The model suggests, that  $^{14}\text{C}$  ages would be much closer to ventilation ages, if we would correct the deep Pacific  $\Delta^{14}\text{C}$  for Southern Ocean surface water instead of local one.

In contrast, the offset is nearly equal at 750 years over the whole Pacific below 2000 m depth (Fig. 5.6a). The origin of this water masses seems to be the Southern Ocean with its modeled reservoir ages of 600–1100 years. Southern Ocean reservoir ages are not “reset” to  $\sim 400$  years like in the North Atlantic because of their short surface-residence time (Adkins and Boyle, 1999). The model suggests that  $^{14}\text{C}$  ages would be much closer to ventilation ages, if we would correct the deep Pacific  $\Delta^{14}\text{C}$  for the Southern Ocean surface water reservoir age instead of the global mean of 400 years or a local surface ocean one. We will continue to discuss this approach in the context of transient  $\Delta^{14}\text{C}_{atm}$  variations.

### 5.5.2 Transient atmospheric $\Delta^{14}\text{C}$ variations

The initial projection age increase, when  $\Delta^{14}\text{C}_{atm}$  starts to decrease (Fig. 5.4), is related to the difference between ideal age and  $^{14}\text{C}$  age. If the projection to the atmospheric curve is done first and the reservoir age correction afterwards, the projection curve intersects

with the atmospheric curve too far in the past. For example, if one chooses a location in the deep northern North Pacific with an ideal age of  $\sim 1500$  years, the  $^{14}\text{C}$  age at the same location will be  $\sim 2200$  years, this way the flat part of the atmospheric curve could be the intersection point when the deep sea starting point of the projection is already decreasing because the 700 years reservoir age correction is done after the projection.

The opposite happens at the time of the atmospheric pulse when the deep ocean  $\Delta^{14}\text{C}$  already starts to increase while the projection curve still intersects with a decreasing part of the atmospheric curve, projection ages decrease. The amplitude of the projection age variation is a function of the amplitude of the deep ocean reaction to the pulse. This response is a combination of mixing effects and reservoir age variations. Another difference to Adkins and Boyle (1997), which seems to be of minor importance, is that the  $\Delta^{14}\text{C}$  at this location is not only influenced by advective transport. Due to mixing and diffusion the deep-water  $\Delta^{14}\text{C}$  changes faster than the advection timescale alone would suggest.

The B-P age curve in Fig. 5.4a and b show the same initial drop as the B-P age curve in Fig. 1f of Adkins and Boyle (1997). However, in Fig. 5.4b the B-P age in the Pacific curve continues to drop while the Atlantic one in Fig. 5.4a and the curve in Fig. 1f of Adkins and Boyle (1997) nearly level out after one ventilation age period. Adkins and Boyle (1997) assumed that a deep-water flow path is similar to advection in a pipe. Obviously this is nearly valid for the chosen Atlantic location in the UVic ESCM but not the case for the Pacific location which is far away from a deep-water formation area and cannot react quickly to atmospheric variations due to damping by the large volume of the ocean and mixing processes.

These processes are also influencing the projection ages but less than other uncertainties. Besides the intersection of the curves to far back in time, projection ages are influenced by unrecognised reservoir age changes.

### **The effect of reservoir-age variations**

B-P as well as projection age calculations are affected by temporal and spatial variations in the reservoir age. Reservoir-age variations can be caused by changes in the atmospheric  $^{14}\text{C}$  production rate, which result in rapid  $\Delta^{14}\text{C}_{atm}$  changes (Laj et al., 2002). Several thousand years of time would be needed to bring the large, slow responding oceanic  $^{14}\text{C}$

reservoir to a new equilibrium state. Until a new equilibrium is reached or as long as the  $^{14}\text{C}$ -production rate is still changing, reservoir ages will vary, too (see Fig. 5.5). Another reason for reservoir-age variations are ocean circulation changes. Both reasons can cause variations of several hundred years, e.g. as reconstructed for the last deglaciation (Cao et al., 2007; Sarin et al., 2007) or modeled for the last 45,000 years (Franke et al., subm.). Here, we focus on changes in the atmospheric  $^{14}\text{C}$  production, as circulation changes are not simulated.

To assess “real” reservoir ages corresponding to a subsurface water parcel, the following information would be required: A surface reservoir-age distribution for the time period of interest and the source region of the subsurface water parcel. One way to determine the contributing source region would be trajectories or transit-time distributions (Peacock and Maltrud, 2006). Their calculation for different circulation states that might have occurred in the late Quaternary might become a promising approach in future. Until now, transit-time distributions have only been determined for the present day state of the ocean. The knowledge about past reservoir-age variations is very scarce, too. Deep sea coral research might solve this part in the future because they recorded temporal  $^{14}\text{C}$  variations at depth. For the North Atlantic there are already measurements (Cao et al., 2007; Eltgroth et al., in prep.). Reconstructions for the Southern Ocean are still lacking. Together with conservative tracer reconstruction, the  $^{14}\text{C}$  measurements on deep sea corals offer a second opportunity to assess mixing effects and reservoir age of the source regions (see section 5.5.2 and Fig. 5.7).

Temporal reservoir age variations (Fig. 5.5) are not taken into account in the original projection-age method. When using a constant reservoir age, the advantage of projection ages compared to B-P ages are regions where reservoir-age variations are small compared to the ventilation age. Because the planktonic surface ocean  $^{14}\text{C}$  value is used in the calculation, B-P ages implicitly consider the local surface-ocean reservoir age. As discussed in Adkins and Boyle (1997), the disadvantage to this method is that ages contain a time lag, but they take the reservoir-age variation partly into account. This is an advantage if reservoir ages change over a longer period in the same direction as the ventilation ages. In regions where the time lag is small in relation to the reservoir-age variations (e.g. in the northern North Atlantic),  $\Delta^{14}\text{C}_{atm}$  variations will influence B-P ages less than projection ages. On the one hand, when atmospheric  $\Delta^{14}\text{C}$  decreases or increases faster than in this simulation, the reservoir-age variations become larger, which would give an advantage to

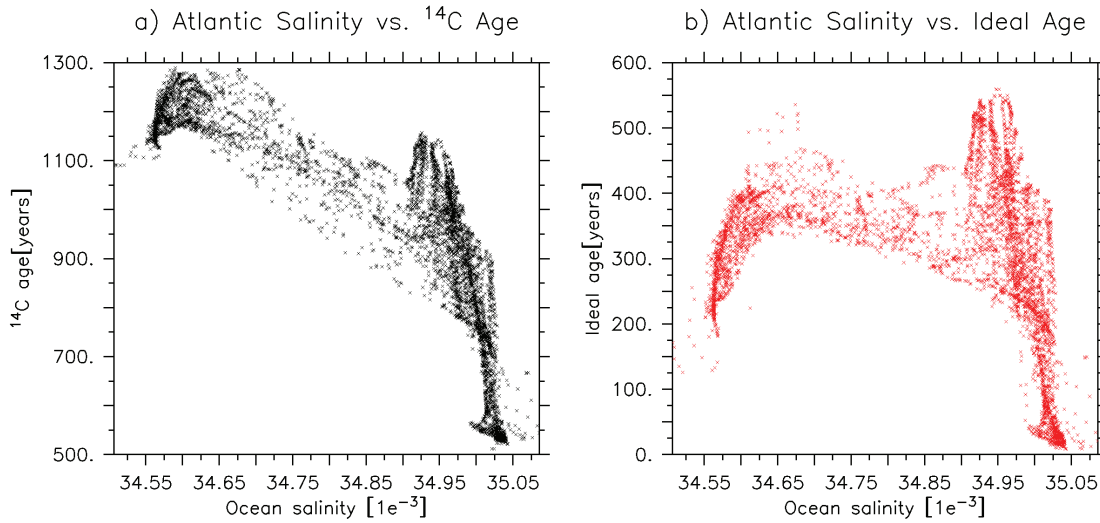


**Figure 5.7:** a) Modeled  $^{14}\text{C}$  age vs. salinity in the Atlantic Ocean (65W–20E, 65N–80S) between 2000 and 4000 m depth. b) Modeled ideal age vs. salinity for the same region.

the B-P age method. On the other hand, in this scenario the time lag introduced error is also becoming larger, giving the projection-age method an advantage. These opposite effects mean that both methods become worse the faster an atmospheric change occurs.

### The effect of ocean mixing

Mixing affects both methods, B-P age and projection age, too. It can be divided into two processes in this context. The first is damping of the atmospheric pulse by limited atmosphere-ocean gas exchange and by diffusion in the deep-sea; in this sense the ocean operates like a low-pass filter. The second is mixing of water-masses with different initial  $^{14}\text{C}$  ages. Both processes together (simply called “mixing” in the following) lead to a subsurface ocean  $\Delta^{14}\text{C}$  time evolution that is a smoothed version of the atmospheric one, e.g. the deep Pacific  $\Delta^{14}\text{C}$  in Phase 2 is hardly increasing relative to the simulated atmospheric pulse (Fig. 5.3b). If the temporal evolution of the subsurface ocean is not parallel to the surface ocean, mixing influences B-P ages in addition to the time lag problem. In a similar way, projection ages are affected by these diverging or converging curves (Fig. 5.3).

The two locations discussed until now are mainly influenced by one deep-water source region. However, much of the interesting oceanography and much of the existing paleo-data comes from regions of the ocean where two deep-water masses are mixing from separate outcrop regions in the north and the south. B-P and projection age variations in the South Atlantic (25W, 20S at 3500 m depth), where both NADW and AABW source waters mix, have characteristics of both previous shown location (Fig. 5.8). B-P ages fall to a nearly stable smaller age like in the North Atlantic, only the offset compared to the equilibrium is larger because of the longer time lag. Projection ages increase again initially and then slowly decrease because of decreasing reservoir ages. The ideal age differs in the South Atlantic much more from B-P age ( $\sim 200$  years, Fig. 5.8) than in North Atlantic ( $\sim 10$  years, Fig. 5.4a). This is caused by the influence of AABW which source region has a higher reservoir age than the local surface at this spot.

If there would be only one deep-water production zone  $^{14}\text{C}$  could be a good ventilation age tracer, mixing between different sources limits this capability. In Fig. 5.7a deep sea  $^{14}\text{C}$  of the Atlantic Ocean was plotted against the conservative tracer salinity. In the North Atlantic with a salinity of 35 psu  $^{14}\text{C}$  ages of 500 years were simulated. Moving southward from the northern North Atlantic salinity decreases the more both water masses mix. At

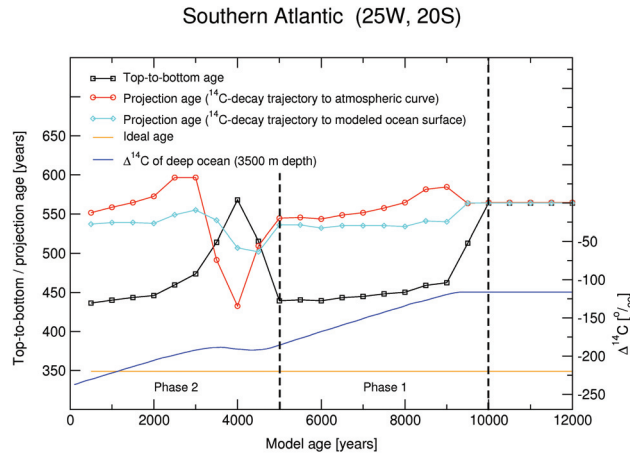


**Figure 5.8:** Changes in the B-P ages and projection ages in the southern Atlantic (25W, 20S). All curves are referenced to the modeled deep ocean  $\Delta^{14}\text{C}_{\text{atm}}$  at 3500 m depth (blue curve). Changes in B-P ages are plotted in black, original projection ages (intersection of  $^{14}\text{C}$ -decay trajectory with atmospheric curve and subsequent reservoir age correction) in red and projection ages (intersection of  $^{14}\text{C}$ -decay trajectory with modeled surface ocean curve) in cyan.

the same time  $^{14}\text{C}$  decays as long as the water is isolated from the surface. Between a salinity of 35 psu and 34.9 psu there is a steep, nearly linear age increase. This represents the North Atlantic deep-water mass, which fills most of the northern Atlantic. The highest  $^{14}\text{C}$  ages are reached in the eastern basin of the southern Atlantic down to Walvis Ridge. In the Atlantic sector of the Southern Ocean with a salinity of around 34.6 psu oldest water range between 1100 and 1300 years (Fig. 5.7a) although Fig. 5.7b shows that it is freshly ventilated young water. This way mixing and the subsequent different initial values of the northern and southern source region limit the  $^{14}\text{C}$  ability as an age tracer.

### 5.5.3 Assessing potential sources of error

The ocean circulation in our model simulations is time-independent, causing the errors that result from mixing of water masses to be time-independent, too. As shown for the reservoir age, the results are strongly dependent on the  $\Delta^{14}\text{C}_{atm}$  variations. If the  $\Delta^{14}\text{C}_{atm}$  decrease is faster, the subsurface, surface ocean and atmosphere  $\Delta^{14}\text{C}$  curves converge faster. The system is further away from equilibrium because the decay of  $^{14}\text{C}$  is too slow to follow the  $\Delta^{14}\text{C}$  in the atmosphere. Periods of such fast  $\Delta^{14}\text{C}_{atm}$  decrease occurred during the last deglaciation. In this case mixing will become less important compared to the overall projection-age shift. In contrast, during periods of quite stable  $\Delta^{14}\text{C}_{atm}$  and reservoir ages, mixing will be the important error source in the ventilation age estimation. Thus, it would not make sense to quantify error sources in detail for one special model simulation because their relative contribution to the overall error will vary in any single case. Although we are far away from a worst case model scenario and do not involve the complicated natural  $\Delta^{14}\text{C}_{atm}$  evolution with much more variations, we already see offsets in the projection and B-P ages of up to 400 years in the Pacific compared to the control run.

In the Atlantic both methods work well, in the northern North Atlantic the B-P age method appears to be superior because the time lag between surface and deep ocean is small (Fig. 5.3b). Mixing of different water masses is unimportant as well. Thus, taking the reservoir-age variations in form of a planktonic age into account is a big advantage.

In the Pacific both methods have large uncertainties of similar magnitude. The B-P ages are influenced by the time lag between the occurrence of an atmospheric signal in the

surface and the deep ocean. Reservoir age variations and the projection to an atmospheric  $\Delta^{14}\text{C}$  to far back in time mainly cause the errors in the projection-age method.

In our model simulation both methods have little uncertainties close to deep-water formation zones and in time periods and regions of little reservoir-age variations, which unfortunately mostly disagree with deep-water production zones. They have large uncertainties where deep water has been isolated from the surface for a long time and in time periods of fast  $\Delta^{14}\text{C}_{atm}$  changes.

#### 5.5.4 Improved projection-age method

Some systematic errors already cause differences between ideal and the projection/B-P ages in the control run, further ones arose from  $\Delta^{14}\text{C}_{atm}$  variations. In the following we will present a potential improvement of the projection-age method.

Reservoir ages need to be chosen depending on the source region of the water mass, especially where local and real reservoir age differ significantly like in the parts of the Pacific where the source region is the Southern Ocean. Furthermore the temporally constant reservoir age should be replaced by a varying one for the past. In the North Atlantic there are already some reconstructions (Cao et al., 2007; Eltgroth et al., in prep.). A temporal history of Southern Ocean reservoir age does not exist by now, but deep-sea coral  $^{14}\text{C}$  reconstructions will close this gap in the nearby future. In regions where NADW and AABW mix, the source region reservoir age can never be estimated perfectly due to non linearity in the  $^{14}\text{C}$  decay. Nevertheless temperature or salinity reconstructions can help to assess the relative portion of northern and southern source water. As first suggested by Adkins and Boyle (1999), the relationship of salinity and  $^{14}\text{C}$  in Fig. 5.7a indicates that these conservative tracer reconstructions could be used to make a guess, how the end member  $^{14}\text{C}$  might have mixed. Knowing both end members would then allow for a time dependent reservoir-age correction.

Another improvement addresses the projection to far back in time to the atmospheric  $\Delta^{14}\text{C}$  curve and an improvement to an additional error source, which has not been mentioned yet. The atmospheric  $\Delta^{14}\text{C}$  curve (e.g. INTCAL04 Reimer et al., 2004) has many high frequency variations, especially in the time period where it is based on tree-ring measurements. The surface ocean reacts more slowly than the atmosphere to  $^{14}\text{C}$  production-rate

changes, which smoothes the atmospheric signal. If the atmospheric curve is used, all high frequency variations will cause errors. A alternative way would be to take the mean ocean surface  $\Delta^{14}\text{C}$  curve, e.g. MARINE04 (Hughen et al., 2004a), to get rid of short term atmospheric variations, which are filtered by the atmosphere-ocean gas exchange (Cook, 2006).

If MARINE04 or a comparable product is used instead of the atmospheric curve, a reservoir age which is already included in the correction curve has to be taken into account (Hughen et al., 2004a). A second correction to adapt the reservoir age of the source region might be necessary. This procedure has the advantage that the projection will lead directly to a surface ocean curve and therefore will not go to far back in time. This will make projection ages much more stable if the reservoir-age correction is made prior to the projection.

Reservoir-age variations in the MARINE04 dataset contain uncertainties until 10.5 kyr BP and a constant reservoir age is applied for the time period before (Hughen et al., 2004a). An option to include reconstructed reservoir-age variations would be a time-series of parallel  $^{14}\text{C}$  and  $^{230}\text{Th}/^{234}\text{U}/^{238}\text{U}$  measurements on shallow water corals. Then a projection-age method can be applied using the well known surface ocean curve from the shallow water coral. Unfortunately shallow water corals do not grow in deep-water formation zones. Thus, another correction for the reservoir age difference between the source region of the deep water and the region where the shallow water coral grow is necessary. The reservoir-age variations will also probably be underestimated because reservoir ages are more variable in high latitudes, but in principal this is a way to combine the advantages of both methods by making the time lag correction like in the projection method and taking the local surface ocean with its partly resolved reservoir-age variations into account like in the B-P method.

The projection ages build to the intersection with the model  $\Delta^{14}\text{C}$ -evolution curve of the surface ocean are least influenced by  $\Delta^{14}\text{C}_{atm}$  variations at any time and location (cyan curve in Fig. 5.3). Errors related to mixing and not taking the “real” temporally varying reservoir age into account stay the same. Thus, there are still projection-age variation, especially in the Pacific (Fig. 5.4a), although the ocean circulation is not changing.



## 5.6 Conclusions

Both, the method of B-P ages as well as the projection-age method, have uncertainties which make it doubtful to interpret age variations as true ventilation-age changes. It has always to be checked if the atmospheric  $^{14}\text{C}$  production rate could be responsible for the  $\Delta^{14}\text{C}_{atm}$  variation. It should be considered that the Atlantic is less influenced than the Pacific by damping of the atmospheric variations and the difference between “local” reservoir age and the “real” one of the source region. Therefore Pacific age predictions are more sensitive to atmospheric  $\Delta^{14}\text{C}$  variations, no matter which method is used.

The projection-age method (Adkins and Boyle, 1997) was oversimplified in sense of reservoir ages and ocean mixing. After some improvements, using an ocean surface  $\Delta^{14}\text{C}$  curve and new reconstructions of source region reservoir-age histories it has potential as a tool to show circulation changes based on  $^{14}\text{C}$  reconstructions, which are only slightly influenced by atmospheric  $\Delta^{14}\text{C}$  variations.



# Chapter 6

## Discussion

The integration of radiocarbon as an additional tracer into the ocean part of the University of Victoria Earth System Climate model allows to study the influence of atmospheric  $^{14}\text{C}$ -concentration changes on  $^{14}\text{C}$  variations in the ocean. This is used to investigate temporal and spatial reservoir-age variations in the past 45 kyr (Chap. 3) and to assess the potential of  $^{14}\text{C}$  as a tool to reconstruct past ocean-circulation changes (Chap. 5).

Reservoir ages are modeled for two different ocean circulation states and using two different forcings of atmospheric  $^{14}\text{C}$  (Chap. 3). The production-rate forcing prescribes the major cause for reservoir-age changes and the calculations are fully consistent in the way they are integrated in the model, but this forcing excludes consequences of carbon-cycle changes, such as variations of deep-water formation in the North Atlantic. The  $\Delta^{14}\text{C}_{atm}$  forcing on the other hand implicitly includes all factors that influenced the atmospheric  $\Delta^{14}\text{C}$  variations, but to generate this dataset constant low latitude reservoir ages have been assumed between 45 and 12.4 kyr BP, a spline is interpolated through data with large scatter and the calculation is not fully consistent in the way of handling all  $\Delta^{14}\text{C}_{atm}$  changes as if they were caused by production-rate variations. Due to this, the experiments with the reduced AMOC need to be interpreted for both atmospheric forcings, if the trigger of the  $\Delta^{14}\text{C}_{atm}$  variation can be related to an ocean-circulation or other carbon-reservoir size change.

The model results tend to be in the lower range of possible reservoir-age variations. Periods of strong reductions or shutdowns of the NADW formation, as reported during Heinrich events (Elliot et al., 2002; Keigwin and Lehman, 1994), caused large reservoir-

age variations (Sarnthein et al., 2007), which are simulated in this work. On the one hand using the  $^{14}\text{C}$  production-rate forcing does not show reservoir-age variation initiated by carbon-cycle changes. On the other hand the atmospheric  $\Delta^{14}\text{C}$  forcing also causes underestimated reservoir-age variations because of the spline interpolation which smoothes the reconstructed variations of  $\Delta^{14}\text{C}_{atm}$  (Sect. 3.3).

Modeled reservoir-age variations for the Holocene are expected to have the smallest uncertainties using the  $\Delta^{14}\text{C}_{atm}$  forcing because the  $\Delta^{14}\text{C}_{atm}$  is known quite precisely for this period and given that the carbon-reservoir sizes were relatively constant and similar to PD. The further back in time, the larger the uncertainties, due to increasing errors in the forcing and divergence of the carbon reservoir sizes from the PD state. The production-rate forcing is found to have an advantage between 27 and 45 kyr BP, where the interpolation of the spline through the  $\Delta^{14}\text{C}_{atm}$  reconstructions caused uncertainties (Sect. 3.3).

The scatter between the different  $\Delta^{14}\text{C}_{atm}$  reconstructions might itself be influenced by the assumption of constant reservoir ages, when marine measurements were converted to an atmospheric  $\Delta^{14}\text{C}$  value. The model experiments of temporally varying  $\Delta^{14}\text{C}_{atm}$  show that  $^{14}\text{C}$  production-rate variations can have shifted low latitude reservoir ages by a few hundred years. Additional reservoir-age changes might have occurred at locations where reconstructions were made, if an ocean-circulation change led to the influx of another water mass with a different reservoir age.

These model experiments present the current state of knowledge and are a useful instrument to correct for the reservoir age of marine samples. However, the applicability of the model results to improve calibration curves is restricted. Concerning the  $\Delta^{14}\text{C}$  forced experiment, the results of this simulation cannot be used to improve calibration curves for marine data, given that the calibration curve itself is used as a forcing factor. In case of the production-rate forcing, there is still too much uncertainty about carbon-cycle changes to improve the atmospheric calibration curves. Another factor are the large error bars of the  $^{14}\text{C}$  dating technique, which prior to 15 kyr BP can exceed  $\pm 100$  years.

Radiocarbon is also a powerful tracer to assess the ocean circulation and its changes (Chap. 5), but merely using  $^{14}\text{C}$  as a tracer to distinguish the past ocean circulation can be misleading, if the gas exchange was enhanced such as in the case of stronger winds (Wunsch, 2003a). The age difference between surface-ocean and deep-sea water, top-to-bottom age, would in contrast allow to draw conclusions on the circulation because

the differences in the gas exchange would be taken into account via the surface-ocean age. Top-to-bottom ages are influenced by variations of  $\Delta^{14}\text{C}_{atm}$  and thus their change is also no clear indication of a circulation change. The projection-age method (Chap. 5) was invented to circumvent this problem but it involves new uncertainties caused by neglecting mixing processes in the ocean and assuming constant reservoir ages to make the method practicable.

Comparing the top-to-bottom and projection-age method in a model simulation demonstrates that both methods are influenced by atmospheric  $\Delta^{14}\text{C}$  variations. They are more affected in the North Pacific than in the North Atlantic, indicating that the distance between the sampling location and the deep-water formation region is a crucial factor. In case of a long continuous trend in atmospheric  $\Delta^{14}\text{C}$ , the projection-age method has the advantage not to produce a similar long term trend in the projection ages. In the North Pacific, the projection-age method is less affected by  $\Delta^{14}\text{C}_{atm}$  changes than the top-to-bottom age method. The reason is that the high ventilation age of the deep water allows for a significant change in the local surface ocean  $\Delta^{14}\text{C}$  since the deep water was produced. In the North Atlantic this time lag is less important and the long term trend in the top-to-bottom ages is small. Hence, the uncertainties of the projection-age method are more notable. This is mainly the initial projection-age increase due to the projection to the reconstructed atmospheric  $\Delta^{14}\text{C}$  curve. The projection reaches too far back in time to a wrong  $\Delta^{14}\text{C}_{atm}$  value because the reservoir-age correction is applied after the projection (Chap. 5). This causes top-to-bottom ages to be slightly more robust than projection ages in the North Atlantic.

When the  $\Delta^{14}\text{C}_{atm}$  evolution is more irregular, as reconstructed for the past, both methods indicate apparent age variations in the same order of magnitude. This complicates the interpretation of circulation changes on the basis of top-to-bottom and projection-age variations. It is thus essential to verify that the apparent age change cannot be explained by an atmospheric  $\Delta^{14}\text{C}$  variation.

An advantage of top-to-bottom ages is that they can be achieved with less input data, for instance in sediment cores by dating benthic and planktonic organisms in the same layer. In order to calculate a projection age an alternative dating method needs to be applied to obtain a real calendar age. This might be impossible in many cases or require further assumptions that introduce additional uncertainty. For the projection-age method it is

optimal to use corals that can be dated using both the U/Th and the  $^{14}\text{C}$  method.

The projection-age method has the potential to be improved as more of the required input information is reconstructed, which was lacking when this method was formulated originally. A major improvement would be the substitution of the atmospheric  $\Delta^{14}\text{C}$  history, which causes an initial projection-age increase at every  $\Delta^{14}\text{C}_{atm}$  variation, by a curve of the marine  $\Delta^{14}\text{C}$  evolution. Conservative tracer reconstruction can help to distinguish mixing of different water masses to estimate the source region or regions of the deep water. Then, reservoir age reconstructions from deep-sea coral  $^{14}\text{C}$  measurements close to deep-water formation regions (Eltgroth et al., 2006; Cao et al., 2007) or the modeled reservoir ages can replace the previously used constant reservoir ages. Removing all these error sources, such a revised projection age method promises to be more robust regarding  $\Delta^{14}\text{C}_{atm}$  variations than the top-to-bottom age method or the original projection-age method.

# Chapter 7

## Conclusions and outlook

This study proved that reservoir ages can be modeled spatially differentiated for all oceans and for the entire time period of  $^{14}\text{C}$  dating, using an earth system climate model of intermediate complexity. The following insights have been gained:

- Reservoir-age variation during the past 45 kyr occurred globally at the same time.
- The amplitude of the reservoir-age variations due to  $\Delta^{14}\text{C}_{atm}$  variations depends on the location and ranges from  $\sim 300$  years in a few subtropic regions to  $\sim 1000$  years in the Southern Ocean.
- LGM boundary conditions cause a  $\sim 30\%$  reduced North Atlantic deep water formation in the model and increase reservoir ages globally between  $\sim 100$  years in low and mid latitudes and up to 500 years in high latitudes.
- The  $^{14}\text{C}$  production-rate forcing leads to reliable reservoir-age variations in periods of relatively constant carbon-reservoir sizes such as in the Holocene and in periods of uncertain  $\Delta^{14}\text{C}_{atm}$  reconstructions, such as between 27 and 45 kyr BP.
- Reservoir-age variations caused by changes of carbon-reservoir sizes, which occurred at the end of the last glacial and the last deglaciation (between 27 and 10 kyr BP) can only be estimated using a  $\Delta^{14}\text{C}_{atm}$  model forcing.

The modeled reservoir-age variations confirm reconstructions of the large reservoir-age variability exceeding a thousand years at high latitudes. At low latitudes the model

simulates reservoir-ages variations of a few hundred years. This suggests that a reservoir-age correction cannot be neglected at low latitudes. Instead, it has to be applied at any location, where a marine sample is dated using the  $^{14}\text{C}$  method. Therefore, the modeling results are a tool to assess past reservoir ages and to improve  $^{14}\text{C}$  dating in regions, depth levels and time periods, where no reconstructions exist.

Atmospheric  $^{14}\text{C}$  calibration curves, which are generated from tropical and subtropical marine  $^{14}\text{C}$  reconstructions neglecting low latitude reservoir-age variations, reveal additional uncertainty by the modeled variations. The potential of the model simulation to improve the current calibration curves is however limited.

To allow for more accurate reservoir-age modeling in the future major transient changes in the carbon cycle could be simulated in the model. To do that more research is needed to understand the reconstructed glacial  $\Delta^{14}\text{C}_{atm}$  levels and the variations in detail. Likewise, the models would also need to be able to simulate all these reconstructed variations.

When  $^{14}\text{C}$  is used as a proxy to reconstruct past ocean-circulation changes, all existing methods involve different uncertainties. Comparing the top-to-bottom and projection-age method in a model simulation allowed to assess how both methods are influenced by atmospheric  $\Delta^{14}\text{C}$  variations:

- The top-to-bottom age method as well as the projection-age method are influenced by  $\Delta^{14}\text{C}_{atm}$  variations of the same order of magnitude.
- Both methods are less influenced by atmospheric  $\Delta^{14}\text{C}$  variations the closer the samples are located to a deep-water formation area.
- An advantage of the projection-age method is that it does not show a long-term trend if such a trend exists in  $\Delta^{14}\text{C}_{atm}$ . The correction for the time lag until an atmospheric signal reaches the deep ocean makes it preferable in regions of old water.
- Top-to-bottom ages have slight advantages close to deep-water formation sites, because they take the surface ocean into account and the aforementioned time lag is not very important.



The top-to-bottom age method can be applied having relatively little information but the potential to improve the method seems to be limited. In contrast, the original projection-age method was oversimplified to be suitable because it requires more input information. Constantly increasing input data as more reconstructions are performed and further development of the method, in particular the substitution of the atmospheric  $\Delta^{14}\text{C}$  evolution by a marine one, appears to be a promising approach to improve the projection-age method. Thus, an updated projection-age method can be more robust regarding to  $\Delta^{14}\text{C}_{atm}$  variation and the quality of  $^{14}\text{C}$  as a proxy in paleoceanography can be improved.



# Bibliography

- Adkins, J., Cheng, H., Boyle, E. A., Druffel, E. R. M., and Edwards, R. L.: Deep-Sea Coral Evidence for Rapid Change in Ventilation of the Deep North Atlantic 15,400 Years Ago, *Science*, 280, 725–728, 1998.
- Adkins, J. F. and Boyle, E. A.: Changing atmospheric  $\Delta^{14}\text{C}$  and the record of deep water paleoventilation ages, *Paleoceanography*, 12, 337–344, 1997.
- Adkins, J. F. and Boyle, E. A.: Age screening of deep-sea corals and the record of deep North Atlantic circulation change at 15.4 ka, in: *Reconstructing Ocean History: A Window Into the Future*, edited by Mix, A. A., pp. 103–120, Springer, New York, 1999.
- Ahagon, N., Ohkushi, K., Uchida, M., and Mishima, T.: Mid-depth circulation in the northwest Pacific during the last deglaciation: Evidence from foraminiferal radiocarbon ages, *Geophysical Research Letters*, 30, 1–4, 2003.
- Andersen, K. K., Svensson, A., Johnsen, S. J., Rasmussen, S. O., Bigler, M., Röthlisberger, R., Ruth, U., Siggard-Andersen, M.-L., Steffensen, J. P., Dahl-Jensen, D., Vinther, B. M., and Clausen, H. B.: The Greenland Ice Core Chronology 2005, 15-42 ka. Part 1: constructing the time scale, *Quaternary Science Reviews*, 25, 3246–3257, 2006.
- Austin, W. E. N., Bard, E., Hunt, J. B., Krooni, D., and Peacock, J. D.: The  $^{14}\text{C}$  age of the Icelandic Vedde ash: Implications for Younger Dryas marine reservoir age corrections, *Radiocarbon*, 37, 53–62, 1995.
- Bard, E.: Correction of accelerator mass spectrometry  $^{14}\text{C}$  ages measured in planktonic foraminifera: paleoceanographic implications, *Paleoceanography*, 3, 635–645, 1988.
- Bard, E., Arnold, M., Mangerud, J., Paterne, M., Labeyrie, L., Duprat, J., Mélières, M.-A., Sønstegaard, E., and Duplessy, J.-C.: The North Atlantic atmosphere-sea surface

- $^{14}\text{C}$  gradient during the Younger Dryas climatic event, *Earth and Planetary Science Letters*, 126, 275–287, 1994.
- Bard, E., Raisbeck, G. M., Yiou, F., and Jouzel, J.: Solar modulation of cosmogenic nuclide production over the last millennium: comparison between  $^{14}\text{C}$  and  $^{10}\text{Be}$  records, *Earth and Planetary Science Letters*, 150, 453–462, 1997.
- Bard, E., Arnold, M., Hamelin, B., Tisneratlaborde, N., and Caboich, G.: Radiocarbon calibration by means of mass spectrometric  $^{230}\text{Th}/^{234}\text{U}$  and  $^{14}\text{C}$  ages of corals: An updated database including samples from Barbados, Mururoa and Tahiti, *Radiocarbon*, 40, 1085–1092, 1998.
- Bard, E., Rostek, F., and Ménot-Combes, G.: Radiocarbon calibration beyond 20.000  $^{14}\text{C}$  yr B.P. by means of planktonic foraminifera of the Iberian Margin, *Quaternary Research*, 61, 204–214, 2004.
- Bard, E. and Ménot-Combes, G. and Rostek, F.: Present status of radiocarbon calibration and comparison records based on Polynesian corals and Iberian margin sediments, *Radiocarbon*, 46, 1189–1202, 2005.
- Beck, J. W., Richards, D. A., Edwards, L., Silverman, B. W., Smart, P. L., Donahue, D. J., Herrera-Osterheld, S., Burr, G. S., Calsoyas, L., Jull, A. J. T., and Biddulph, D.: Extremely Large Variations of Atmospheric  $^{14}\text{C}$  Concentration During the Last Glacial Period, *Science*, 292, 2453–2458, 2001.
- Beer, J., Muscheler, R., Wagner, G., Laj, C., Kissel, C., Kubik, P. W., and Synal, H.-A.: Cosmogenic nuclides during Isotope Stages 2 and 3, *Quaternary Science Reviews*, 21, 1129–1139, 2002.
- Berger, W. H.: Carbon dioxide excursions and the deep-sea record, in: *The fate of fossil-fuel  $\text{CO}_2$  in the oceans*, edited by Andersen, N. R. and Malahoff, A., pp. 505–542, Plenum, New York, 1977.
- Berger, W. H.: The Younger Dryas cold spell - a quest for causes, *Global and Planetary Change*, 3, 219–237, 1990.

- Bitz, C. M., Holland, M. M., Weaver, A. J., and Eby, M.: Simulating the ice-thickness distribution in a coupled climate model, *Journal of Geophysical Research*, 106, 2441–2464, 2001.
- Björck, S., Bennike, O., Possnert, G., Wohlfahrt, B., and Digerfeldt, G.: A high-resolution  $^{14}\text{C}$  dated sediment sequence from southwest Sweden: age comparisons between different components of the sediment, *Journal of Quaternary Science*, 13, 85–89, 1998.
- Bondevik, S., Birks, H. H., Gulliksen, S., and Mangerud, J.: Late Weichselian Marine  $^{14}\text{C}$  Reservoir Ages at the Western Coast of Norway, *Quaternary Research*, 52, 104–114, 1999.
- Bondevik, S., Mangerud, J., Birks, H. H., Gulliksen, S., and Reimer, P.: Changes in North Atlantic Radiocarbon Reservoir Ages During the Allerød and Younger Dryas, *Science*, 312, 1514–1517, 2006.
- Bowman, S.: Radiocarbon dating - Interpreting the past, British Museum Press, London, 2. edn., 1995.
- Braconnot, P., Otto-Bliesner, B., Harrison, S., Joussaume, S., Peterschmitt, J.-Y., Abe-Ouchi, A., Crucifix, M., Driesschaert, E., Fichefet, T., Hewitt, C. D., Kageyama, M., Kitoh, A., Lainé, A., Loutre, M.-F., Marti, O., Merkel, U., Ramstein, G., Valdes, P., Weber, S. L., Yu, Y., and Zhao, Y.: Results of PMIP2 coupled simulations of the Mid-Holocene and Last Glacial Maximum - Part 1: experiments and large-scale features, *Climate of the Past*, 3, 261–277, 2007.
- Broecker, W., Peng, T.-H., Ostlund, G., and Stuiver, M.: The Distribution of Bomb Radiocarbon in the Ocean, *Journal of Geophysical Research*, C90, 6953–6970, 1985.
- Broecker, W., Klas, M., Ragano-Beavan, N., Mathieu, G., and Mix, A.: Accelerator Mass Spectrometry Radiocarbon Measurements on Marine Carbonate Samples from Deep Sea Cores and Sediment Traps, *Radiocarbon*, 30, 261–295, 1988.
- Broecker, W. S.: Was the Younger Dryas Triggered by a Flood?, *Science*, 312, 1146–1148, 2006.
- Broecker, W. S. and Peng, T.-H.: Tracers in the Sea, Tech. rep., Lamont-Doherty Earth Observatory, Palisades, N.Y., 1982.

- Broecker, W. S., Ledwell, J. R., Takahashi, T., Weiss, R., Merlivat, L., Memery, L., Peng, T.-H., Jahne, B., and Munnich, K. O.: Isotopic versus micrometeorologic ocean CO<sub>2</sub> fluxes, *Journal of Geophysical Research*, 91, 10 517–10 527, 1986.
- Broecker, W. S., Sutherland, S., Smethie, W., Peng, T.-H., and Ostlund, G.: Oceanic radiocarbon: Separation of the natural and bomb components, *Global Biogeochemical Cycles*, 9, 263–288, 1995.
- Bryan, K. and Lewis, L. J.: A water mass model of the world ocean circulation, *Journal of Geophysical Research*, C84, 2503–2517, 1979.
- Burr, G. S., Beck, J. W., Taylor, F. W., Recy, J., Edwards, L., Cabioch, G., Correge, T., Donahue, D. J., and O'Malley, J. M.: A high-resolution radiocarbon calibration between 11,700 and 12,400 calendar years BP derived from <sup>230</sup>Th ages of corals from Esperitu Santo Island, Vanuatu, *Radiocarbon*, 40, 1093–1151, 1998.
- Butzin, M., Prange, M., and Lohmann, G.: Radiocarbon simulations for the glacial ocean: The effects stress, Southern Ocean sea ice and Heinrich events, *Earth and Planetary Science Letters*, 235, 45–61, 2005.
- Cao, L., Fairbanks, R. G., Mortlock, R. A., and Risk, M. J.: Radiocarbon reservoir age of high latitude North Atlantic surface water during the last deglacial, *Quaternary Science Reviews*, 26, 732–742, 2007.
- Carstens, J., Hebbeln, D., and Wefer, G.: Distribution of planktic foraminifera at the ice margin in the Arctic (Fram Strait), *Marine Micropaleontology*, 29, 257–269, 1997.
- Cook, M. S.: The paleoceanography of the Bering Sea during the last glacial cycle, Ph.D. thesis, Massachusetts Institute of Technology and Woods Hole Oceanographic Institution, 2006.
- Cutler, K. B., Gray, S. C., Burr, G. S., Edwards, R. L., Taylor, F. W., Cabioch, G., Beck, J. W., Cheng, H., and Moore, J.: Radiocarbon Calibration and Comparison to 50 Kyr BP with Paired <sup>14</sup>C and <sup>230</sup>TH Dating of Corals from Vanuatu and Papua New Guinea, *Radiocarbon*, 46, 1127–1160, 2004.

- Delaygue, G., Stocker, T. F., Joos, F., and Plattner, G.-K.: Simulation of atmospheric radiocarbon during abrupt oceanic circulation changes: trying to reconcile models and reconstructions, *Quaternary Science Reviews*, 22, 1647–1658, 2003.
- Druffel, E.: Decade time scale variability of ventilation in the North Atlantic: High-precision measurements of bomb radiocarbon in banded corals, *Journal of Geophysical Research*, C94, 3271–3285, 1989.
- Druffel, E. and Griffin, S.: Variability of surface ocean radiocarbon and stable isotopes in the southwestern Pacific, *Journal of Geophysical Research*, C104, 493–502, 1999.
- Duplessy, J.-C., Arnold, M., Bard, E., Juillet-Leclerc, A., Kallel, N., and Labeyrie, L.: AMS  $^{14}\text{C}$  Study of Transient Events and of the Ventilation Rate of the Pacific Intermediate Water During the Last Deglaciation, *Radiocarbon*, 31, 493–502, 1989.
- Eiriksson, J., Larsen, G., Knudsen, K. L., Heinemeier, J., and Simonarson, L. A.: Marine reservoir age variability and water mass distribution in the Iceland Sea, *Quaternary Science Reviews*, 23, 2247–2268, 2004.
- Elliot, M., Labeyrie, L., and Duplessy, J.-C.: Changes in North Atlantic deep-water formation associated with the Dansgaard-Oeschger temperature oscillations (60-10 ka), *Quaternary Science Reviews*, 21, 1153–1165, 2002.
- Ellis, J., Fields, B. D., and Schramm, D. N.: Geologic Isotope Anomalies As Signatures of Nearby Supernovae, *Astrophysical Journal*, 470, 1227, 1996.
- Eltgroth, S. F., Adkins, J. F., Southon, J., and Franke, J.: The Transfer of Bomb Radiocarbon to the Deep Ocean: Observations from a North Atlantic Deep-sea Coral, in prep.
- Eltgroth, S. F., Adkins, J. F., Robinson, L. F., and Southon, J.: A deep-sea coral record of North Atlantic radiocarbon through the Younger Dryas: Evidence for intermediate water/deepwater reorganization, *Paleoceanography*, 21, 1–12, 2006.
- England, M. H.: The Age of Water and Ventilation Timescales in a Global Ocean Model, *Journal of Physical Oceanography*, 25, 2756–2777, 1995.

- Fairbanks, R. G., Mortlock, R. A., Chiu, T.-C., Cao, L., Kaplan, A., Guilderson, T. P., Fairbanks, T. W., Bloom, A. L., Grootes, P. M., and Nadeau, M.-J.: Radiocarbon calibration curve spanning 0 to 50,000 years BP based on paired  $^{230}\text{Th}/^{234}\text{U}/^{238}\text{U}$  and  $^{14}\text{C}$  dates on pristine corals, *Quaternary Science Reviews*, 24, 1781–1796, 2005.
- Fanning, A. F. and Weaver, A. J.: An atmospheric energy-moisture balance model: climatology, interpentadal climate change, and coupling to an ocean general circulation model, *Journal of Geophysical Research*, D101, 15 111–15 128, 1996.
- Franke, J., Paul, A., and Schulz, M.: Modeling variations of marine reservoir ages during the last 45,000 years, submitted to *Climate of the Past*.
- Gagan, M. K., Ayliffe, L. K., Beck, J. W., Cole, J. E., Druffel, E. R. M., Dunbar, R. B., and Schrag, D. P.: New views of tropical paleoclimates from corals, *Quaternary Science Reviews*, 19, 45–64, 2000.
- Ganopolski, A. and Rahmstorf, S.: Rapid changes of glacial climate simulated in a coupled climate model, *Nature*, 409, 153–158, 2001.
- Gent, P. R. and McWilliams, J. C.: Isopycnal mixing in ocean circulation models, *Journal of Physical Oceanography*, 20, 150–155, 1990.
- Goslar, T., Arnold, M., Tisnerat-Laborde, N., Czernik, J., and Wieckowski, K.: Variations of Younger Dryas atmospheric radiocarbon explicable without ocean circulation changes, *Nature*, 405, 877–880, 2000.
- Griffies, S. M.: *Fundamentals of ocean climate models*, Princeton University Press, Princeton, USA, 2004.
- Guilderson, T. P., Schrag, D. P., Goddard, E., Kashgarian, M., M., W., and Linsley, B. K.: Southwest subtropical Pacific surface water radiocarbon in a high-resolution coral record, *Radiocarbon*, 42, 249–256, 2000.
- Hemming, S.: Heinrich events: massive late Pleistocene detritus layers of the North Atlantic and their global climate imprint, *Reviews of Geophysics*, 42, 1–43, 2004.
- Hesshaimer, V., Heimann, M., and Levin, I.: Radiocarbon evidence for a smaller oceanic carbon dioxide sink than previously believed, *Nature*, 370, 201–203, 1994.



- Hibler, W. D.: A dynamic thermodynamic sea ice model, *Journal of Physical Oceanography*, 9, 815–846, 1979.
- Hua, C. and Barbetti, M.: Review of tropospheric bomb  $^{14}\text{C}$  data for carbon cycle modeling and age calibration purposes, *Radiocarbon*, 46, 1273–1298, 2004.
- Hughen, K. A., Baillie, M. G. L., Bard, E., Beck, J. W., Bertrand, C. J. H., Blackwell, P. G., Buck, C. E., Burr, G. S., Cutler, K. B., Damon, P. E., Edwards, R. L., Fairbanks, R. G., Friedrich, M., Guilderson, T. P., Kromer, B., McCormac, G., Manning, S., Ramsey, C. B., Reimer, P. J., Reimer, R. W., Remmele, S., Southon, J. R., Stuiver, M., Talamo, S., Taylor, F. W., Plicht, J. v. d., and Weyhenmeyer, C. E.: MARINE04 Marine Radiocarbon Age Calibration, 0–26 cal kyr BP, *Radiocarbon*, 46, 1059–1086, 2004a.
- Hughen, K. A., Lehman, S., Southon, J., Overpeck, J., Marchal, O., Herring, C., and Turnbull, J.:  $^{14}\text{C}$  Activity and Global Carbon Cycle Changes over the Past 50,000 Years, *Science*, 303, 202–207, 2004b.
- Hughen, K. A., Lehman, S., Southon, J., Overpeck, J., Marchal, O., Herring, C., and Turnbull, J.: Marine-derived  $^{14}\text{C}$  calibration and activity record for the past 50,000 years updated from the Cariaco Basin, *Quaternary Science Reviews*, 25, 3216–3227, 2006.
- Hunke, E. C. and Dukowicz, J. K.: An elastic-viscous-plastic model for sea ice dynamics, *Journal of Physical Oceanography*, 27, 1849–1867, 1997.
- Joos, F.: Imbalance in the budget, *Nature*, 370, 181–182, 1994.
- Jöris, O. and Weninger, A.: Extension of the  $^{14}\text{C}$  calibration curve to ca. 40,000 cal BC by synchronizing Greenland  $^{18}\text{O}/^{16}\text{O}$  ice core records and North Atlantic foraminifera profiles: a comparison with U/Th coral data, *Radiocarbon*, 40, 495–504, [www.calpal.de](http://www.calpal.de), updated 2007, 1998.
- Kalnay, E., Kanamitsu, M., Kistler, R., Collins, W., Deaven, D., Gandin, L., Iredell, M., Saha, S., White, G., Woollen, J., Zhua, Y., Leetmaa, A., Reynolds, B., Chelliah, M., Ebisuzaki, W., Higgins, W., Janowiak, J., Mo, K. C., Ropelewski, C., Wang, J., Jenne, R., and Joseph, D.: The NCEP/NCAR 40-year reanalysis project, *Bulletin of the American Meteorological Society*, 77, 437–471, 1996.

- Keeling, C. D.: The Suess Effect:  $^{13}\text{C}$  Carbon and  $^{14}\text{C}$  Carbon interactions, *Environment International*, 2, 229–300, 1979.
- Keeling, C. D.: The modelling of rare isotopic carbon with regard to notations, in: *Carbon cycle modelling*, edited by Bolin, B., vol. 16 of *SCOPE*, pp. 89–94, John Wiley and Sons, Chichester, 1981.
- Keigwin, L. D. and Lehman, S. J.: Deep circulation change linked to Heinrich event 1 and Younger Dryas in a mid-depth North Atlantic core, *Paleoceanography*, 9, 185–194, 1994.
- Keigwin, L. D. and Schlegel, M. A.: Ocean ventilation and sedimentation since the glacial maximum at 3 km in the western North Atlantic, *Geochemistry, Geophysics, Geosystems*, 3, 1–14, 2002.
- Key, R. M., Kozyr, A., Sabine, C. L., Lee, K., Wanninkhof, R., Bullister, J. L., Feely, R. A., Millero, F. J., Mordy, C., and Peng, T.-H.: A global ocean carbon climatology: Results from Global Data Analysis Project (GLODAP), *Global Biogeochemical Cycles*, 18, 1–23, 2004.
- Kitagawa, H. and Plicht, J. v. d.: Atmospheric radiocarbon calibration beyond 11,900 cal BP from Lake Suigetsu laminated sediments, *Radiocarbon*, 42, 369–380, 2000.
- Kovanen, D. and Easterbrook, D.: Paleodeviations of radiocarbon marine reservoir values for the NE Pacific, *Geology*, 30, 243–246, 2002.
- Laj, C., Mazaud, A., and Duplessy, J.-C.: Geomagnetic intensity and  $^{14}\text{C}$  abundance in the atmosphere and ocean during the past 50kyr, *Geophysical Research Letters*, 23, 2045–2048, 1996.
- Laj, C., Kissel, C., Mazaud, A., Channell, J. E. T., and Beer, J.: North Atlantic paleointensity stack since 75ka (NAPIS-75) and the duration of the Laschamp event, *Philosophical Transactions Royal Society*, 358, 1009–1025, 2000.
- Laj, C., Kissel, C., Mazaud, A., Michel, E., Muscheler, R., and Beer, J.: Geomagnetic field intensity, North Atlantic Deep Water circulation and atmospheric  $^{14}\text{C}$  during the last 50 kyr, *Earth and Planetary Science Letters*, 200, 177–190, 2002.

- Laj, C., Kissel, C., and Beer, J.: high Resolution Global Paleointensity Stack Since 75 kyr (GLOPIS-75) Calibrated to Absolute Values, *Geophysical Monograph Series*, 145, 255–265, 2004.
- Libby, W. F.: Accuracy of Radiocarbon Dates, Apparent discrepancies are examined for geophysical significance and for a general principle of correction., *Science*, 140, 278–280, 1963.
- Lynch-Stieglitz, J., Adkins, J. F., Curry, W. B., Dokken, T., Hall, I. R., Herguera, J. C., Hirschi, J. J.-M., Ivanova, E. V., Kissel, C., Marchal, O., Marchitto, T. M., McCave, I. N., McManus, J. F., Mulitza, S., Ninnemann, U., Peeters, F., Yu, E.-F., and Zahn, R.: Circulation During the Last Glacial Maximum, *Science*, 316, 66–69, 2007.
- Marchal, O., Stocker, T. F., Indermühle, A., Blunier, T., and Tschumi, J.: Modelling the concentration of atmospheric CO<sub>2</sub> during the Younger Dryas climate event, *Climate Dynamics*, 15, 341–354, 1999.
- Marchal, O., Francois, R., Stocker, T. F., and Joos, F.: Ocean thermohaline circulation and sedimentary <sup>231</sup>Pa/<sup>230</sup>Th ratio, *Paleoceanography*, 15, 625–641, 2000.
- Marchitto, T. M., Lehman, S.J. Ortiz, J. D., Flückiger, J., and Geen, A. v.: Marine Radiocarbon Evidence for the Mechanism of Deglacial Atmospheric CO<sub>2</sub> Rise, *Science*, 316, 1456–1459, 2007.
- Marshall, J. C., Williams, R. W., and Nurser, A. J. G.: Inferring the Subduction Rate and Period over the North Atlantic, *Journal of Physical Oceanography*, 23, 1315–1329, 1993.
- Masarik, J. and Beer, J.: Simulations of particle fluxes and cosmogenic nuclide production in the earth’s atmosphere, *Journal of Geophysical Research*, D104, 12 099–13 012, 1999.
- McCave, I. N., Manighetti, B., and Robinson, S. G.: Sortable silt and fine sediment size/composition slicing: Parameters for paleocurrent speed and paleoceanography, *Paleoceanography*, 10, 593–610, 1995.
- McManus, J. F., Francois, R., Gherardi, J.-M., Keigwin, L. D., and Brown-Leger, S.: Collapse and rapid resumption of Atlantic meridional circulation linked to deglacial climate changes, *Nature*, 428, 834–837, 2004.

- Meese, D. A., Gow, A. J., Grootes, P., Stuiver, M., Mayewski, P. A., Zielinski, G. A., Ram, M., Taylor, K. C., and Waddington, E. D.: The Accumulation Record from the GISP2 Core as an Indicator of Climate Change Throughout the Holocene, *Science*, 266, 1680–1682, 1994.
- Meissner, K. J., Schmittner, A., Weaver, A. J., and Adkins, J. F.: Ventilation of the North Atlantic Ocean during the Last Glacial Maximum: A comparison between simulated and observed radiocarbon ages, *Paleoceanography*, 18, 1023, 2003.
- Muscheler, R., Beer, J., Gerhard Wagner, G., Carlo Laj, C., Kissel, C., Raisbeck, G. M., Yiou, F., and Kubik, P. W.: Changes in the carbon cycle during the last deglaciation as indicated by the comparison of  $^{10}\text{Be}$  and  $^{14}\text{C}$  records, *Earth and Planetary Science Letters*, 219, 325–340, 2004.
- Muscheler, R., Beer, J., Kubik, P. W., and Synal, H.-A.: Geomagnetic field intensity during the last 60,000 years based on  $^{10}\text{Be}$  and  $^{36}\text{Cl}$  from the Summit ice cores and  $^{14}\text{C}$ , *Quaternary Science Reviews*, 24, 1849–1860, 2005.
- Naegler, T., Ciais, P., Rodgers, K., and Levin, I.: Excess radiocarbon constraints on air-sea gas exchange and the uptake of  $\text{CO}_2$  by the oceans, *Geophysical Research Letters*, 33, 1–4, 2006.
- Orr, J.: Global Ocean Storage of Anthropogenic Carbon (GOSAC), Tech. rep., IPSL/CNRS, 2002.
- Orr, J., Najjar, R., Sabine, C., and Joos, F.: Abiotic HOWTO, Tech. rep., LSCE/CEA Saclay, Gif-sur-Yvette, France, 2000.
- Orsi, A. H., Whitworth, T., and Nowlin, W. D.: On the meridional extent and fronts of the Antarctic Circumpolar Current, *Deep-Sea Research I*, 42, 641–673, 1995.
- Pacanowski, R. C.: MOM 2 Documentation, User’s Guide and Reference Manual, Technical report, GFDL Ocean Group, NOAA, GFDL, Princeton, New Jersey, 1995.
- Pacanowski, R. C. and Griffies, S. M.: MOM 3.0 Manual, Technical report, GFDL Ocean Group, GFDL, Princeton, New Jersey, 2000.

- Palmer, J., Lorrey, A., Turney, C. S. M., Hogg, A., Baillie, M., Fifield, K., and Ogden, J.: Extension of New Zealand Kauri (*Agathis australis*) tree-ring chronologies into Oxygen Isotope Stage (OIS) 3, *Journal of Quaternary Science*, 21, 779–787, 2006.
- Peacock, S.: Debate over the ocean bomb radiocarbon sink: Closing the gap, *Global Biogeochemical Cycles*, 18, 1–15, 2004.
- Peacock, S. and Maltrud, M.: Transit-Time Distributions in a Global Ocean Model, *Journal of Physical Oceanography*, 36, 474–495, 2006.
- Peltier, R.: Ice age paleotopography, *Science*, 265, 195–201, 1994.
- Peltier, R.: Global Glacial Isostasy and the Surface of the Ice-Age Earth: The ICE-5G (VM2) Model and GRACE, *Earth Planetary Science*, 32, 111–149, 2004.
- Raynaud, D., Jouzel, J., Barnola, J. M., Chappellaz, J., Delmas, R. J., and Lorius, C.: The ice record of greenhouse gases, *Science*, 259, 926–934, 1993.
- Reimer, P. J. and Reimer, R. W.: A marine reservoir correction database and on-line interface, *Radiocarbon*, 43, 461–463, 2001.
- Reimer, P. J., Baillie, M. G. L., Bard, E., Bayliss, A., Beck, J. W., Bertrand, C. J. H., Blackwell, P. G., Buck, C. E., Burr, G. S., Cutler, K. B., Damon, P. D., Edwards, R. L., Fairbanks, R. G., Friedrich, M., Guilderson, T. P., Hogg, A. G., Hughen, K. A., Kromer, B., McCormac, G., Manning, S., Ramsey, C. B., Reimer, R. W., Remmele, S., Southon, J. R., Stuiver, M., Talamo, S., Taylor, F. W., Plicht, J. v. d., and Weyhenmeyer, C. E.: INTCAL04 Terrestrial Radiocarbon Age Calibration, 0–26 cal kyr BP, *Radiocarbon*, 46, 1029–1058, 2004.
- Saenko, O. A. and Weaver, A. J.: Atlantic deep circulation controlled by freshening in the Southern Ocean, *Geophysical Research Letters*, 30, 1–4, 2003.
- Sarnthein, M., Stattegger, K., Dreger, D., Erlenkeuser, H., Grootes, P., Haupt, B. J., Jung, S., Kiefer, T., Kuhnt, W., Pflaumann, U., Schäfer-Neth, C., Schulz, H., Schulz, M., Seidov, D., Simstich, J., Kreveld, S. v., Vogelsang, E., Völker, A., and Weinelt, M.: Fundamental Modes and Abrupt Changes in North Atlantic Circulation and Climate

- over the last 60 ky - Concepts, Reconstruction and Numerical Modeling, in: The Northern North Atlantic, edited by Schäfer, P., Ritzrau, W., Schlüter, M., and Thiede, J., pp. 365–410, Springer Verlag, New York, 2001.
- Sarnthein, M., Kennett, J. P., Allen, J. R. M., Beer, J., Grootes, P., Laj, C., McManus, J., Ramesh, R., and 117, S.-I. W. G.: Decadal-to-millennial-scale climate variability-chronology and mechanisms: summary and recommendations, *Quaternary Science Reviews*, 21, 1121–1128, 2002.
- Sarnthein, M., Grootes, P. M., Kennett, J. P., and M.-J., N.:  $^{14}\text{C}$  Reservoir Ages Show Deglacial Changes in Ocean Currents, in: *Ocean Circulation: Mechanisms and Impacts*, Geophysical Monograph Series 173, edited by Schmittner, A., Chiang, J., and Hemming, S., pp. 175–197, American Geophysical Union, Washington, DC, 2007.
- Schiebel, R. and Hemleben, C.: Modern planktic foraminifera, *Paläontologische Zeitschrift*, 79, 135–148, 2005.
- Schimmelmann, A., Lange, C. B., Roark, B., and Ingram, L.: Resources for paleoceanographic and paleoclimatic analysis: A 6,700-year stratigraphy and regional radiocarbon reservoir-age ( $\Delta R$ ) record based on varve counting and  $^{14}\text{C}$ -AMS dating for the Santa Barbara Basin, offshore California, U.S.A., *Journal of Sedimentary Research*, 76, 74–80, 2006.
- Schmidt, A., Burr, G. S., Taylor, F. W., O'Malley, J., and Beck, J. W.: A semiannual radiocarbon record of a modern coral from the Solomon Islands, *Nuclear Instruments and Methods in Physics Research B*, 223, 420–427, 2004.
- Schmittner, A., Meissner, K. J., Eby, M., and Weaver, A. J.: Forcing of the deep ocean circulation in simulations of the Last Glacial Maximum, *Paleoceanography*, 17, 26–35, 2002.
- Semtner, A. J.: A model for the thermodynamic growth of sea ice in numerical investigations of climate, *Journal of Physical Oceanography*, 6, 379–389, 1976.
- Shackleton, N. J., Duplessy, J.-C., Arnold, M., Maurice, P., Hall, M. A., and Cartledge, J.: Radiocarbon age of last glacial Pacific deep water, *Nature*, 335, 708–711, 1988.

- Shackleton, N. J., Fairbanks, R. G., Tzu-chien, C., and Parrenin, F.: Absolute calibration of the Greenland time scale: implications for Antarctic time scales and for  $\Delta^{14}\text{C}$ , *Quaternary Science Reviews*, 23, 1513–1522, 2004.
- Shi, N., Schneider, R., Beuga, H.-J., and Dupont, L. M.: Southeast trade wind variations during the last 135 kyr: evidence from pollen spectra in eastern South Atlantic sediments, *Earth and Planetary Science Letters*, 187, 311–321, 2001.
- Siani, G., Paterne, M., Michel, E., Sulpizio, R., Sbrana, A., Arnold, M., and Haddad, G.: Mediterranean Sea Surface Radiocarbon Reservoir Age Changes Since the Last Glacial Maximum, *Science*, 294, 1917–1920, 2001.
- Siegenthaler, U., Heimann, M., and Oeschger, H.:  $^{14}\text{C}$  Variations caused by changes in the global carbon cycle, *Radiocarbon*, 22, 177–191, 1980.
- Sikes, E. L., Samson, C. R., Guilderson, T. P., and Howard, W. R.: Old radiocarbon ages in the southwest Pacific Ocean during the last glacial period and deglaciation, *Nature*, 405, 555–559, 2000.
- Simstich, J., Sarnthein, M., and Erlenkeuser, H.: Paired  $\delta^{18}\text{O}$  signals of *Neogloboquadrina pachyderma* (s) and *Turborotalita quinqueloba* show thermal stratification structure in Nordic Seas, *Marine Micropaleontology*, 48, 107–125, 2003.
- Southon, J. R., Nelson, D. E., and Vogel, J. S.: A record of past ocean-atmosphere radiocarbon difference from the northeast Pacific, *Paleoceanography*, 5, 197–206, 1990.
- Stuiver, M. and Braziunas, T. F.: Modeling atmospheric  $^{14}\text{C}$  influences and  $^{14}\text{C}$  ages of marine samples to 10,000 BC, *Radiocarbon*, 35, 137–189, 1993.
- Stuiver, M. and Polach, H. A.: Discussion reporting of  $^{14}\text{C}$  data, *Radiocarbon*, 19, 355–363, 1977.
- Stuiver, M., Reimer, P. J., Bard, E., Beck, J. W., Burr, G. S., Hughen, K. A., Kromer, B., McCormac, G., Plicht, J. v. d., and Spurks, M.: INTCAL98 Radiocarbon Age Calibration, 24,000–0 cal BP, *Radiocarbon*, 40, 1041–1083, 1998.
- Stuut, J.-B. W., Prins, M. A., Schneider, R. R., Weltje, G. J., Jansen, J. H. F., and Postma, G.: A 300-kyr record of aridity and wind strength in southwestern Africa: inferences

- from grain-size distributions of sediments on Walvis Ridge, SE Atlantic, *Marine Geology*, 180, 221–233, 2002.
- Sweeney, C., Gloor, E., Jacobson, A. R., Key, R. M., McKinley, G., Sarmiento, J. L., and Wanninkhof, R.: Constraining global air-sea gas exchange for CO<sub>2</sub> with recent bomb <sup>14</sup>C measurements, *Global Biogeochemical Cycles*, 21, 1–10, 2007.
- Talley, L. D., Reid, J. L., and Robbins, P. E.: Data-based meridional overturning stream-functions for the global ocean, *Journal of Climate*, 16, 3213–3226, 2003.
- Thiele, G. and Sarmiento, J. L.: Tracer dating and ocean ventilation, *Journal of Geophysical Research*, C95, 9377–9391, 1990.
- Turney, C. S. M., Fifield, L. K., Palmer, J. G., Hogg, A. G., Baillie, M. G. L., Galbraith, R., Ogden, J., Lorrey, A., and Tims, S. G.: Towards a radiocarbon calibration for oxygen isotope stage 3 using New Zealand Kauri (*Agathis Australis*), *Radiocarbon*, 49, 447–457, 2007.
- Valet, J.-P., Meynadier, L., and Guyodo, Y.: Geomagnetic dipole strength and reversal rate over the past two million years, *Nature*, 435, 802–805, 2005.
- Voelker, A. H. L.: Global distribution of centennial-scale records for Marine Isotope Stage (MIS) 3: a database, *Quaternary Science Reviews*, 21, 1185–1212, 2002.
- Voelker, A. H. L., Sarnthein, M., Grootes, P. M., Erlenkeuser, H., Laj, C., Mazaud, A., and Nadeau, M.-J.: Correlation of marine <sup>14</sup>C ages from the Nordic Seas with the GISP2 isotope record: Implications for <sup>14</sup>C calibration beyond 25 ka BP, *Radiocarbon*, 40, 517–534, 1998.
- Vonmoos, M., Beer, J., and Muscheler, R.: Large variations in Holocene solar activity: Constraints from <sup>10</sup>Be in the Greenland Ice Core Project ice core, *Journal of Geophysical Research*, 111, 1–14, 2006.
- Waelbroeck, C., Duplessy, J.-C., Michel, E., Labeyrie, L., Paillard, D., and Dupart, J.: The timing of the last deglaciation in North Atlantic climate records, *Nature*, 412, 724–727, 2001.



- Weaver, A. J., Eby, M., Wiebe, E. C., Bitz, C. M., Duffy, P. B., Ewen, T. L., Fanning, A. F., Holland, M. M., MacFadyen, A., Matthews, H. D., Meissner, K. J., Saenko, O., Schmittner, A., Wang, H., and Yoshimori, M.: The UVic Earth System Climate Model: Model Description, Climatology, and Applications to Past, Present and Future Climates, *Atmosphere-Ocean*, 39, 361–428, 2001.
- Weber, S., Drijfhout, S., Abe-Ouchi, A., Crucifix, M., Eby, M., Ganopolski, A., Murakami, S., B., Otto-Bliesner, B., and Peltier, W. R.: The modern and glacial overturning circulation in the Atlantic ocean in PMIP coupled model simulations, *Climate of the Past*, 3, 51–64, 2007.
- Weiss, R. F. and Price, B. A.: Nitrous oxide solubility in water and seawater, *Marine Chemistry*, 8, 347–359, 1980.
- Williams, R. G., Spall, M. A., and Marshall, J. C.: Does Stommel’s Mixed Demon Work?, *Journal of Physical Oceanography*, 25, 3089–3102, 1995.
- Williams, T. and Kelley, C.: gnuplot - An Interactive Plotting Program, 2007.
- Wunsch, C.: Determining paleoceanographic circulations, with emphasis on the Last Glacial Maximum, *Quaternary Science Reviews*, 22, 371–385, 2003a.
- Wunsch, C.: Greenland-Antarctic phase relations and millennial time-scale climate fluctuations in the Greenland ice-cores, *Quaternary Science Reviews*, 22, 1631–1646, 2003b.
- Zhang, X. and Cai, W.-J.: On some biases of estimating the global distribution of air-sea CO<sub>2</sub> flux by bulk parameterizations, *Geophysical Research Letters*, 34, 1–6, 2007.



# Appendix A

## The Live Access Server

### A.1 Installation and operation of the server

The technology of LAS changed in the year 2007. While LAS 6.x was written in Perl and used CGI, the newly developed version 7.x, called “Armstrong”, is programmed in Java. In the following it is described how the first stable alpha release of LAS Armstrong (<ftp://ftp.pmel.noaa.gov/pub/las/las.armstrong.1.0.tar.gz>) and all other required software is installed on the web server

<http://reservoirage.palmod.uni-bremen.de> (134.102.241.130). Different procedures can be necessary when newer versions of LAS and its required software will be available in future.

LAS is unpacked using the command: `tar xvfz las.armstrong.1.0.tar.gz` into the directory `/opt` and linked to `/opt/las` with `ln -s las.armstrong.1.0.tar.gz las`.

The installation requires the following software to be installed:

- Apache HTTP Server
- Java 1.5 or higher (the full SE JDK not just JRE)
- Tomcat 5 or higher
- The THREDDS Data Server (TDS) 3.16 or higher

- mySQL 3 or higher
- Perl 5.8 or higher
- ant 1.6 or higher
- Ferret 6.07 or higher

Apache, Java, mySQL, Perl and ant are installed with the operating system in form of rpm packages using the program yum. They can be updated easily with the regular system update. `system-config-services` is used to configure that the mySQL and Apache (httpd) servers are running and automatically started when the computer is started.

The Apache HTTP server is started in its standard configuration, but a few parameters have to be set in `/etc/httpd/conf/httpd.conf`:

```
User apache
Group apache
ServerName reservoirage.palmod.uni-bremen.de:80
DocumentRoot "/var/www/html"
<Directory />
    Options FollowSymLinks
    AllowOverride None
</Directory>
<Directory "/var/www/html">
    Options Indexes SymLinksifOwnerMatch
    AllowOverride None
    Order allow,deny
    Allow from all
</Directory>
```

MySQL configuration:

1. The mySQL daemon can be started manually, if not already running, with:  
    `/usr/bin/mysqld_safe`  
    and can be shutdown with:  
    `/usr/bin/mysqladmin shutdown -p`

2. A user root without password exists after the installation. A new password is set:

```
mysqladmin -u root password 'new_password'
```

The Tomcat Server has to be installed manually because it is not provided by the distribution in the required version 5. Hence, Tomcat is installed following the instructions on the webpage

<http://ferret.pmel.noaa.gov/LAS/documentation/installer-documentation/installation/preliminaries>:

1. The latest version is downloaded from `tomcat.apache.org`
2. The archive is decompressed and unpacked: `tar zxvf apache-tomcat-5.5.25.tar.gz`
3. A symbolic link from the directory `/opt/apache-tomcat-5.5.25` is set to `/opt/tomcat`
4. The HTTP port number is left unchanged at its standard: 8080
5. The Java environment is set in `/etc/profile`:

```
export JAVA_HOME=/usr/java/jdk1.5.0_14/
export JAVA_OPTS="-Djava.awt.headless=true -Xms256M
-Xmx256M"
export PATH="$PATH:/usr/java/jdk1.5.0_14/bin"
```

The TDS installation is following next:

1. The `thredds.war` file is downloaded from <http://www.unidata.ucar.edu/projects/THREDDS/tech/TDS.html#download>
2. The file is saved in the Tomcat webapps directory, `/opt/tomcat/webapps`

Then the TDS is tested following the instructions on <http://www.unidata.ucar.edu/projects/THREDDS/tech/tutorial/GettingStarted.html>. First the environment variable is set (`export TOMCAT_HOME=/opt/tomcat`) and then the tomcat server is started with the start script `/opt/tomcat/startup.sh`. Afterwards the browser displays the test dataset at <http://localhost:8080/thredds/>.

TDS needs to be configured following <http://ferret.pmel.noaa.gov/LAS/documentation/installer-documentation/installation/installing-and-integrating-tds-with-las>:

1. Directories and other services in

`/opt/tomcat/content/thredds/catalog.xml` are configured:

```
<service name='`gridded`' serviceType='`Compound`'
  base='`'`' >
<service name='`opendap`' serviceType='`OpenDAP`'
  base='`/thredds/dodsC/'`'/>
<service name='`wcs`' serviceType='`WCS`'
  base='`/thredds/wcs/'`'/>
</service>
<datasetScan name='`Data From LAS`' path='`las`'
  location='`/opt/las/conf/server/data`'
  serviceName='`gridded`'>
<filter>
  <include wildcard='`*.nc`' />
  <include wildcard='`*.fds`' />
  <include wildcard='`*.jnl`' />
</filter>
</datasetScan>
```

2. `/opt/tomcat/content/thredds/threddsConfig.xml` is configured to use plug-ins that allow TDS to serve data opened in a Ferret journal:

```
<datasetSource>gov.noaa.pmel.tmap.ioisp.FerretDataSource
</datasetSource>    <nj22Config>
  <ioServiceProvider class=
    ``gov.noaa.pmel.tmap.ioisp.FerretIOServiceProvider`` />
</nj22Config>
```

Then Ferret is installed following the instructions on the webpage

[http://ferret.pmel.noaa.gov/static/Downloads/ferret\\_installation\\_and\\_update\\_guide\\_v600.html](http://ferret.pmel.noaa.gov/static/Downloads/ferret_installation_and_update_guide_v600.html):

1. `fer_executables.tar.Z` and `fer_environment.tar.Z` and `fer_dsets.tar.Z` are downloaded from [http://www.ferret.noaa.gov/Ferret/Downloads/ferret\\_downloads.html](http://www.ferret.noaa.gov/Ferret/Downloads/ferret_downloads.html)
2. A directory `/opt/ferret` is created
3. The support file archive is extracted with the command `tar xvfz`  
`/[download_dir]/fer_environment.tar.Z` in the directory `/opt/ferret`
4. A directory `/usr/local/ferret/fer_dsets` is created
5. The sample data archive is extracted to this directory `tar xvfz`  
`/[download_dir]/fer_dsets.tar.Z`
6. The Ferret executables are installed running  
`/usr/local/ferret/bin/Finstall`
7. The `ferret_paths` script is generated
8. The created script needs to be customized to run in the bash by changing `setenv` to `export` and adding “=” signs and is saved as `/opt/ferret/ferret_bash`
9. The script is included into `/etc/bashrc` to automatically set the `PATH` variables for Ferret.

At this point all prerequisites are installed and configured and the main LAS installation can be performed, following the instructions on the webpage:

<http://ferret.pmel.noaa.gov/LAS/documentation/>

`installer-documentation/installation/installing-armstrong:`

1. The LAS configuration script `./configure` is executed in the directory  
`/opt/las`.

In our case some Perl modules are missing at the first start. LAS offers the option to build the modules as part of the LAS distribution (2). This is chosen but still the installation of the following modules fails:

`Bit-Vector-6.4`

`Date-Calc-5.4`

```
Log-Agent-0.301
```

```
XML-DOM-1.39
```

They have to be installed manually in the CPAN shell by using the name of the package, where the minus sign in the name is substituted by two colons and the version number has to be skipped:

```
perl -MCPAN -e shell;
install Bit::Vector
install Date::Calc
install Log::Agent
install XML::DOM
```

Then the `./configure` script can be executed without error messages, and the following parameters have to be set (mostly to the default parameter in brackets):

```
Location of perl executable [/usr/bin/perl]
Location of ferret executable:
    [/usr/local/ferret/bin/ferret]/opt/ferret/bin/ferret]
Location of java executable:  [/usr/bin/java]
Full path of Tomcat JAKARTA_HOME directory where you
    would like to deploy the servlet:  [/opt/tomcat]
Which HTTP port does the Tomcat server use:  [] 8080
Enter the full domain name of the Tomcat
    Server (do not include the port number):
    [reservoirage.palmod.uni-bremen.de]
Enter name of mysql host:
    [reservoirage.palmod.uni-bremen.de] localhost
MySQL account name:  [root]
Enter password:  []
Enter the fully qualified domain name of the mysql host:
    [reservoirage.palmod.uni-bremen.de] localhost
Enter the full domain name of the Web Server
    (including port number if non standard):
    [reservoirage.palmod.uni-bremen.de]
Do you plan to use a proxy pass or connector from the
    HTTP server to the tomcat server (recommended;
```



```

instructions below):  [yes]no
Enter path name for LAS: [/las]
Enter a title for the LAS server:  [Reservoir Age
Database]
Enter a blank separated list email address(es):
[joerg@palmod.uni-bremen.de]
Enter a directory path for F-TDS temporary files:
[/opt/las/conf/server/temp]
Enter the directory path you configured for LAS F-TDS
data files:  [/opt/las/conf/server/data]
The directories to store journal and temporary files
/opt/las/conf/server/data and ../temp are created automatically in
the configuration process.

```

If run the second time:

```

You already have a config file for your Ferret backend
environment.  Do you want to use this file?  [yes]
You have an existing XML file in server/las.xml Do you
want to set up the server to use this file?  [yes]
I need to know the group your Web server runs as.
Group name?  [apache]
(can be checked in: /etc/httpd/conf/httpd.conf)
Configuration completed successfully

```

The option to use a proxy module to hide the Tomcat port in the URLs is deactivated in LAS `./configure` script because it is not working. To redirect requests without any port specification to the Tomcat port 8080 the following lines are added to the Apache configuration file `/etc/httpd/conf/httpd.conf`:

```

Redirect permanent /las
http://reservoirage.palmod.uni-bremen.de:8080/las

```

The Scientific Linux operating system of the reservoir-age server has Security Enhanced Linux (SELINUX) enabled in the standard configuration. This omits the redirection in the `httpd` configuration. Thus, SELINUX is disabled by editing `/etc/selinux/config`: `SELINUX=disabled`

After rebooting the system the redirect works.

Now the Live Access Server can be started, stopped and rebooted with:

1. `./opt/las/startserver.sh`
2. `./opt/las/stopserver.sh`
3. `./opt/las/rebootserver.sh`

To activate a script that checks and automatically restarts the Tomcat UI server when necessary the following entry is added to `/etc/crontab`:

```
55 0-23 * * * /opt/las/bin/las-ui-check.sh
```

When the server is running, it can be accessed under the URL:

```
http://reservoirage.palmod.uni-bremen.de/las/servlets/dataset or
http://reservoirage.palmod.uni-bremen.de:
8080/las/servlets/dataset
```

If problems arise the log file `[TOMCAT_HOME]/logs/catalina.out` and `http://ferret.pmel.noaa.gov/LAS/documentation/installer-documentation/installation/installation-error-messages` may help.

## A.2 LAS modifications

Finally a few modifications are carried out to improve the LAS user interface. In the banner at the top left of the web page a logo is added, which can be used as a “Home” button to go back to the main web page. Therefore

`/opt/tomcat/webapps/las/VM_global_library.vm` is edited:

```
<td valign="center" align="left">
  <a <link rel="up" title="Home"
    href="http://reservoirage.palmod.uni-bremen.de/
    index.php?thispage=home">
  
```

```

</a>
</td>
<!-- <td class='`bannertitle`' align='`left`'>$title</td>
--> comment this line

```

The image file of the logo (`ra_logo.gif`) has to be copied to `/opt/tomcat/webapps/las/images`. Afterwards the website has to be generated again by running `/opt/las/xml/perl/genLas.pl las.xml` in the directory `/usr/opt/las/conf/server/` and the server has to be rebooted by `sh /opt/las/rebootserver.sh`.

For LAS Armstrong version 1.1 and above the internal handling of the date/time variable in the NetCDF data file will be changed. This needs to be switched off to follow using the modeled reservoir ages. The second line of `/opt/las/WebContent/luis/velocity/constrain.vm` and the fourth line of `/opt/las/WebContent/luis/velocity/constrain_compare.vm` need to be changed from:

```

set($date_widget = ``true``) to
set($date_widget = ``false``)

```

## A.3 Preparing model data for LAS

The output of the UVic ESCM contains data which needs to be converted or cannot be directly processed by LAS. It includes dissolved inorganic carbon (dic) and dissolved inorganic  $^{14}\text{C}$  (dic14) instead of the reservoir ages. The model was run forward in time, but the output in the database is supposed to contain the data in “years BP”. Therefore the timescale has to be inverted. Furthermore the description of some variables in the NetCDF file have to be changed because the used NetCDF tools or LAS cannot deal with descriptions made by the model, e.g. for the time unit or calendar. Finally the output also has to be rotated back on a regular grid, which can be done with a script `rot_nc.f` included in the `/util` directory of the UVic ESCM code.

A script, written for the bash under UNIX, processes all transformation steps at once. It requires the grid rotation tool of the UVic ESCM including the extension for the newly included tracer. The vector and scalar fields that need to be rotated are added in

the file `rot.nc.f`:

```
! 3d in ocean depth
s3d(1,1) = ``temp``
...
s3d([last value + 1],1) = ``dic14``
```

The “cdo” NetCDF tools

(<http://www.mpimet.mpg.de/fileadmin/software/cdo/>) and the “nco” NetCDF tools (<http://nco.sourceforge.net/>) are required to reformat the NetCDF files. The following extract of the script `tm2db.sh` shows the major steps to modify the model output NetCDF file in a manner that it can be included into LAS:

```
...
<UVic directory>/<version number>/util/rot.nc/mk.exe
...
ncap -s 'time=(time-55001)/(-10)' out2.nc out3.nc
ncatted -a axis, time, c, c, 't' -a long_name, time,
c, c, 'time since initial condition' -a standardname,
time, c, c, 'time' -a units, time, c, c, 'years since
0000-01-01 00:00:00' ... out3.nc out4.nc
cdo splityear out4.nc out4_
cdo mergetime out4_????.nc out5.nc
...
cdo merge out6.nc out8.nc out9.nc
ncatted -a calendar, time, c, c, 'noleap' -a axis, time,
c, c, 't' -a long_name, time, c, c, 'time since initial
condition' -a standardname, time, c, c, 'time' -a units,
time, m, c, 'common_year since 0000-01-01 00:00:00'
...
```

## A.4 Time-axis conversion

In practice marine  $^{14}\text{C}$  ages are measured. Hence the web interface should provide calendar ages and reservoir ages for a given uncalibrated ages. Thus, a second conversion

is necessary to convert the modeled reservoir ages to a new dataset that is based on a  $^{14}\text{C}$ -time axis instead of the calendar-time axis.

The program `c14cal.f90` is written to do this conversion. It searches in time steps of 10 years in the modeled  $^{14}\text{C}$  ages of every grid cell for the corresponding calendar and reservoir age and saves them in a new variable `res_age` for the reservoir ages and `cal_age` for the calendar ages. If more than one calendar age exists at a given  $^{14}\text{C}$  age ( $^{14}\text{C}$  plateau), an arithmetic mean of the calendar ages and reservoir ages is calculated, respectively. If no value exists in the  $^{14}\text{C}$  age time step, it is interpolated linearly from the next available neighbors on the time axis. If no calendar and reservoir age is corresponding to the  $^{14}\text{C}$  age at the beginning or end of the dataset in time, a value of  $9.9 \cdot 10^{36}$  is set to indicate missing data.

The entire dataset cannot be converted at once due to a lack of computer memory.

Therefore it is split by depth levels as the whole time period has to be processed at once to find all reservoir and calendar ages corresponding to a  $^{14}\text{C}$  age. This is done in `ferret` using the command `SAVE/clobber/FILE=ra-c14age_k19.nc`

`RA[k=19],C14AGE[k=19]` on the NetCDF descriptor file e.g. `dc14_pd_circ.des` after increasing the memory size set `memory/size=500`. After the transformation of the time axis with the aforementioned program the NetCDF files are merged together using the `nco` tools. The following extract of the script `cat_z-levels.sh` shows the major steps to concatenate the 19 depth levels of the model output after the splitting for the time-axis conversion:

```
...
ncap -s "Time=Time/10" $in1 out1.nc
...
ncap -s "Time=Time/10" $in19 out19.nc
ncecat -O out1.nc out21.nc
...
ncecat -O out19.nc out39.nc
ncpdq -O -a Depth,record,Latitude,Longitude,Time out21.nc
      out41.nc
...
ncpdq -O -a Depth,record,Latitude,Longitude,Time out39.nc
```

```

out59.nc

ncrcat out41.nc out42.nc ... out59.nc out90.nc

ncpdq -O -a record,Longitude,-Latitude,Depth,Time out90.nc
out91.nc

ncwa -O -a record out91.nc $out

```

## A.5 NetCDF descriptor file

In order to keep the size of the files manageable and due to memory limitation when the time axis is converted (Appendix A.4), the model output is split to files of less than 2 GB size. For the database they have to be merged again, otherwise time series plots spanning data of multiple files would be impossible. For NetCDF files a simple way of writing a so-called “multifile NetCDF descriptor” exists that describes how single NetCDF files are connected. These files, usually ending in `.des` instead of `.nc`, can be read and analyzed by Ferret like usual NetCDF files.

A program to automatically generate descriptor files is e.g. `make_des` ([http://www.gfdl.noaa.gov/~atw/ferret/make\\_des](http://www.gfdl.noaa.gov/~atw/ferret/make_des)). The descriptor file produced by typing `make_des in-files > out-file.des` needs manual editing of the calendar type and the time unit.

By convention the variable year in NetCDF files has only four digits, but the database has to store the reservoir ages for the last 45,000 years.

Therefore, a special definition of the time axis has to be applied in the NetCDF file and in LAS. The data consisted of 4500 time slices of 10 yearly mean values. In the NetCDF files they have a number for the year divided by 10, resulting in year 0 to 4500. In the descriptor file the time range and the time step is adjusted to the range from 0 to 45,000 with a 10 year time step:

```

&FORMAT_RECORD
  D_TYPE = ' MC'
  D_FORMAT = ' 1A'
/
&BACKGROUND_RECORD

```

```

    D_TITLE = 'Reservoir Age'
    D_T0TIME = '01-JUL-0000'
    D_TIME_UNIT = 31536000
    D_TIME_MODULO = .FALSE.
    D_CALTYPE = 'NOLEAP'
/
&MESSAGE_RECORD
    D_MESSAGE = ' '
    D_ALERT_ON_OPEN = .FALSE.
    D_ALERT_ON_OUTPUT = .FALSE.
/
&EXTRA_RECORD
/
&STEPFILE_RECORD
    S_FILENAME = 'PATH and name of first NetCDF file'
    S_AUX_SET_NUM = 0
    S_START = 00000
    S_END = 04000
    S_DELTA = 10
    S_NUM_OF_FILES = 1
    S_REGVARFLAG = ' '
/
&STEPFILE_RECORD
    S_FILENAME = 'PATH and name of second NetCDF file'
    S_AUX_SET_NUM = 0
    S_START = 05000
    S_END = 09000
    S_DELTA = 10
    S_NUM_OF_FILES = 1
    S_REGVARFLAG = ' '
/
...
&STEPFILE_RECORD

```

```
S_FILENAME = ' **END OF STEPFILES** '
```

If a data request from LAS is sent to Ferret at this point, it can not deal with year variables exceeding 9999. To allow for this Ferret needs to treat the x-axis as a regular axis with decimal numbers instead of a time axis with dates. This can be achieved with the command: `CANCEL MODE CALENDAR` when a data request in the Ferret initialization scripts of LAS is made. `LAS_initialize_data.jnl` initializes the dataset first, then calls special initialization scripts like in our case `tm_dc14_forc_initialize.jnl` and finally initializes the variable.

The script `tm_dc14_forc_initialize.jnl` to cancel the time axis contains the following:

```
CANCEL MODE CALENDAR
EXIT
```

and has to be saved in the directory

```
/opt/tomcat/webapps/las/WEB-INF/classes/resources/ferret/scripts/.
```

When LAS is generated all scripts are copied to this directory ensuring that the new script is available in the same directory.

In the dataset configuration XML file (`/opt/las/conf/server/las.xml`), the name of the initialization script has to be set as a Ferret property called

`init_script`:

```
<properties>
  <ferret>
    <init_script>tm_dc14_forc_initialize</init_script>
  </ferret>
</properties>
```

Alternatively the script can be called directly by editing `LAS_initialize_data.jnl`.

## A.6 Adding files to LAS

To include the modeled data into LAS, an utility called `addXML` is used. It generates a XML configuration file for an existing NetCDF formatted data file. This utility is available at `ftp://ftp.pmel.noaa.gov/ferret/pub/las/addXML/`. `AddXML`



is extracted to `/opt/las.armstrong.1.0/addXML-1.4.1` with the command `tar xvfz addXML-1.4.1.tar.gz`.

In `/opt/las.armstrong.1.0/addXML-1.4.1/addXML.sh` the pathes are set:

```
``$JAVA_HOME`` == ``/usr/java/jdk1.5.0_11``
``$ADDXML_HOME`` == ``/opt/las.armstrong.1.0/addXML-1.4.1``.
```

Then the XML file is created by running the following command in the directory

`/opt/las.armstrong.1.0/conf/server:`

```
sh /opt/las.armstrong.1.0/addXML-1.4.1/addXML.sh -v -x las.xml
-n /opt/las.armstrong.1.0/data/dc14_forc_pd_05-00.nc
dc14_forc_pd_circ.
```

This command creates a file named `dc14_forc_pd_circ.xml`. The option `-v` is set for detailed messages when running the script, `-n` to signify reading from a NetCDF data source and the option `-x` to create a new `las.xml` configuration file called `dc14_forc_pd_circ_las.xml`, which includes the previous `las.xml` and additionally the entries for the new dataset. The existing `las.xml` is not changed. The script needs to be run calling a `[file_name].nc` NetCDF file and not the `[file_name].des` descriptor file.

In the generated `dc14_forc_pd_circ_las.xml` the `lasdata` section has to be edited to define, which files will be displayed in the web interface:

```
<!ENTITY dc14_forc_pd_circ SYSTEM ``dc14_forc_pd_circ.xml``>
  &dc14_forc_pd_circ;
  ...
```

Then the file is finally saved as `las.xml`.

The new xml file `dc14_forc_pd_circ.xml` that describes the data has to be edited manually in order to enter a dataset name, to comment the variables that should not to be offered in the web interface, to edit the time axis and to replace the NetCDF file name with the descriptor file name:

```
<datasets>
  <id-6165bc3a62 name=``10-yearly mean Reservoir Age
    (calculated with PD circulation)``
  <variables>
```

```

<!-- <tlat-id-6165bc3a62 name='`tracer grid latitude`'
units='`degrees' url='`#tlat`' />
<link match='`/lasdata/grids/grid-xt-yt-id-6165bc3a62`' />
</tlat-id-6165bc3a62>-->

<time-t-id-6165bc3a62 type='`t`' units='`year`'>
<arange start='`0`' size='`4500`' step='`10`' />
</time-t-id-6165bc3a62>

```

This time axis description creates a dropdown menu in the range between timestep 0 and 45,000 with a spacing of 10 years.

To include the updated xml configurations into LAS, the webpages are rebuild with the command `/opt/las.armstrong.1.0/xml/perl/genLas.pl las.xml` in the directory `/opt/las.armstrong.1.0/conf/server` and the server is restarted with `/opt/las.armstrong.1.0/rebootserver.sh`.

Name: Jörg Franke  
Anschrift: Mühlenkampstr. 61  
31515 Wunstorf

Datum: 04.02.2008

## Erklärung

Hiermit versichere ich, dass ich

1. die Arbeit ohne unerlaubte fremde Hilfe angefertigt habe,
2. keine anderen als die von mir angegebenen Quellen und Hilfsmittel benutzt habe und
3. die den benutzen Werken wörtlich oder inhaltlich entnommenen Stellen als solche kenntlich gemacht habe.

Bremen, den 04.02.2008

---

(Unterschrift)